LBL-10888
UC-34c
CONF-800320

Lawrence Berkeley Laboratory
UNIVERSITY OF CALIFORNIA

WORKSHOP ON NUCLEAR DYNAMICS

17-21 March 1980

Granlibakken, Tahoe City, California

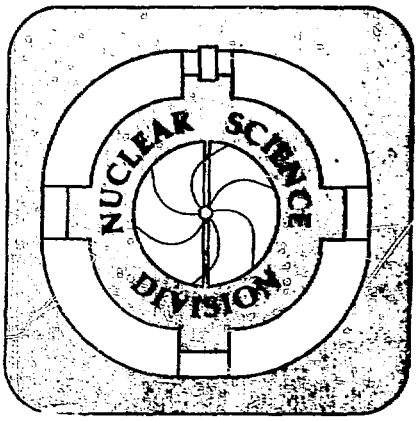

Prepared for the U.S. Department of Energy under Contract W-7405-ENG-48

PREFACE

We chose the title "Nuclear Dynamics" for our workshop because it was broad enough to cover the wide range of subjects that characterize the frontiers of nuclear physics today. The macroscopic aspects of nuclear collisions at all energies (from the lowest to the highest currently available) occupied our attention for a week and we were delighted with how well the discussions served to emphasize the unity and coherence of the field. The participants were just as much at home discussing the chemical properties and low energy nuclear structure of the elements as they were discussing pion production correlation functions and quark confinement. Conventional nuclear physics, and its extension to higher energies that is now underway, is a broad, interesting and exciting field.

The workshop consisted of nine scheduled sessions with discussions centered around current research themes presented by some of the participants. Summaries of these presentations make up the bulk of this report. These summaries give a good impression of the subjects covered but they can not convey the contents of the associated discussions, which took up most of the time, and which were the most important part at the meeting.

Some of the administrative costs and the costs of preparing these proceedings were covered by a grant from the Director's Office at Lawrence Berkeley Laboratory. We are indebted to Sue Ovuka of Conference Coordination for help in setting up the workshop, to Jeannette Mahoney for handling all of the on-site administration and to Cathy Webb for program assistance and for editing these proceedings. The staff of Granibakken provided a pleasant and comfortable atmosphere for the workshop, but, of course, it was the enthusiasm of the participants themselves that was the decisive element in making this such an enjoyable and profitable week. We want to take this opportunity to thank all concerned.

The Organizers:

Bill Myers
Jørgen Randrup
Gary Westfall

PROGRAM

Page

PROGRAM (continued)

PROGRAM (continued)

LIGHT-PARTICLE EMISSION IN REACTIONS INDUCED WITH CARBON AND OXYGEN IONS*

F. Plasil, J. R. Beene, R. L. Ferguson, A. Gavron, D. C. Hensley,
F. E. Obenshain, G. R. Young, M. P. Webb
Oak Ridge National Laboratory, Oak Ridge, Tennessee 37830

G. A. Petitt
Georgia State University, Atlanta, Georgia 30303

K. A. Geoffroy, M. Jaaskelainen, D. G. Sarantites
Washington University, St. Louis, Missouri 63130

C. F. Maguire
Vanderbilt University, Nashville, Tennessee 37215

In this work preliminary results are presented from three different experiments in which light particles emitted during the course of heavy-ion-induced reactions have been studied. The common primary motivation for undertaking these studies was to determine the nature and extent of nonequilibrium particle emission. The three experiments involved measurements of energies, angular correlations, and multiplicities of neutrons or alpha particles emitted in coincidence with deeply inelastic (DI) products or with evaporation residues (ER) produced as follows: 1) neutrons from reactions of ^{16}O with ^{93}Nb at 12.9 MeV/u; 2) alphas produced in the same system; and 3) neutrons produced in ^{12}C reactions with ^{158}Gd and in ^{13}C reactions with ^{157}Gd at about 12.4 MeV/u.

Earlier experiments in which neutrons from heavy-ion-induced reactions were measured directly have failed to yield evidence for nonequilibrium neutron emission,[1-3] except for experiments carried out at ORNL with relatively light heavy ions at energies above 10 MeV/nucleon.[4] The number of α-emission studies is considerably larger, and while there is some evidence that nonequilibrium alpha particles are emitted, they do not dominate the observed distributions. Furthermore, the interpretation of the alpha measurements is complicated and, as will be pointed out, subject to pitfalls which may lead to questionable conclusions.

In the two neutron experiments described here, heavy-ion detectors were located inside a thin-walled spherical reaction chamber, and eight liquid scintillator neutron detectors were deployed at fixed angles around

the chamber. The energies of neutrons were deduced from measurements of their time-of-flight. DI products were identified by means of ΔE-E telescopes having silicon ΔE elements. ER were identified with a gas ΔE-E telescope in the O + Nb experiment and by means of time-of-flight measurements in the C + Gd experiment. In the O + Nb case, the silicon ΔE-E telescope was located at -22° and the gas ΔE-E telescope at +27° with respect to the beam. In the C + Gd measurements the two silicon time-of-flight ER detectors were located at 6.5° and -9° and the silicon ΔE-E telescope at 18°.

An analysis of measurements of neutrons in coincidence with DI projectile-like (PL) fragments was described earlier[5] for the O + Nb reaction. It was based on the initial assumption that all neutrons observed in a detector at 46° (located on the other side of the beam from the coincident PL products) were emitted from the target-like (TL) fragments. The neutron spectrum observed in this detector was transformed (assuming isotropic emission from the TL fragments) to the corresponding spectra at laboratory angles of all other detectors, resulting in calculated spectra that were then compared with measured spectra. In Fig. 1.a we show the velocity spectrum of neutrons in coincidence with PL products, measured with detectors located at -13.7° and 11.4°. The appropriate calculated spectrum is also shown. It is clear that in these two forward detectors, there is a large excess of neutrons that cannot be attributed to statistical emission from TL fragments. In Fig. 1.b the differences between calculated and measured neutron velocity spectra are shown for each of the detectors located at -28°, -14°, 11°, and 24°. From the angular correlation and from the velocities involved, it can be shown that very few, of the excess neutrons are evaporated from the PL fragments. Thus, a large fraction (~50%) of the neutrons emitted in the forward direction are not due to evaporation from fully accelerated fragments, but are due to some form of nonequilibrium emission. While we do not propose a mechanism for the production of these nonequilibrium neutrons, it should be noted that their most probable velocity is similar to the beam velocity of 5 cm nsec^{-1}. This indicates that projectile breakup could be one of the mechanisms

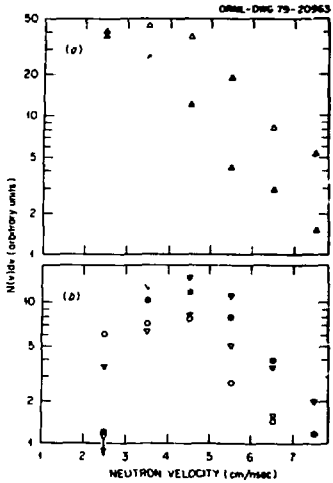

Fig. 1. (a) Measured (open triangles) and calculated (closed triangles) velocity spectra of neutrons in coincidence with DI products produced in the 208-MeV ^{16}O reactions with ^{93}Nb. (b) Differences between measured and calculated spectra for detectors located at -28° (closed circles), -11° (closed triangles), 11° (open triangles), and 24° (open circles). For method of calculation, see text.

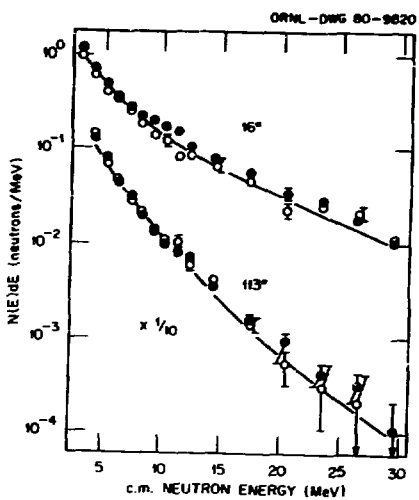

Fig. 2. Spectra of neutrons in coincidence with ER produced in the reactions 150-MeV ^{12}C + ^{158}Gd (open circles) and 160-MeV ^{13}C + ^{157}Gd (closed circles). Solid curves are from calculations which are described in the text.

involved in their production. Empirically, however, it is also possible to explain both the observed anisotropy and the energy spectra by assuming that 60% of all neutrons were emitted from fully accelerated TL fragments, while 40% were evaporated from a source moving with half the beam velocity.

Next, we present results from the 150-MeV ^{12}C + ^{158}Gd and 160-MeV ^{13}C + ^{157}Gd reactions. The neutrons discussed here were measured in coincidence with ER, which were detected at 6.5° and at -9°. Nonequilibrium neutrons in coincidence with specific ER have been observed earlier in the case of ^{12}C + ^{158}Gd at 152 MeV.[4] From gamma multiplicity measurements it was deduced that they are associated with the highest partial waves which contribute to ER (or to detected partial-fusion products[5]). In view of the peripheral nature of the reactions leading to the emission of the energetic neutrons, it was expected that effects of the difference in neutron binding energies in the projectiles might become apparent when ^{12}C- and ^{13}C-induced reactions are compared with each other. In Fig. 2 we present neutron spectra at 36° and 113° obtained in coincidence with ER from the ^{12}C + ^{158}Gd and ^{13}C + ^{157}Gd reactions at about the same energy per nucleon. It is clear that there is no significant difference between the spectra obtained from the two different systems. The curves in Fig. 2 indicate fits to data performed at four angles (36°, 54°, 90°, and 113°) on the assumption that the observed spectra resulted from two moving sources. The first source was assumed to be the compound nucleus, emitting neutrons with a Maxwellian energy distribution characterized by a temperature of 1.6 MeV. The velocity and temperature of the second source, which was also assumed to produce a Maxwellian spectrum, were adjustable parameters. A good fit was obtained to both reactions simultaneously when it was assumed that 60% of all observed neutrons (~1.6 neutrons) were associated with a source moving with one-third of the beam velocity (i.e., $v_{source} = \frac{1}{3} v_{beam}$) and having a temperature of 4 MeV. This suggests that the high-energy neutrons were produced during the deceleration stage of the nuclear collisions.

The final results we wish to present are for α emission associated with DI collisions between 200-MeV ^{16}O and ^{232}Th. The α particles and fragments were detected at -21°, and the correlated α particles were

measured at several angles, both in- and out-of-plane, on both sides of the beam. From the data it is possible to generate a diagram of Galilean invariant α multiplicity, $dM_\alpha/dv^3 d\Omega_{RI}$. The resulting contour-polar velocity plot has the advantage that it represents results that are invariant with respect to transformations into any frame of reference, and thus a choice of a specific emission mechanism need not be made in order to make some appropriate lab to rest frame transformation. The experimental results for alphas in coincidence with carbon ions are shown in this representation in Fig. 3.c. It can be seen that a large number of alphas are concentrated on the other side of the beam from the coincident carbon nuclei, between the beam and the TL recoils. Similar results have been obtained by other groups, and in some cases claims have been made that the α particles result from some type of nonequilibrium emission process.

In order to interpret our results, we have carried out a Monte Carlo simulation calculation in which alphas were allowed to evaporate from excited ^{16}O and ^{93}Nb reaction products. In this calculation we have made use of average n, p, and α energy spectra and of multiplicities calculated from a modified version of the Monte Carlo evaporation code JULIAN.[7] The total kinetic energy and angular distributions of PL products were obtained experimentally from a separate singles measurement. First, we neglected the effect of the sharp variation in the angular distributions of PL products and obtained the velocity plot shown in Fig. 3.a. When this calculated distribution is compared with the measured one, it is clear that there is little resemblance between the two, even in their gross features. We then took the angular distribution of the ^{16}O products into account and obtained the contour plot of Fig. 1.b. If we allow for the fact that our α detectors did not cover the angular range close to the beam and had an energy threshold equivalent to 2 cm nsec^{-1}, the calculated distribution (Fig. 3.b) is in fairly good agreement with the measured distribution (Fig. 3.c). We conclude that while there may be a small number of nonequilibrium alphas produced in this reaction, most of the alphas can be accounted for in terms of equilibrium emission from fully accelerated fragments. It also follows from the simulation that most of

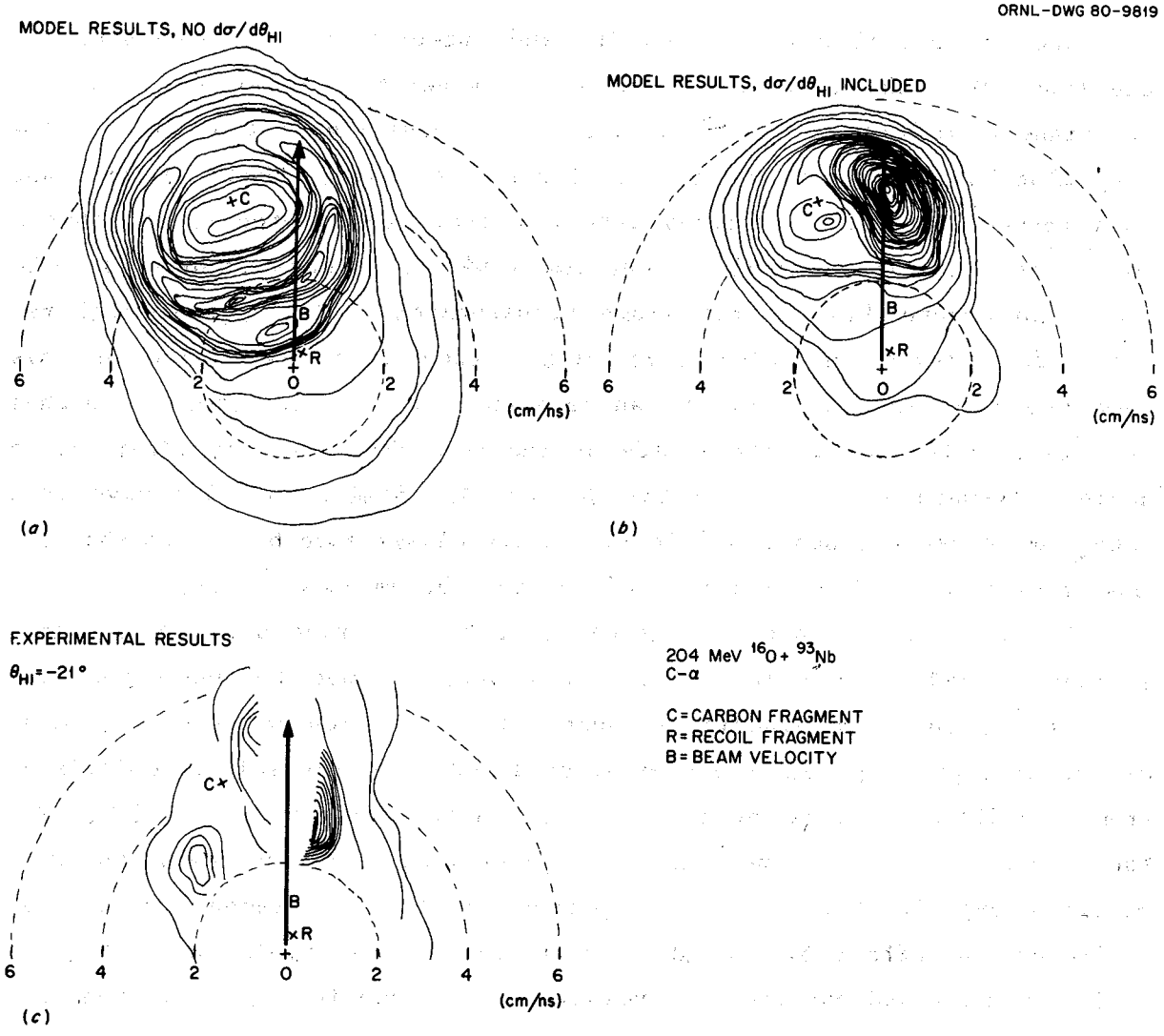

Fig. 3. Linear contour plots of invariant a multiplicities, $dM_a/dv^3 d\Omega_{HI}$ of alphas in coincidence with DI carbon ions produced in reactions of 204-MeV ^{16}O with ^{93}Nb. Calculated results are given in (a) and (b). For a description of the calculations, see text.

the alpha yield in the intense-yield region of Fig. 3 is due to the emission from the PL fragment and not from the TL products, as one might have been tempted to conclude from a cursory examination of the experimental velocity contour diagram. This result, however, is not inconsistent with excitation energy sharing proportional to the masses of the products.

References

*Research sponsored in part by the Division of High Energy and Nuclear Physics, U. S. Department of Energy, under contract W-7405-eng-26 with the Union Carbide Corporation.

1. D. Hilscher et al., Phys. Rev. C20, 576 (1979).
2. Y. Eyal et al., Phys. Rev. Lett. 41, 625 (1978).
3. B. Tamain et al., Nucl. Phys. A330, 253 (1979).
4. L. Westerberg et al., Phys. Rev. C18, 796 (1978).
5. G. A. Pettitt et al., Proc. Int. Symp. on Heavy-Ion Reactions (San Antonio, Texas, 1979).
6. K. Siwek-Wilczynska et al., Phys. Rev. Lett. 42, 1599 (1979).
7. A. Gavron, Phys. Rev. C21, 230 (1980).

BOMBARDING ENERGY DEPENDENCE OF NUCLEON EXCHANGE AND ENERGY DISSIPATION IN THE STRONGLY DAMPED REACTION $^{209}Bi + ^{136}Xe$*

W.W. Wilcke, W.U. Schröder, J.R. Huizenga and J.R. Birkelund
Departments of Chemistry and Physics
Nuclear Structure Research Laboratory
University of Rochester
Rochester, New York 14627

J. Randrup
Nuclear Science Division
Lawrence Berkeley Laboratory
Berkeley, California 94720

I. Introduction

Although considerable progress has been achieved in the understanding of strongly damped reactions at energies several MeV/u above the Coulomb barrier, some important experimental results are not yet clearly understood.

Among these is the degree of correlation between the nucleon exchange and the large energy losses observed. In a model[1] proposed by Swiatecki nucleons upon crossing a window between the colliding nuclei deposit their relative momentum within the recipient nucleus and thus convert kinetic energy of relative motion into intrinsic excitation energy. Although such a mechanism is consistent with experimental data, it has not yet been proven that energy loss induced by nucleon exchange is so dominant a mode of dissipation as to exclude other mechanisms such as the excitation of isoscalar giant resonances. Investigation of the bombarding-energy dependence of reaction phenomena is expected to yield essential information bearing on this question. In the following, experimental evidence is discussed, suggesting nucleon exchange as described by a one-body model to be the major component of the dissipation mechanism.

II. Experimental results

In an experiment[2] similar to the one described by Schröder et al.[3] the system $^{209}Bi + ^{136}Xe$ has been studied by measuring the triple-differential cross section $d^3\sigma/d\Omega dZdE$ at a bombarding energy of E_L=940 MeV. An overview of the data is shown in Fig. 1. The qualitative results are similar to the study[3] of this system at E_L = 1130 MeV, yielding Gaussian Z-distributions with variances σ_Z^2 strongly increasing with energy loss. In Fig. 2, the variances σ_Z^2 are plotted as a function of the energy loss for both bombarding energies. In the framework of one-body nucleon exchange models there is a simple relation between the variance σ_A^2 of the mass distribution and the energy loss, since both are produced by the same nucleon flux. In the classical limit and for peripheral collisions this relation can be written as

$$\ln (T_o/T) = \frac{m}{\mu} \sigma_A^2 \qquad (1)$$

where $T_o = E_{cm} - V_c$ and $T = T_o - E_{Loss}$ are the kinetic energies in the entrance and exit channels, respectively, μ denotes the reduced mass and m the nucleon mass. If a unique proportionality between σ_A^2 and σ_Z^2 exists throughout a reaction, a classical model of nucleon exchange predicts a linear relationship also between

*Work supported by the U.S. Department of Energy.

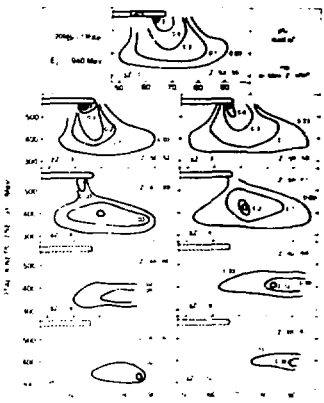

Figure 1

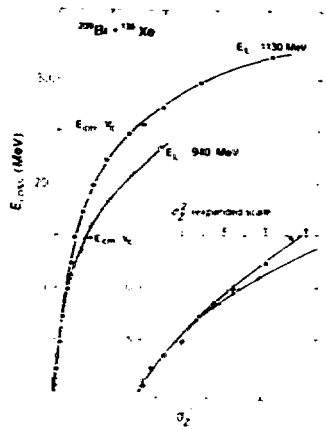

Figure 2

the quantities σ_z^2 and $\ln(T_o/T)$, with a slope given by $\frac{m}{\mu}\left(\frac{A}{Z}\right)^2$, if the relation $\sigma_A^2 = (A/Z)^2 \sigma_Z^2$ is assumed to hold. In Fig. 3 is shown that the data indeed follow straight lines, but quite in contrast to the prediction of Eq. 1, the slopes are strongly dependent on the bombarding energy.

It has been pointed out by Randrup[4] that it is important to incorporate the effect of the Pauli principle into models of nucleon exchange. Since the exclusion principle decreases the nucleon flux, the associated variances are reduced too. On the other hand, it can be shown, that the energy loss rate is not affected, since only nucleons with high relative momentum can participate in the nucleon exchange, which just compensates for the reduced flux. Therefore, the value $\ln(T_o/T)$ for a given σ_A^2 has to be increased by a factor $\alpha \approx j_{class}/j_{q.m.} \geq 1$ with respect to the one given by Eq. 1 in order to account for the Pauli principle. Three quantities determine the magnitude of α: the thermodynamic temperature of the colliding nuclei, the relative position of the Fermi-surfaces for non-identical nuclei and - most importantly - the relative momentun of the nuclei, which displaces the Fermi spheres with respect to each other. A straightforward geometrical calculation of the overlap volume of two intersecting Fermi spheres of equal radius T_F yields a universal energy dependence

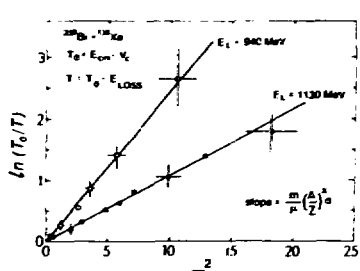

Figure 3

for α:

$$\alpha \approx \frac{2}{3}\left(\mu\, T_p/m(E_{cm} - V_c)\right)^{1/2}, \qquad (2)$$

approximately valid for peripheral collisions of cold nuclei. Consistent with experiment, α increases strongly with decreasing bombarding energy. These results are not restricted to the Xe + Bi system. In Fig. 4 experimental α-values for numerous systems are shown, where the broken line is calculated using Eq. 2. Although this simple model reproduces the qualitative trend of the data, there are still strong systematic deviations of the data from a universal curve. They are mainly associated with reactions induced by ^{56}Fe projectiles.

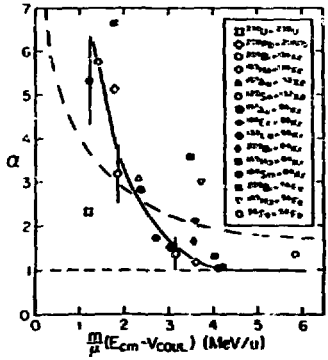

Figure 4

III. Trajectory calculations

The discussion so far has been restricted to peripheral reactions. For more penetrating collisions it is not possible to treat α as a constant during the interaction time. More detailed trajectory calculations have to be performed to allow a meaningful comparison with the data over a wide range of impact parameters. In Fig. 5 results of a partial-wave decomposition of experimental data are compared to a trajectory calculation using a model[5] with four degrees of freedom: the position vector (r,θ) connecting the centers of spherical nuclei and their respective angles of rotation. It should be pointed out, that theoretical values of none of the quantities depicted in Fig. 5 are affected by inclusion of the Pauli principle. Thus the effect of various potentials or a different set of degrees of freedom can be studied decoupled from the effect of the exclusion principle.

As can be inferred from Fig. 5, the calculation is unable to reproduce the large energy losses observed. This is not unexpected, since no deformation degrees of freedom are included, which puts an upper limit on the kinetic energy that can be dissipated. Therefore, an extended model,[6,7] where the two spherical nuclei are joined by a cylindrical neck has been adopted. Its radius and the mass and charge numbers of the projectile-like fragment are treated as three additional degrees of freedom. The proximity formalism and the liquid-drop

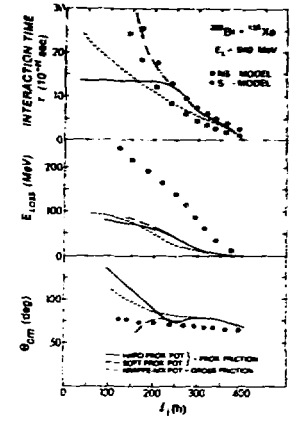

Figure 5

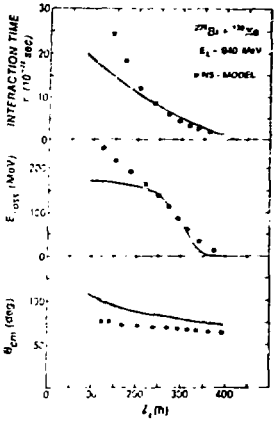

Figure 6

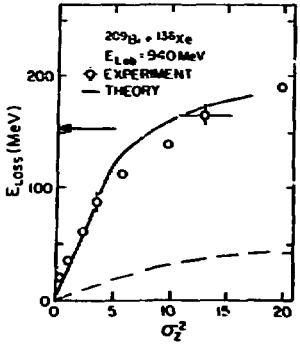

Figure 7

potential energy surface has been used to define the conservative and dissipative forces. In Fig. 6 the results of a calculation (without any adjusted parameters) are shown. Consistent with experiment, the calculated energy loss has strongly increased. The charge variances σ_Z^2 calculated by integrating the time-dependent proton flux for each trajectory are shown in Fig. 7 as a function of energy loss. It can be seen, that the inclusion of the Pauli principle (solid line) leads to good agreement with the data, whereas a classical treatment fails.

In conclusion, it appears, that the previously unexplained bombarding energy dependence between energy loss and fragment charge dispersion can be understood on the basis of a nucleon exchange model, provided the Pauli exclusion principle is taken into account. No necessity is seen to invoke further energy dissipation mechanisms to explain the present data, although such processes cannot be ruled out on basis of this comparison.

---

1. J. Błocki et al., Ann. Phys. 113, 330 (1977).
2. W.W. Wilcke et al., Phys. Rev. C (in press).
3. W.U. Schröder et al., Phys. Rep. 45, 301 (1978).
4. J. Randrup, Nucl. Phys. A307, 319 (1978); ibid. A327, 490 (1979).
5. J.R. Birkelund at al., Phys. Rev. Lett. 40, 1123 (1978).
6. W.J. Swiatecki, Report LBL-8950 (1979).
7. W.U. Schröder et al., Phys. Rev. Lett. 44, 308 (1980).

FRAGMENT SPIN ORIENTATION IN THE DEEP-INELASTIC REACTION $^{165}Ho + ^{165}Ho$ FROM ANISOTROPY MEASUREMENTS OF CONTINUUM γ-RAYS

G.J. Wozniak, R.J. McDonald, D.J. Morrissey, A. J. Pacheco, C. Shuck, S. Shih, R.M. Diamond, C.C. Hsu, H. Kluge, L.G. Moretto, L. G. Sobotka, and F. S. Stephens

Large amounts of orbital angular momentum can be transferred into fragment spin during the deep-inelastic collision process. Simple friction models suggest that the transferred spin should be aligned perpendicular to the reaction plane. This spin alignment should yield a large ratio for the in-plane to out-of-plane continuum γ-ray yield, $W(in/\perp)$, if most of the spin is carried off by stretched E2 transitions. For symmetric products from the 1064-MeV $^{136}Xe + ^{197}Au$ reaction, the observed small values of $W(in/\perp)$ have been interpreted[1] as evidence for a reaction depolarization mechanism, caused by the thermal excitation of angular-momentum bearing collective modes[2,3] in the rotating di-nuclear system.

To investigate the Q-value dependence of this depolarization process, we have investigated the $^{165}Ho + ^{165}Ho$ system at 8.5 MeV/A. A symmetric entrance channel was chosen to minimize ℓ-fractionation effects[1,4] and because at this bombarding energy ($\ell_{rms} \cong 36\hbar$) a large amount of angular momentum can be transferred into intrinsic spin ($I_1 + I_2 \sim 100\hbar$) if either the sticking or rolling limit is achieved. Secondly, this spin is primarily carried away by the γ-ray cascade because the product nuclei in this mass region have large fission barriers and large coulomb barriers which inhibit

the fission process and charged particle emission, respectively. Thirdly, the nuclei in this mass region are good rotors[5] whose γ-ray cascade multipolarity is relatively pure (~80% E2)[5]. Lastly, for a symmetric system there is no drift in the mass distribution and its width is narrow due to the steep ion-ion potential as a function of mass asymmetry, thus eliminating the need for A or Z-identification.

A schematic representation of our experimental setup is shown in Fig. 1a. To define two reaction planes, three particle detectors were placed at identical angles from the beam direction (two in a horizontal plane, Si1 & Si3, and a third, Si2, in a vertical plane). Si1 and Si2 consisted of a single E-detector each and Si3 was a ΔE-E telescope to monitor the width of the product charge/mass distribution. To detect the continuum γ-rays, three 5x6" NaI detectors collimated by 3" diameter Pb aperatures were placed 24" from the target. Two of these detectors, NaI1 & NaI3, were placed in the same horizontal plane as Si1 & Si3 and NaI2 was placed in the same vertical plane as Si2. With the above detector arrangement, 9 separate determinations of the in-plane to out-of-plane γ-yield could be made. Two examples of one such class of detector combinations are shown in Figs. 1b&c. In this preliminary analysis of the data only four such combinations were analyzed.

For the ^{165}Ho + ^{165}Ho system, the grazing angle is ~25^{o} in the lab. A particle energy spectrum taken at 27^{o} is shown in Fig. 2 (solid curve). This spectrum shows a kinematically broadened elastic peak which falls

off into the quasi-elastic (QE) region and a distinct deep-inelastic(DI) bump with a mean Q-value of about -300 MeV. The continuum γ-ray energy measured in coincidence with reaction products showed a peominent E2 bump whose mean position and upper edge moved to higher energies as the particle Q-value became increasingly negative in the QE region, but remained constant throughout the entire Q-value range (~-200 to -400 MeV) of the DI region. For each Q-value bin, the average γ-ray multiplicity was calculated employing the following expression:

$$M_\gamma = N_c(\gamma)/\varepsilon(\gamma)N_s(\text{particles}),$$

where N_c and N_s are the number of coincidence and singles particle events and ε is the γ-ray detection efficiency of the NaI detectors. The amount of angular momentum transferred into the intrinsic spin of the two fragments was calculated from M_γ with the following transformation:

$$I_1 + I_2\ (\hbar) = 2\left[M_\gamma + 8 - 6\right] + 1.0\ E^*/12.$$

It was assumed that there were 6 E1 transitions and that eitht E2 transitions lay below the 0.3 MeV cutoff which was set to exclude the backscatter energy region. Furthermore, it was assumed that one neutron was emitted for each 12 MeV of excitation energy and that each neutron carried off on the average one unit of $\hbar$.

The amount of spin deposited in one product fragment is plotted (squares) versus the reaction Q-value in Fig. 2. For the first 200 MeV of energy loss the transferred spin increases rapidly and saturates at ~50 $\hbar$ in the DI

region, which is essentially the value of the sticking limit for ℓ_{rms}. The above dependence of I_1 of Q-value mirrors the change of the values of the mean and upper edge of the quadrupole bump in the E spectra. This behavior can be easily understood when one recognizes that for rotational nuclei E_γ is proportional to the spin of the emitting nucleus.

The ratio of the in-plane to out-of-plane continuum γ-ray yield $W(in/\perp)$ is also plotted (open circles) versus the reaction Q-value. This ratio is unity for elastic events and rises rapidly with increasing energy loss reaching a maximum value of 2.2 at the upper edge of the DI region, before decreasing back to near unity for the largest energy losses. The rapid rise of $W(in/\perp)$ across the QE region tracks the rapid increase in the spin of the fragments. Since $W(in/\perp)$ is approximately proportional to I^2/σ^2, where σ^2 is the rms misalignment vector and I^2 is the fragment spin, and because I rapidly increases with increasing energy loss one would expect $W(in/\perp)$ to increase if σ was only slowly varying with Q-value. However, in the DI region I is essentially constant, while $W(in/\perp)$ decreases, indicating that the misalignment σ is increasing with energy loss.

The magnitude of the spin misalignment can be extracted from the experimental ratios by assuming[2,3] that the probability function for misalignment is a gaussian distribution peaked at the Z-axis. For 80% E2 transitions and a Q-value of -250 MeV, the experimental value of σ^2/I^2 is 0.070 which corresponds to a misalignment angle of approximately 26°. The depolarization model of Moretto and Schmitt[2,3] predicts that $\sigma^2 \simeq \vartheta/I^2$, where ϑ is

the moment of inertia of one of the two touching spheres and T is the temperature. For the -250 MeV Q-value bin, T = 2.3 MeV and the model predicts a value of σ^2/I^2 = 0.064 and a misalignment angle of 25° which are in close agreement with the experimental values.

In summary, from this preliminary analysis we have observed in the ^{165}Ho + ^{165}Ho reaction, large values for the spin transfer ($I_1 + I_2 \sim 100\ \hbar$) and large values for the in-plane to out-of-plane continuum γ-ray ratio, W(in/⊥) = 2.2. Both the spin transfer and W(in/⊥) are strong functions of the reaction Q-value and the latter also shows a dependence on E_γ. For a reasonable value of the γ-ray cascade multipolarity (80% E2s), a misalignment angle of 26° is extracted for the deep-inelastic region. These data have been compared with the statistical model of Moretto and Schmitt which correctly predicts the magnitude of the observed misalignment and qualitatively explains the trend of W(in/⊥) with Q-value. We conclude that continuum γ-ray anisotropy measurements are a powerful technique for probing the deep-inelastic collision process.

References

1. P. Aguer, R.P. Schmitt, G.J. Wozniak, D. Habs, R.M. Diamond, C. Ellegaard, D.L. Hillis, C.C. Hsu, G.J. Mathews, L.G. Moretto, [illegible] Rattazzi, C.P. Roulet, and F.S. Stephens, Phys. Rev. Lett. 43. 1778 (1979).

2. L. G. Moretto and R. P. Schmitt, Phys. Rev. C21, 204 (1980).

3 L.G. Moretto, LBL Report No. LBL-10493.

4. M.T. Aleonard, G.J. Wozniak, P.Glassel, M.M. Deleplanque, R.P. Dia[illegible], L.G. Moretto, R.P. Schmitt and F.S. Stephens, Phys. Rev Lett. 40, (1978) 622.

5. M.A. Deleplanque et al., Phys. Rev. Lett. 41 1105 (1978).

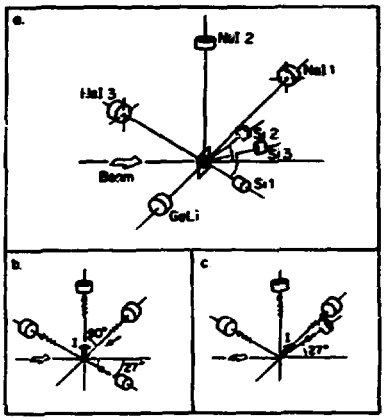

XBL 803-520

Fig. 1. A schematic diagram of the experimental set-up.

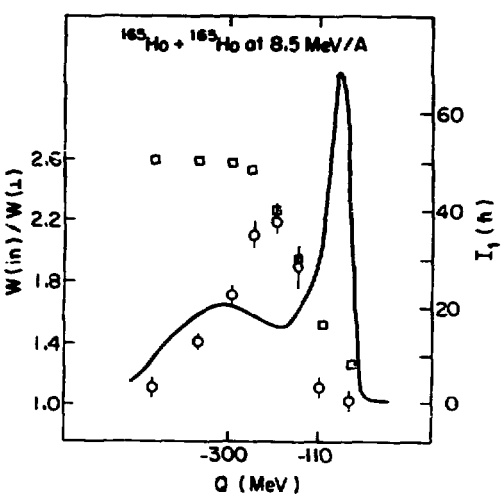

XBL 803-521

Fig. 2. Plots of particle yield (solid curve), spin transfer (squares) and the continuum γ-ray in- to out-of-plane ratio W(in/⊥)(circles) versus the reaction Q-value for ^{165}Ho + ^{165}Ho at 8.5 MeV/A.

DISTRIBUTION OF PRODUCTS IN THE REACTION ^{20}Ne + Al*

R. L. Ferguson, A. Gavron, F. E. Obenshain, F. Plasil,
R. L. Robinson, D. Shapira, A. H. Snell and G. R. Young
Oak Ridge National Laboratory
P. O. Box X, Oak Ridge, Tennessee 37830

We report here our measurement and preliminary analysis of the distribution of products with $2 \leq Z \leq 21$ and $3 \leq A \leq 43$ from reactions of ^{20}Ne with Al. Experimental conditions were adequate to allow resolution of individual isotopes over this entire range, and measurements were made at several angles for each of two bombarding energies. Measured relative cross sections of the heavier products are compared with predictions of a statistical model evaporation calculation.

The measurement of distributions of evaporation residues (ER) with simultaneous single charge and mass resolution provides a sensitive test of evaporation models. In a systematic study of fusion reactions, it is possible to test various assumptions involved in the calculations, as well as to obtain values for various nuclear parameters. Information can be obtained, for example, on the variation of level density parameters with nuclear deformation and on deformation-enhanced particle emission. Effects of incomplete fusion may also be apparent in the observed distributions.

Experiments were performed using energy-analyzed, well-collimated beams of ^{20}Ne from the Oak Ridge Isochronous Cyclotron incident on 100 $\mu g\text{-}cm^{-2}$ aluminum targets. For reaction products, the flight time was measured between two channel-plate electron multiplier assemblies 122 cm apart, and the energy loss in a gas-filled ionization chamber as well as residual energy in a silicon surface-barrier detector were also determined. Our time resolution of $\sim$ 150 ps FWHM and energy resolution of $\sim$ 0.6-MeV FWHM (measured for elastically scattered ^{20}Ne) gave a mass resolution of $\sim$ 0.4 FWHM. Resolution in Z was $\sim$ 0.6 FWHM. Differences in charge-collection times in the parallel plate ΔE ionization chamber were used to correct for small differences in path length between the channel-plate detector foils, which were oriented at 45° with respect to the detected particle's flight path. The data were analyzed by first constructing Z-masks in the ΔE-vs-E plane and then forming maps of an ET^2 function vs E for each Z. From these maps, A-masks were constructed, and an energy spectrum of each isotope was projected. Our present results are presented as relative yields.

Figure 1 indicates the energy- and angle-integrated yields of the observed products. As is to be expected, yields of the heaviest products from the 167-MeV bombardment can be seen to lie further from the compound nucleus than in the 118-MeV case.

In Fig. 2 are shown comparisons between our experimental results for the heavier products and the ER yields that are predicted by the evaporation code JULIAN (as modified by Gavron [1]). The calculated values

have been normalized to experiment by the ratio of total experimental to theoretical σ_{ER}. For this purpose, the experimental σ_{ER} was defined to be the sum of yields for all nuclides with $Z \geq 12$ and $A \geq 24$.

The Monte Carlo evaporation code JULIAN (Hillman and Eyal), includes proper angular momentum coupling to final states. The calculations shown were performed with the code's default options, which include: (i) Gilbert-Cameron level densities, (ii) the Bass model fusion cross section, (iii) the Cohen-Plasil-Swiatecki rotating liquid drop yrast line, and (iv) nuclear masses from the Wapstra 1977 table. One thousand cascades were calculated for each bombarding energy.

As is apparent in the Z and A projections of these comparisons (Fig. 3), the overall agreement between experiment and theory is rather good. With the calculational parameters used, the theoretical distribution is somewhat narrower than the experimental, both in Z and A at both bombarding energies. Variation of the input quantities will very likely improve the agreement. Hopefully, such variations will enable us to define level densities and the yrast line appropriate to this case, but it remains to be seen whether a unique fit can be obtained.

It is likely that even with the variations in input conditions mentioned above, it may not be possible to remove the discrepancies between calculation and experiment for low Z and A at 167 MeV. Lehr et al.,[2] were able to account for a similar underprediction of yield for light ER in their study of the system $^{20}Ne + {}^{26}Mg$ by including the effect of incomplete fusion in the reaction. It may, of course, be possible that we are seeing a corresponding effect here. The underprediction of yield for heavier ER, especially noticeable at 118 MeV, could be due to an overemphasis on α-emission. In this case, agreement between experiment and calculation is likely to improve with other choices of input conditions.

We have also made comparisons with the computer code ALICE,[3] which does not involve the couplings to all final angular momentum states but treats angular momentum removal by particle emission only approximately. The purpose was to see if such a calculation, which requires less computing time than JULIAN, can give a rough description of the observed yields. It was found that ALICE results in distributions that have much higher Z and A values, and the effect is easily understood in terms of an underestimation of α-emission. We conclude that for such light systems ALICE calculations are inappropriate.

REFERENCES

1. A. Gavron, Phys. Rev. C 21, 230 (1978).
2. H. Lehr, W. v. Oertzen, W. Bohne, H. Morgenstern, K. Grosch, and F. Pühlhofer, Hahn-Meitner-Institut für Kernforschung Berlin, Preprint HMI-P 1/80.
3. F. Plasil, Oak Ridge National Laboratory Report ORNL/TM-6054 (1977).

*Research sponsored by the Division of High Energy and Nuclear Physics, Office of Energy Research, U. S. Department of Energy, under contract W-7405-eng-26, with the Union Carbide Corporation.

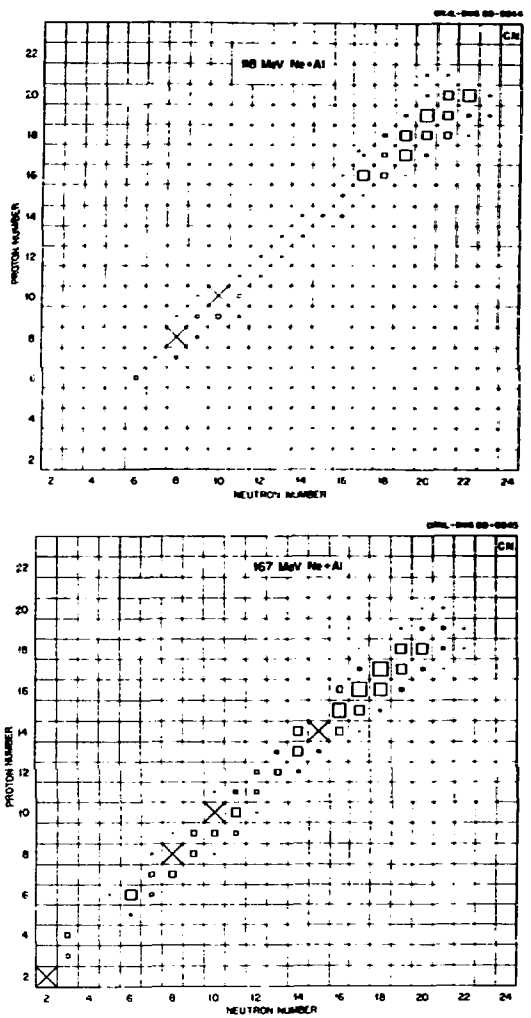

Fig. 1. Yields of all observed products from the reactions studied. Relative yields are proportional to the length of the side of the squares. The X's represent "overflow" values in the scale chosen.

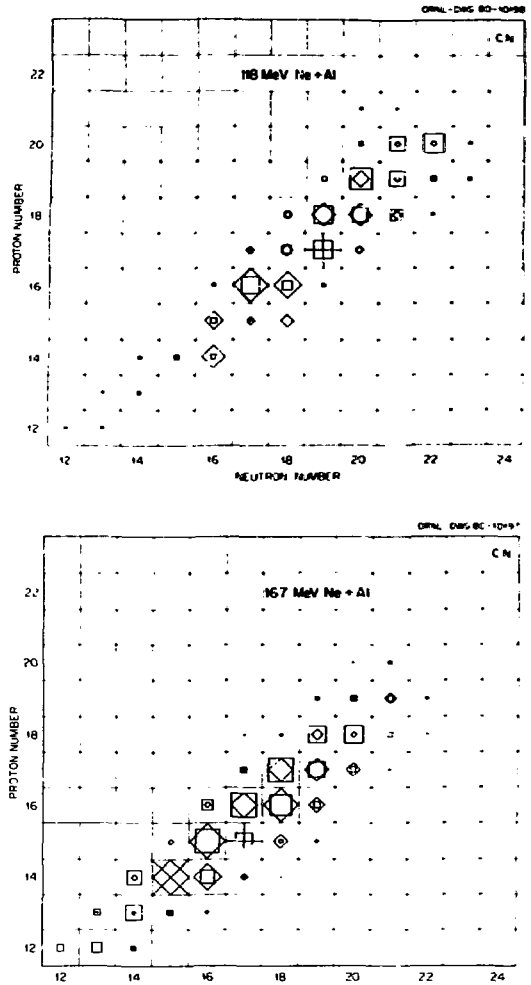

Fig. 2. Comparisons between measured yields (□,X) and Monte Carlo evaporation calculations (◇,+). Cf. Fig. 1.

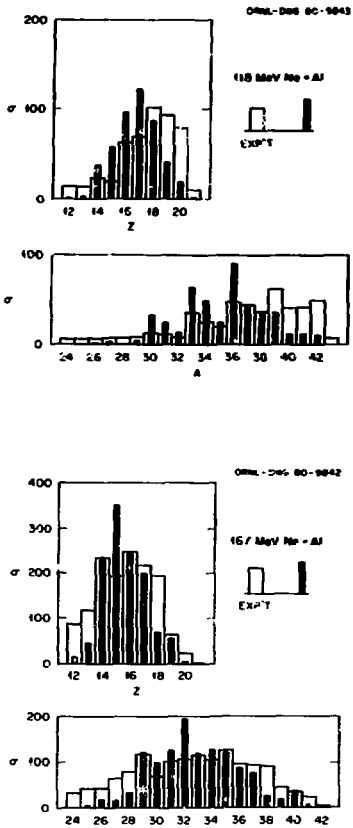

Fig. 3 Comparisons between experiment and calculations summed over A or Z to give the respective Z or A distribution.

LIGHT PARTICLE EMISSION AS A PROBE OF THE ROTATIONAL DEGREES OF FREEDOM IN DEEP-INELASTIC REACTIONS

L. G. Sobotka, G. J. Wozniak, C. C. Hsu, G. U. Rattazzi, R. J. McDonald, A. J. Pacheco, S. K. Blau, L. G. Moretto

A prominent feature of deep-inelastic collisions is the transfer of orbital angular momentum into intrinsic spins of the fragments. The experimental techniques commonly used to study this phenomenon have been gamma-ray multiplicity, and anistropy measurements and sequential fission angular distributions. Unfortunately the above techniques suffer from some severe limitations. The interpretation of continuum gamma-ray data is complicated by the emission of neutrons or light charged particles, which preceed gamma emission and can remove a substantial amount of angular momentum, and by uncertainties in the ratio of statistical vs. stretched γ-rays. In addition, it is not known which fragment emitted the detected γ-rays. While in- and out-of-plane sequential fission angular distributions are quite sensitive to the fissioning fragment's spin and the alignment of its spin relative to the orbital angular momentum, this technique is confined to very heavy systems.

The emission of light particles complements sequential fission in that medium and light regions of the periodic table can be examined. For example, recent work (1) on the angular correlation of evaporated light charged particles from the reaction 280 MeV ^{40}Ar + ^{58}Ni was used to infer the angular momentum of one of the deep-inelastic fragments. We have improved upon this already powerful technique by

simultaneously measuring the gamma multiplicity (M_γ), as well as the out-of-plane alpha emission from one of the deep-inelastic fragments produced in the reaction 664 MeV ^{84}Kr + ^{nat}Ag. We would like to discuss some preliminary results from this experiment, which we believe will prove extremely enlightening upon completion of the data reduction. Our results are interpreted with the aid of a straight forward statistical mechanical formalism.

The 664 MeV ^{84}Kr + ^{nat}Ag system was selected for study for several reasons. The Ag-like fragment is light enough to have an appreciable probability of evaporating an α-particle, but heavy enough so that second-chance light-particle emission is unlikely. Furthermore, it is possible to select an experimental configuration (see figure 1) where the detected α-particles should be predominately emitted from the target-like fragment. The system has a large angular momentum, ℓ (rms) $\cong$ 194 , and thus can deposit reasonably large spins into the two fragments (2).

The experimental configuration is outlined in figure 1. An ^{84}Kr beam from the superHILAC impinged upon a 586 $\mu g/cm$ ^{nat}Ag target. A ΔE-E (11μm-300μm) solid-state telescope with a 6.8 msr acceptance was positioned just behind the grazing angle to detect the projectile-like fragment and to define the reaction plane. On the opposite side of the beam an arc containing 4 light-particle telescopes (40μm-5mm) was positioned so that these telescopes had an in-plane projection approximately coinciding with the target recoil direction. Thick, 10.1 mg, Ta absorbers were placed in front of the light particle

telescopes to reduce the counting rates of HI's and noise due to x-rays and electrons striking these counters. In addition, an array of 7 NaI detectors was positioned above the reaction plane with an out-of-plane angle of 45° to measure M_γ. An eighth NaI was employed to obtain gamma energy spectra.

After each event was reconstructed, the energy of the alpha particles were transformed into the c.m. of the undetected Ag-like fragment. The energy spectra obtained are consistent with evaporation from tne slower moving Ag-like recoils.

A detailed treatment of the formalism for the angular distributions has been presented elsewhere (3), here we give only a brief discription. In a statistical model the spin alignment of one of the deep-inelastic fragments is described by gaussian distributions in cartesian components of angular momentum with widths σ_x, σ_y, and σ_z.

Using these misalignments it has been shown (4) that the decay width is:

$$W = \frac{1}{S(\theta,\phi)} \exp\left[- \frac{I_z^2 \cos^2\theta}{2S^2(\theta,\phi)} \right] \qquad 1.$$

where $S^2(\theta,\phi) = K_0^2 + \sigma_x^2\cos^2\phi\sin^2\theta + \sigma_y^2\sin^2\phi\sin^2\theta + \sigma_z^2\cos^2\theta$. Here, K_0 is the width of the out-of-plane distribution arising from the light particle emission. The alpha-particle need not be emitted perpendicular to the spin axis.

If one integrates over the fragment's angular momentum distribution up to some I(max) and assumes that the bulk of the total decay width is due to neutron emission, then the out-of-plane angular distribution is given by:

$$\omega(\theta,\phi) = \frac{1}{SA}[1 - \exp(-A)] \qquad 2.$$

where $A = I_{max}^2\left(\frac{\cos^2\theta}{2S^2} - B\right)$, $B = \frac{\hbar^2}{2T}\left(\frac{1}{\mathcal{J}_n} - \frac{1}{\mathcal{J}_\perp}\right)$

The moments of inertia $\mathcal{J}_n$ and $\mathcal{J}_\perp$ are those of the nucleus after neutron emission and perpendicular to the separation axis at the critical shape for decay. Using a value for I(max) obtained by assuming rigid rotation, the data in figures 2 and 3 have been fit to equation 2 by adjusting the value of S. If one makes the simplifing assumption that $\sigma_x = \sigma_y = \sigma_z = \sigma$ then $S^2 = K_o^2 + \sigma^2$.

The in-to-out of-plane ratios and the values of S/I(max) calculated by the formalism described above are indicated in figures 2 and 3. One clearly sees that the angular distributions become more focused in-plane, (indicating a higher degree of alignment or increased spin of the emitting fragment) as the number of coincident γ-rays(Nfold), TKE or charge asymmetry is increased. The trend seen in figure 2 results because gating on a higher number of coincident γ-rays creates a bias toward high fragment spins.

In figure 3 the dependencies on charge asymmetry and TKE are shown. The TKE bins span only the deep-inelastic region. The trend

with TKE could result from an increase in the misalignment with increasing energy damping. Another possiblity is that one selects higher angular momentum events with increasing TKE. The trend with asymmetry is most likely a consequence of the division of the angular momentum between the two DI fragments. If the dinuclear complex reaches rigid rotation, the partitioning of angular momentum between the two fragments goes as the moments of inertia or $(M_1/M_2)^{5/3}$. As asymmetry increases, the spin of the emitter (the heavy fragment) increases, causing the angular distribution to be more focused in-plane. The values of S support the attainment or near attainment of rigid rotation. Within a TKE window the values of S are reasonably constant, indicating that the change in the sharpness of the angular distributions is primarily due to a changing I(max).

We are presently attempting to calculate values for K_0 so that σ as a function of TKE and asymmetry can be extracted. Though the data analysis is still in the early stages we have already seen trends that if quantitatively understood could greatly increase our understanding of the rotational degrees of freedom in DIC.

References

1. D. Guerreau, J. Galin, R. Babinet, Preprint IPNO-R.C.79-07.

2. M. M. Aleonard et al., Phys. Rev. Lett. 40, 622 (1978).

3. L. G. Moretto, LBL Report No. LBL-10493.

4. R. A. Broglia, G. Pollarolo, C. H. Dasso and T. Dossing, Phys. Rev. Lett. 43, 1649 (1979).

Figure Captions

Figure 1: Vector diagram for reaction system. Circles are for 1 Coulomb barrier alpha particle emission. Arrow for light-particle telescopes indicates in-plane projection.

Figure 2: Angular distributions integrated over the deep-inelastic region for different Z bins, indicated by the detected Z's, as a function of the number of coincident gamma-rays.

Figure 3: Angular distributions as a function of total kinetic energy and charge asymmetry.

FIGURE 1

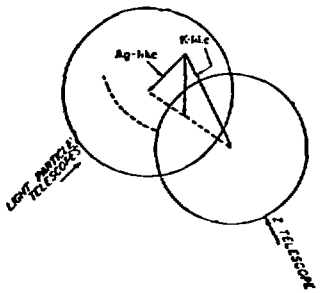

FIGURE 2

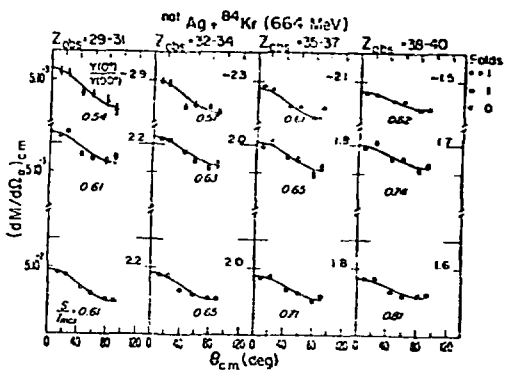

FIGURE 3

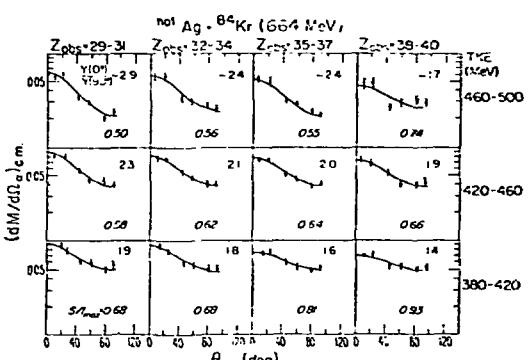

Planning for VENUS

Howel G. Pugh

Lawrence Berkeley Laboratory
Berkeley, California 94720

Abstract: VENUS (Variable Energy Nuclear Synchrotron) is a major new heavy ion accelerator to be proposed for construction at LBL. Some aspects of planning its scientific program are discussed.

1. History

Over the past several years staff of LBL's Nuclear Science Division (NSD) and Accelerator and Fusion Research Division (AFRD) have been working together to consider what new accelerator(s) should be planned for the eventual replacement of LBL's facilities (the 88-inch Cyclotron, the SuperHILAC, and the Bevalac). In addition to questions of technical feasibility, appropriateness to the institution and the interests of the existing staff and outside user groups, the requirement was imposed that the new accelerator(s) should put the Laboratory into a position of clear leadership on the national and international scene.

Extensive internal discussions groups and the annual series of LBL/GSI meetings contributed greatly, culminating in the May, 1979 1st Workshop on Ultra-Relativistic Heavy Ion Collisions (1). In June, 1979 the LBL staff issued a report (2) on The VENUS Project, which forms the basis for current planning. The VENUS facility, replacing the Bevalac, and injected by the SuperHILAC, would provide ions up to U and up at energies from 40 MeV/amu to 1 TeV/amu equivalent, the latter being obtained by a colliding beam capability. The accelerator, using superconducting iron-free magnets, would fit comfortably on to the existing LBL site, and cost roughly $100M (1978). The overall capability of the facility, added to the 88-inch Cyclotron (assumed to continue operation with appropriate upgrading) would permit an extremely wide range of physics to be addressed: atomic, nuclear, elementary particle, cosmic ray, and astrophysics. In addition it would provide expanded capability for the biomedical research program currently carried out at the Bevalac.

In July-August 1979, the DOE/NSF Nuclear Science Advisory Committee, chaired by Professor Herman Feshbach, held a major

Long Range Planning Study and projected national construction and operating budgets for the coming decade (3). The committee stated that $100M projects such as VENUS, or a kaon-antiproton facility, would require funds supplemental to those projected for the national base program, and would have to "be justified separately as required by important national goals, requiring special construction allocations, and ... substantial (additional) operating costs". The Committee recommended that research and development be conducted on such facilities, noting: "It is essential in all these cases that the R&D is not confined only to accelerator and other technical developments. A serious investigation into the scientific case... must be mounted... Scientific feasibility, that is the demonstration that one will be able to obtain results, is equally essential". These considerations form the basis of current LBL planning for VENUS.

2. The VENUS Project

The details of the accelerator will not be presented here in detail, since they are well described in reference (2) and have also continued to evolve in the intervening period. For the purposes of discussion of the science, and as a goal for further enterprise by the staff of AFRD, we assume:

Fixed target mode:	10 MeV/amu to 20 GeV/amu: 3 beams independently variable in energy, duty factor and intensity.
Colliding beam mode:	1 GeV/amu to 20 GeV/amu (1 TeV/amu fixed target equivalent), 3 intersection regions.
Proton capability:	50 GeV fixed target or colliding beams (5 TeV fixed target equivalent)

3. General Observations

The energy range is sufficiently unfamiliar that some comments are worth making to fix in ones mind the consequences of the high energies to be achieved:

1) At 20 GeV/amu the projectile is 20 times heavier than its rest mass. Only a fraction of its total energy can be made available in the c.m. system by collision with a stationary target.

2) The above problem is overcome by the colliding beam capability. For 20 GeV/amu colliding beams of equal mass

nuclei, all the energy is available in the c.m. This provides the equivalent of 1 TeV/amu projectiles striking a stationary target, with all the experimental advantages of having the c.m. system at rest in the laboratory.

3) The collisions are truly "ultra-relativistic", i.e., the rest mass can be neglected to a first approximation. Particle creation is the order of the day: no description of the collision process can succeed which ignores particle creation.

4) While the above three comments apply as much to proton-proton collisions as to collisions involving nuclei, the extreme Lorentz contraction and time dilatation introduce new features when nuclei are involved. These features warrant a special section:

1. Lorentz Contraction and Time Dilatation

The projectile, target, and c.m. frames are all of interest. A 20 GeV/amu on 20 GeV/amu collision is equivalent, for equal masses to a 1 TeV/amu projectile (target) striking a stationary target (projectile).

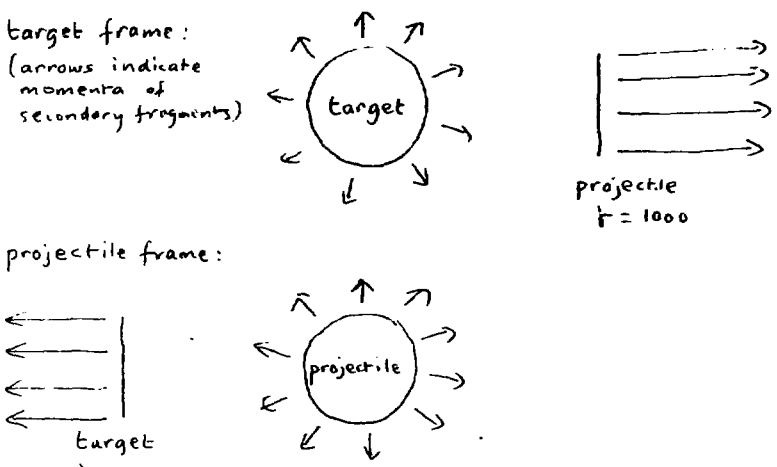

In the target frame, the target is entirely a normal nucleus. The projectile, longitudinally contracted by a factor of one thousand is only about 10^{-2} fm thick, resembling a piece of

paper in its proportions. We must therefore expect an entire row of nucleons in the projectile to collide with each component of the target in an extremely short time, as the projectile passes through. Symmetry, of course, indicates that the target looks to the projectile equally like a piece of paper. This brings us to the c.m. frame.

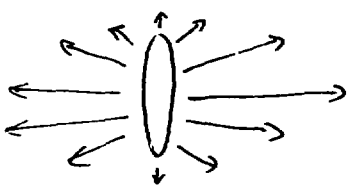

In the c.m. frame, the Lorentz contraction is less extreme, a factor of 20, but applies to each nucleus. This still suffices to reduce the Uranium nucleus to a thickness of less than 1 fm., the diameter of a proton. It becomes clear for all these reference frames that the collision is physically one of rows of nucleons on rows of nucleons.

In the c.m. frame, if the two nuclei were to be stopped completely by the collision (a very unlikely possibility) the energy density would be 20 GeV x 2 x 238 in a volume 1/20 that of a Uranium nucleus, i.e. 800 times larger than that of a normal nucleus. Statistical considerations of such energy densities provide a highly successful basic description of, for example, pion multiplicities in high energy p-p collisions, and such p-nucleus and nucleus-nucleus data as are available in this high energy regime.

A very interesting consequence of the Lorentz effect is the absence of cascading in the nuclear collision. The highly excited products of the internal collisions escape from the nuclear environment before decay. This has been verified experimentally in the decay of 3-pion systems produced coherently on nuclei and in comparisons of the secondary particle multiplicities for high energy p-p and p-nucleus collisions.

Such conditions offer possibilities to study the space-time evolution of hadronic interactions which would not be available in p-p collisions or in lower-energy collisions involving

nuclei. They also offer severe theoretical challenges for work in a relativistic many-body problem. It is hoped, however, that by going to the very high energies of VENUS, asymptotic simplicities will arise, and new approximations can be utilized.

5. Scope of the Research

Following the broad original concept and heeding the guidelines of the DOE/NSF Nuclear Science Advisory Committee, it will be necessary to outline a program of experimental work in the various areas to be addressed, to show how the results can be related to theory, and to indicate what group will expect to carry out the work. This is the basis of the current stage of LBL planning.

With various degrees of emphasis, work is proceeding on defining an experimental program related to

- atomic physics
- nuclear physics
- elementary particle physics
- cosmic ray physics
- astrophysics
- biomedical research.

Of these, the first and last items should be considered as among the many surprise benefits of the accelerator. Atomic physics would, for example, benefit from the capability to make one- or two-electron Uranium or other heavy nuclei. It is assumed that by the time VENUS is constructed, LBL will have a medical accelerator, but that biomedical research will continue to need unusual and exotic beams such as can be provided by VENUS.

The remaining topics have close connecting links, which are perhaps stronger at this time than they have been for many years. Investigations in all four areas require greater knowledge of the other areas as understanding of each improves. This results from parallel lines of development, all pointing to a need to understand better higher energies, higher densities and small substructures of particle and nuclear systems, including stars.

The program of the accelerator will be developed in all these areas. As nuclear physicists developing the proposal, it behooves us to look outwards from our own specialities to their implications for other fields and to try to look at ourselves from the outside and try to place our work in a context understandable and appreciable by others.

6. Some Subjects Which Must be Addressed

The following subjects are ones which demand to be addressed. They are presented in a connected order, not the only possible order. Other connecting themes would be of interest.

1) Quantum Chromo Dynamics - particle and nuclear physics have to be looked at in an entirely new light subsequent to discovery of the psi, and the great successes of quantum chromodynamics. This theory must provide the basic framework for the higher energy phenomena to be observed with VENUS.

2) Quark Structure of Nuclei - quarks are becoming part of the every day language even of low energy nuclear physics. We must understand the successes and limits of quark descriptions of nuclear properties and the extent to which these limits are of fundamental importance, limits of present knowledge, limits of complexity, or limits to be expected from such a model.

3) Equations of State of Nuclear Matter - much of present low-energy and high energy heavy ion physics is focused on equations of state. It will be necessary to reconsider the successes and limits of this approach, to what extent interesting nuclear phenomena are undesirable complexities, and to what extent conditions can be arranged such that an equation of state has real applications, e.g. in astrophysics.

4) Phase Transitions in Nuclei - to focus more clearly on the previous question, illustrations of known phase transitions in nuclei need to be presented with a careful thermodynamic discussion. It would be important to understand whether the macroscopic approach really has predictive power, or whether the recognition of phase transitions is a post hoc, strained analogy for phenomena better described in a microscopic way.

5) Quark Matter - this topic of wide current discussion refers to the energy regime where quarks are liberated from their parent nucleons. Intrinsically a nuclear relativistic many-body object, it needs to be defined as closely as possible, and it should be examined whether the approach of items 3 and 4 alone is the best way to address it. This item is also shorthand for other exotic objects such as pion condensate, abnormal nuclear matter, etc. which have been discussed but perhaps not always in a hard-nosed enough way.

6) Astrophysics - the melting pot of all branches of physics. What nuclear information is really needed and to what level of accuracy, if one takes into account other

uncertainties? How are predictions of conditions in the early universe limited by theory, and to what extent would some experimentation help, or confuse, the issue?

7) Nuclear Reactions - a great amount of information has been accumulated from low energy heavy ion experiments, Bevalac experiments, and high energy p-p and p-nucleus experiments, and cosmic ray experiments, all of which could help us define the relevance of experimentation to the question raised in 1-6 above. This crucial link must be described in both its strengths and its weaknesses.

7. The Next Steps

As you might guess, we believe strongly that the experimental program to be defined for VENUS will help answer some of the most interesting and difficult questions in modern physics. We will, in addition to working out the logistics of such a major project, have to articulate clearly this belief. We plan in the coming months to hold further study of these topics, and ask for any help and suggestions that you may offer. The intellectual value of such studies will be substantial, independent of whether or not LBL gets its VENUS!

8. Conclusion

I thank the organizers of this workshop for the opportunity to present this tentative framework for a proposal. The atmosphere of workshops such as this enables new connections to be made between superficially disparate areas of research. This is to some extent what VENUS is about, too.

9. References

1) 1st Workshop on Ultra-Relativistic Nuclear Collisions, May 21-24, 1979, LBL Report LBL-8957.

2) The VENUS Project, LBL Staff, June 1979, LBL Report PUB-5025.

3) A Long-Range Plan for Nuclear Science, The DOE/NSF Nuclear Science Advisory Committee, Chairman H. Feshbach, December 1979.

LOW ENERGY PIONS AND DENSITY EVOLUTION IN RELATIVISTIC NUCLEAR COLLISIONS[†]

J. Cugnon[††] and S. E. Koonin[†††]

W. K. Kellogg Radiation Laboratory, Caltech, Pasadena, CA 91125

The recent discovery of differences in the π^+ and π^- yields at $\theta_{lab} = 0°$ [1] as well as the observation of different low energy π^+ and π^- spectra in relativistic nucleus-nucleus collisions raise the possibility that such data are sensitive to the matter density distribution during the collision process. There is no way at present to extract such information from proton inclusive cross sections. In a symmetric N = Z system, π^+/π^- differences arise solely from electromagnetic forces and reflect, in principle, the properties of the charge distribution after the pion is created. We report here on some aspects of a classical calculation of these phenomena.

1. Model for the collision process. The nuclear collision is pictured as a succession of relativistic, on-shell, binary, baryon-baryon collisions. The evolution of the system is calculated by means of a Monte-Carlo method [2], which embodies the following important features: (i) relativistic kinematics, (ii) empirical elementary cross sections, (iii) pionic degrees of freedom are accounted for by allowing Δ-production, (iv) Δ's are considered stable against pion emission until the end of the collision process; they may, however, be destroyed in collisions with nucleons. This last point is a reasonable approximation given the present knowledge of the behavior of Δ resonances in nuclear matter [3].

The present model is a very successful parameter-free description of inclusive cross sections (see fig. 1) and two proton correlations at 800 MeV/A [4].

2. Matter distribution. During the collision process, our calculation reveals that the matter can be compressed substantially ($\rho \approx 2\rho_0$) and then expands rapidly. However, pions should not be sensitive to these early stages of the process. At the end of the collision process and at later times, the calculated matter (and charge) distribution of a symmetric system can be

---

[†]Supported in part by NSF grants PHY77-[illegible] and PHY[illegible].

[††]Permanent address: University of Liège, Institut de Physique, B-[illegible] Sart-Tilman, Belgium.

[†††]Alfred P. Sloan Foundation Fellow.

REACTION THEORY FOR A NONLINEAR DYNAMICS:

THE S-MATRIX TIME-DEPENDENT HARTREE-FOCK THEORY

James J. Griffin, Maria Dworzecka,
Peter C. Lichtner, and Kit-Keung Kan

Department of Physics and Astronomy
University of Maryland, College Park, Maryland 20742 U.S.A.

ABSTRACT

A single-determinantal TDHF reaction theory structurally analogous with the S-matrix Schrödinger theory is constructed. It involves time averaging in an essential way, displays the interpretatively crucial properties of asymptoticity and channel specificity, and excludes the effects of multi-channel spurious cross channel correlations.

SUMMARY

Several recent developments in the nonlinear single-determinantal (Time-Dependent Hartree-Fock) approximation to the many-body Schrödinger reaction theory are drawn together. By modelling the single-determinantal reaction theory, not upon the initial-value Schrödinger theory, but on its (entirely equivalent) S-matrix formulation, one obtains a description of complex reactions (labelled TD-S-HF) different from the initial-value TDHF theory.

Although the initial-value TDHF generates a single wave function whose behavior at late times summarizes all the effects of the collision, in fact no specific method has ever been proposed for the exhaustive physical inter-

pretation of that wave function. Perhaps this is because the solution, and therefore its statement about the internal states of the emergent fragments, continues to vary with time long after the collision because of its self-consistent nonlinear time evolution. Thus it predicts that the results of physical measurements will depend upon precisely where the distant apparatus is located.[1] One concludes immediately that in principle, the interpretative structure of the initial-value TDHF description contrasts qualitatively with that of the exact theory.

The alternative TD-α-HF formulation discussed here provides the calculation,[2] by means of a specific time average over the TDHF analog of the S-matrix reaction amplitude, of the probability for the system to make the transition to any specific one of a set of asymptotic channel states, each characterized by the internal states of two fragments and their relative motion. These asymptotic channel states are constructed upon the set of gauge invariant periodic "TDHF-Eigensolutions," which provide the nearest single-determinantal analog of the Schrödinger eigenfunctions.[3-5,9] Being periodic, they submit naturally to a time-averaged interpretation of their physical characteristics. In addition, they lead to a time-averaged orthogonality among the asymptotic channel states.[2]

The upshot is remarkable: a reaction theory for the nonlinear TDHF dynamics which is completely analogous structurally to the exact linear Schrödinger reaction theory. This theory prescribes amplitudes to a set of (presumably complete) asymptotic channel states whose (time-averaged) physical properties remain constant as the fragments move far away from the collision (asymptoticity). In addition, the (time-averaged) overlaps among these asymptotic channel states vanish, allowing a given reaction amplitude to pre-

dict specifically under the statistical interpretation of the wave functions in the theory the probability of measuring that channel's properties, rather than those of some other nonorthogonal final channel (specificity). Finally, the reaction amplitudes are, by virtue of their specific time-averaged definition, completely free of the spurious cross channel correlations[8] which arise outside the collision region whenever a single TDHF determinant is obliged to describe simultaneously more than one reaction channel.

The authors wish to acknowledge the support of the U. S. Department of Energy, and the Alexander von Humboldt Foundation.

REFERENCES

1. J. J. Griffin, P. C. Lichtner and M. Dworzecka, A.I.P. Conf. Proc. No. 47, Clustering Aspects of Nuclear Structure and Nuclear Reactions (Winnipeg, 1978), ed. by W. T. H. Van Oers, et al. (A.I.P., New York, 1978), p. 114; Nukleonika 24 (1979) 309, 343 and 359, and earlier references cited therein.
2. J. J. Griffin, P. C. Lichtner and M. Dworzecka, Phys. Rev. C21 (1980) 1351. Also, U. of Md. Tech. Rpt. No. 79-115 (ORO 5126-67) and 79-121 (ORO 5126-68).
3. K.-K. Kan, J. J. Griffin, P. C. Lichtner and M. Dworzecka, Nucl. Phys. A332 (1979) 109. See also Refs. 4 and 5 where another approach yields similar solutions, and Ref. 6 where the states are applied further.
4. S. Levit, J. Negele and Z. Paltiel, M.I.T. Report, CTP #781 and priviate communication. This reference follow the method of Refs. 7.
5. H. Reinhardt, to be published in Nucl. Phys. A. This reference follows the method of Refs. 6.
6. K.-K. Kan, P. C. Lichtner, M. Dworzecka and J. J. Griffin, Phys. Rev. C21 (1980) 1098.
7. R. Dashen, B. Hasslacher, and A. Neveu, Phys. Rev. D10 (1974) 4114, 4130, 4138; D11 (1975) 3424; D12 (1975) 2443.

8. J. J. Griffin, Proc. of the Topical Conf. on Heavy Ion Collisions (Fall Creek Falls, Tennessee, June, 1977) (O.R.N.L. Rpt. No. CONF-770602, Oak Ridge, Tennessee), p. 1; Fizika (Zagreb) 9 (1977) 415; Nukleonika (Warsaw) 24 (1979) 309, 343 and 359.

9. P. C. Lichtner, J. J. Griffin, H. Schultheis, R. Schultheis and A. B. Volkov, Phys. Rev. C20 (1979) 945; Phys. Lett. 88B (1979) 221.

FIGURE CAPTION

Fig. 1: The figure symbolizes a time-dependent solution $\Phi(\vec{x},t)$ by a line in the fragment separation-time plane. Solutions $\Phi_i^{(+)}(\vec{x},t)$ obey simple single-channel initial conditions before the collision; they exhibit multi-channel spurious cross channel correlations after their breakup (at the time T_2). Solutions $\Phi_f^{(-)}(\vec{x},t)$ are simple single-channel solutions at late times, exhibiting multi-channel spurious cross channel correlations for early times, less than T_1. The interval (T_1,T_2) therefore is the largest interval during which neither of the wave functions determining the reaction amplitude, $\bar{\cdot}_{fi}$, involves multi-channel spurious cross channel correlations.

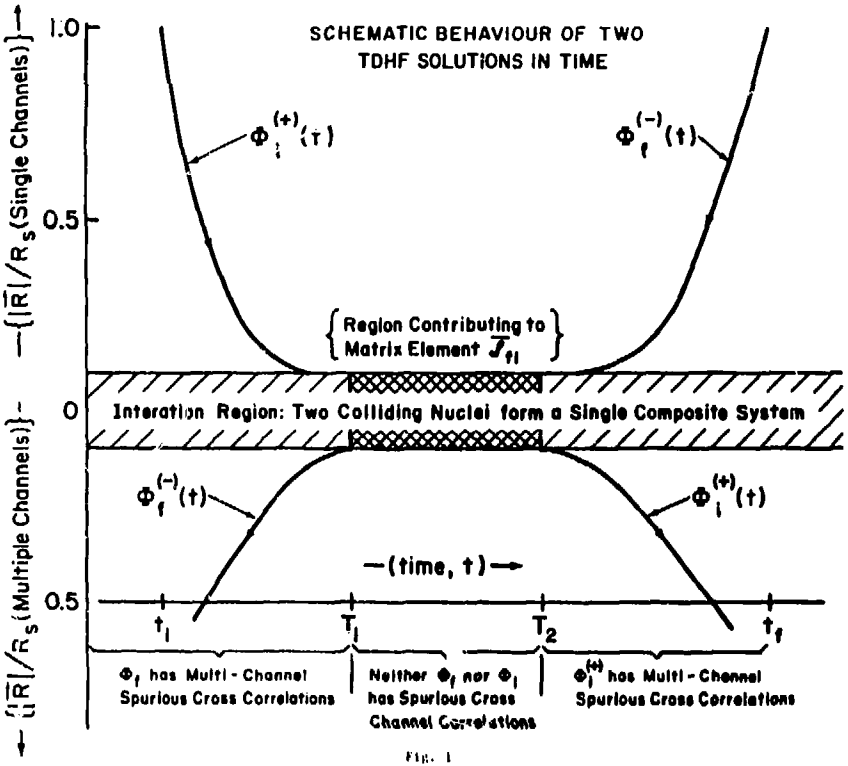
SCHEMATIC BEHAVIOUR OF TWO
TDHF SOLUTIONS IN TIME
1.0
0.5
0
0.5
$\{|\bar{R}|/R_s$ (Single Channels)$\}$
$\{|\bar{R}|/R_s$ (Multiple Channels)$\}$
$\Phi_i^{(+)}(t)$
$\Phi_f^{(-)}(t)$
Region Contributing to Matrix Element $\bar{T}_{fi}$
Interation Region: Two Colliding Nuclei form a Single Composite System
$\Phi_f^{(-)}(t)$
$\Phi_i^{(+)}(t)$
—(time, t)→
t_i
T_1
T_2
t_f
Φ_f has Multi-Channel Spurious Cross Correlations
Neither Φ_f nor Φ_i has Spurious Cross Channel Correlations
$\Phi_i^{(+)}$ has Multi-Channel Spurious Cross Correlations

FIG. 1

TIME DEPENDENT MEAN FIELD APPROXIMATION TO THE MANY-BODY S-MATRIX*

Y. Alhassid† and S. E. Koonin††
W. K. Kellogg Radiation Laboratory, Caltech, Pasadena, CA 91125

Time Dependent Hartree-Fock (TDHF) calculations are a good description of some inclusive properties of deep inelastic heavy-ion collisions. However, it has so far proven impossible to calculate specific reaction cross-sections by any TDHF-like approximation, since the TDHF wave-function at large times does not decompose into a linear combination of channel eigenstates whose coefficients have a time independent modulus.

Here we present the first steps toward a mean-field theory which approximates specific elements of the many-body S-matrix: We consider a many-body system with pairwise interactions, $v(x_i - x_j)$, excited by an external, time-dependent one-body field, $V(\tau)$. Our goal is to calculate the excitation amplitudes, $\langle\beta'|S|\beta\rangle$, where $|\beta\rangle$ and $|\beta'\rangle$ are exact (or approximate) eigenstates of the unperturbed hamiltonian. Scattering problems can be reduced to this situation in an approximation which treats the relative motion classically.

In a second-quantized notation, with the one body density operator $\rho(x) \equiv \psi^\dagger(x)\psi(x)$, the hamiltonian can be written as

$$H(t) = K + \frac{1}{2}(\rho, v\rho) + (V(t),\rho) = H_o + V(t) \quad , \qquad (1)$$

where K is the kinetic energy operator corrected by the self-energy interaction term, and $(A,B) \equiv \int dx\, A(x)\, B(x)$ for any functions A, B.

The scattering operator S is defined as the long-time limit of the interaction picture evolution operator

$$S = \lim_{t\to\infty} U^{(o)}(o,t)\, U(t,-t)\, U^{(o)}(-t,o) \quad , \qquad (2)$$

where $U^{(o)}$ evolves with H_o only, and U with H. To evaluate S we use a technique first introduced by Hubbard[1] and Stratonovich[2] in statistical mechanics and applied recently to nuclear physics by Kleinert[3] and Levit[4]. The details

---

*Supported in part by NSF grants PHY77-21602 and PHY79-23783.

†Chaim Weizmann Postdoctoral Fellow.

††Alfred P. Sloan Foundation Fellow.

can be found in these references. Loosely speaking, this technique expresses an evolution operator containing a two-body interaction as a functional integral over a time-dependent auxilliary field, $\sigma(x,\tau)$, which linearizes the quadratic form $(\rho, v\rho)$. The many-body propagator is thus expressed as a continuous superposition of one-body propagators. Upon introducing a different auxilliary field for each of the three U's in (2), we obtain

$$S = \lim_{t\to\infty} \iiint D[\sigma_i]\, D[\sigma]\, D[\sigma_f]\, \exp\left[\frac{i}{2}\oint(\sigma, v\sigma)\right] U_{\sigma_f}(0,t)\, U_{\sigma}(t,-t)\, U_{\sigma_i}(-t,0) \quad , \tag{3}$$

where

$$\oint d\tau(\sigma, v\sigma) = \int_0^{-t} d\tau(\sigma_i, v\sigma_i) + \int_{-t}^{t} d\tau(\sigma, v\sigma) + \int_t^0 d\tau(\sigma_f, v\sigma_f) \quad , \tag{4}$$

and the integration in (3) is over all possible fields with the corresponding measures D defined in Ref. [4]. In writing (3), we have neglected certain exchange terms, which can be included in a tedious but straightforward manner. For convenience, we shall frequently use the subscript $\ell = -1, 0, 1$, to denote i, no subscript, or f, respectively.

Each of the U_{σ_ℓ}'s in (3) is a one body propagator: $U_{\sigma_\ell} = T \exp[-i \int d\tau\, H_{\sigma_\ell}(\tau)]$, corresponding to the one body σ_ℓ-dependent hamiltonian:

$$H_{\sigma_\ell}(\tau) = K + (\rho, v\sigma_\ell(\tau)) + \delta_{t0}(\rho, V(t)) \quad . \tag{5}$$

The integrand of Eq. (3) can be visualized by the simple diagram shown in Fig. 1a. Evolution is represented by motion along a loop, which consists of 3 sections:

(i) The "preparation" process: the system starts at $\tau = 0$ in the lower middle and moves backward in time along the lower left hand side of the loop (to time $-t$) with the mean field σ_i and with the interaction V turned off.

(ii) The interaction process: the system evolves forward from $-t$ to t along the upper section of the loop with the field σ and the interaction V turned on.

(iii) The "analysis" process: the system moves backward from t to 0 along the lower right hand portion of the loop, with a field σ_f and the interaction V turned off.

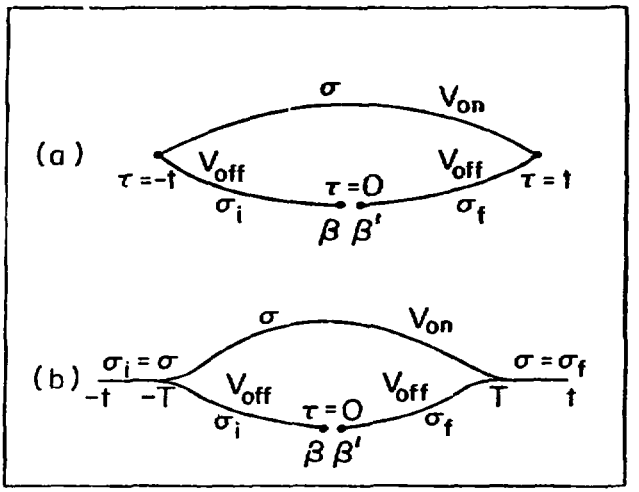

Fig. 1. (a) The loop. (b) The "collapsed" loop. $V(\tau) \neq 0$ for $|\tau| < T$, with $T < t$. (See text for details).

To find a specific matrix element of (3), we approximate the integral by the stationary phase method. There may, of course, be several stationary field configurations. Under certain reasonable approximations, the "quadratic corrections" to the integrand evaluated at each stationary point can be shown to be unity, so that each contributes to S as

$$S_{\beta'\beta} \simeq \lim_{t\to\infty} \exp\left[\frac{i}{2}\oint(\sigma, v\sigma)d\tau\right] \langle\beta'| U_{\sigma_i} U_{\sigma} U_{\sigma_f} |\beta\rangle \quad . \tag{4}$$

Here, the σ_ℓ are the stationary fields. To exhibit them explicitly, we define the wave functions $|\beta_\ell(\tau)\rangle$, $\langle\beta'_\ell(\tau)|$ along different sections of the loop by two simple rules:

(i) To find $|\beta_\ell(\tau)\rangle$ at any point τ on the loop, evolve $|\beta\rangle$ from $\tau = 0$ (in the lower portion) clockwise along the loop to the given point.

(ii) For $\langle\beta'_\ell(\tau)|$, evolve $\langle\beta'|$ counter-clockwise from $\tau = 0$.

As an example, for τ on the upper section of the loop, we have explicitly: $|\beta(\tau)\rangle = U_\sigma(\tau,-t)\, U_{\sigma_i}(-t,o)|\beta\rangle$, $\langle\beta'(\tau)| = \langle\beta'|\, U_{\sigma_f}(o,t)\, U_\sigma(t,\tau)$. Note that these wave functions have one body TDHF-like equations of motion

$$i\frac{\partial}{\partial\tau}|\beta_\ell(\tau)\rangle = H_{\sigma_\ell}(\tau)|\beta_\ell(\tau)\rangle \quad , \tag{7a}$$

$$-i\frac{\partial}{\partial\tau}\langle\beta'_\ell(\tau)| = \langle\beta_\ell'(\tau)|H_{\sigma_\ell}(\tau) \quad . \tag{7b}$$

The stationary fields can then be shown to satisfy

$$\sigma_\ell(x,\tau) = \mathrm{Re}\left[\frac{\langle\beta_\ell'(\tau)|\rho(x)|\beta_\ell(\tau)\rangle}{\langle\beta_\ell'(\tau)|\beta_\ell(\tau)\rangle}\right] \quad ; \tag{8}$$

where the denominator is independent of τ and ℓ. Eq. (8) is a self-consistent equation in the sense that both $|\beta_\ell(\tau)\rangle$ and $\langle\beta_\ell'(\tau)|$ have a complicated functional dependence upon the values of the σ's at all times. Note that Eqs. (7) would be identical with TDHF along the loop if we were to replace (8) by $\sigma_{\ell,\mathrm{TDHF}}(\tau) = \langle\beta_\ell(\tau)|\rho|\beta_\ell(\tau)\rangle/\langle\beta_\ell(\tau)|\beta_\ell(\tau)\rangle$.

The approximate amplitude (8) has the property of being independent of the time t, when t is larger than the interaction time. This is a consequence of the asymptotic behaviour of the σ fields which can be investigated from Eq. (8). At any point in space σ coincides with σ_i before the interaction starts and with σ_f after the interaction ceases, so that the evolution caused by U_σ is cancelled by U_{σ_i} for very early times and by U_{σ_f} for very late times. This can be illustrated by the "collapsed" ends of the loop as in fig. 1b. It is also interesting to note that the above mean field approximation, unlike the usual TDHF, preserves any time reversal symmetry present in the exact problem. Specifically, both the exact and approximate S-matrix ve $S_{\beta'\beta} = S_{\bar{\beta}\bar{\beta}'}$. For a T-reversal invariant situation, it can also be shown that for elastic propagation, $\beta' = \beta$, $\sigma_i(-\tau) = \sigma_f(\tau)$ and $\sigma(\tau) = \sigma(-\tau)$.

The determination of the stationary σ fields defined by (8) represents a self-consistent time dependent problem. A possible iterative scheme for its solution proceeds by alternatively evolving $\beta(\beta')$ clockwise (counter-clockwise) around the loop, using the σ fields generated from the previous wave functions. The problem is thus made equivalent to a number of TDHF-like calculations.

However, for a number of non-trivial model hamiltonians, where the relevant operators form a finite Lie algebra, the mean field equations may be reduced to a set of time local evolution equations for the group parameters. These equations must be solved self-consistently, but only with a small, finite number of iterative parameters.

To illustrate our methods we have solved two such group-theoretic hamiltonians: the forced harmonic oscillator (to be discussed elsewhere), for which the zero'th order mean-field approach yields the exact result, and the forced Lipkin model.

The Lipkin model [5] is a non-trivial many-body system: N distinguishable fermions with pair-wise interactions of strength V. Each fermion is labeled by a quantum number $p = 1,\ldots,N$ and can occupy an upper or lower single particle level with energy $\pm \frac{\mathcal{E}}{2}$. By defining total quasi-spin operators $\vec{J} \equiv \sum_p \vec{j}^{(p)}$, which satisfy an SU(2) algebra, the hamiltonian can be written as

$$H_o = \mathcal{E} J_z + V(J_x^2 - J_y^2) \quad . \tag{9}$$

We take the time dependent perturbation to have the general form: $V(t) = f_x(t)J_x + f_y(t)J_y + f_z(t)J_z$.

To construct the mean field approximation to the S-matrix, we introduce an auxilliary field $\sigma^{(p)}_{x,y}$ for each one body operator $j^{(p)}_{x,y}$ appearing in the two-body term of H_o. The stationary field equations are then

$$\sigma^{(p)}_{\ell\, x,y}(\tau) = \mathrm{Re}\left[\frac{\langle \beta_\ell{}'(\tau)|\, j^{(p)}_{x,y}\, |\beta_\ell(\tau)\rangle}{\langle \beta_\ell{}'(\tau)|\beta_\ell(\tau)\rangle}\right] \tag{10}$$

where $|\beta_\ell(\tau)\rangle$, $\langle\beta_\ell{}'(\tau)|$ evolve with the mean-field hamiltonian

$$H_{\sigma_\ell} = \sum_p \left[\mathcal{E} j^{(p)}_z + \delta_{\ell o}\vec{f}\cdot\vec{j}^{(p)} + 2V \sum_{p'\neq p} \sigma_{\ell x}{}^{(p')} j^{(p)}_x - \sigma_{\ell y}{}^{(p')} j^{(p)}_y\right] \tag{11}$$

Since any of the H_{σ_ℓ} generates the SU(2) algebra, the evolution to any point along the loop can be parametrized by three parameters describing a rotation in quasi-spin space. These group parameters satisfy σ-dependent equation of motion. However, the SU(2) algebra can be used to express σ in terms of the instantaneous group parameters and the $\sigma^{(p)}_{ix,y}(\sigma)$ via (10). We then

obtain equations of motion solely for the group parameters which have to be solved self-consistently with only a few iterative parameters. The solutions of these equations determine the stationary configuration.

For β,β' we can either choose exact eigenstates of H_o, or the ground HF state $|0\rangle_{HF}$ (which corresponds for $\chi = \frac{(N-1)V}{\mathcal{E}} < 1$ to all particles in the lower level).

The results for the ground state transition $0_{HF} \cdot 0_{HF}$ are shown in fig. 2 for $(f_x, f_y, f_z) = \exp(-t^2\mathcal{E}^2/\hbar^2)(1,1,1)$.

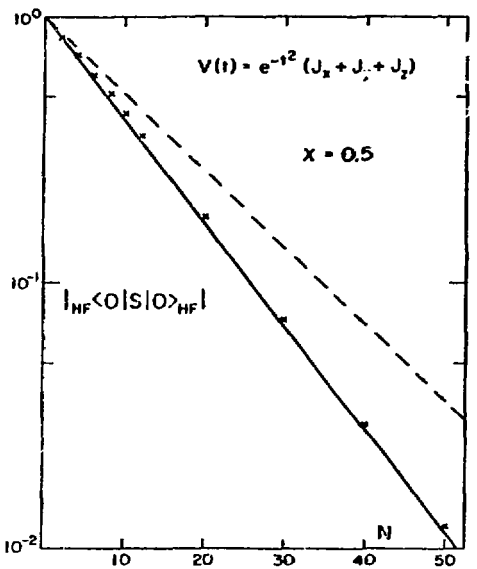

Fig. 2. The modulus of elastic amplitude $|_{HF}\langle 0|S|0\rangle_{HF}|$ vs. the number of fermions (N) in the forced Lipkin model: exact (x), ordinary TDHF along the loop (dashed line) and zero'th order mean field approximation (continuous line).

Since our primary interest in this paper is testing the mean-field approximation to the S-matrix, and not the HF approximation for the initial and final states we are comparing in fig. 2 the mean field approximation to $_{HF}\langle 0|S|0\rangle_{HF}$ with the exact $_{HF}\langle 0|S|0\rangle_{HF}$ rather than with the exact $\langle 0|S|0\rangle$.

Fig. 3 compares the exact excitation amplitudes $\langle n|S|0\rangle$ for the transition between the exact ground and n'th excited states with the mean field approximation for N = 30 and the same parameters. Both figures correspond to the weak-coupling regime $|\chi| < 1$. The strong-coupling limit is now being investigated.

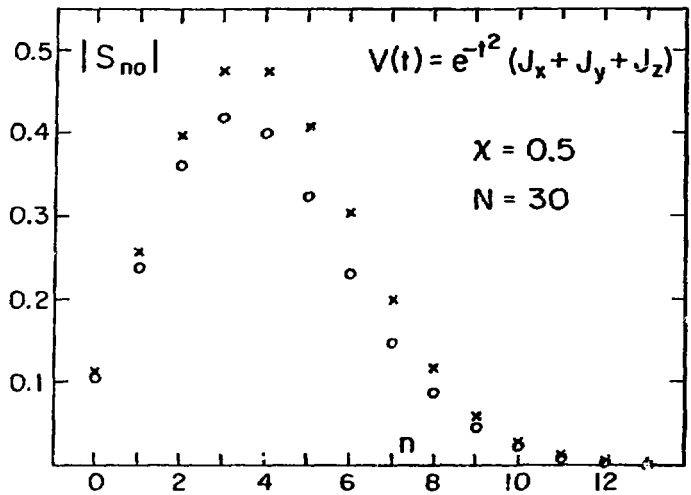

Fig. 3. The moduli of the excitation amplitudes $|\langle n|S|0\rangle|$ in the forced Lipkin model: exact (x) and mean field approximation (o).

Although the Lipkin model is certainly schematic, the good agreement exemplified by figs. 2 and 3 encourages the application of these techniques to more realistic situations. Specifically, we are currently considering atomic or nuclear reactions in which the relative matrix is treated semi-classically and the intrinsic degrees of freedom via the mean-field method. A scheme can also be formulated to allow for the effects of intrinsic excitation on the relative motion. It should therefore be possible to perform microscopic, non-perturbative calculations of elastic, inelastic, and transfer reactions.

REFERENCES

1. J. Hubbard, Phys. Lett. 3, 77 (1963).
2. R. L. Stratonovich, Soviet Phys. Doklady 2, 416 (1958).
3. H. Kleinert and H. Reinhardt, Nucl. Phys. A332, 331 (1979).
4. S. Levit, MIT Preprint CTP #780, submitted to Phys. Rev. C.; S. Levit, J. W. Negele and Z. Paltiel, MIT Preprint CTP #781, submitted to Phys. Rev. C.
5. H. J. Lipkin, N. Meshkov and A. J. Glick, Nucl. Phys. 62, 188, 199, 211 (1965); D. Agassi, H. J. Lipkin and N. Meshkov, Nucl. Phys. 86, 321 (1966).

GIANT COLLECTIVE VIBRATIONS AS TDHF EIGENSOLUTIONS†

M. Dworzecka, K.-K. Kan and J. J. Griffin

Department of Physics and Astronomy
University of Maryland, College Park, Maryland 20742 U.S.A.

It has recently been shown[1] that the TDHF variational principle prescribes a unique TDHF "Hamiltonian," $\mathcal{H}_C$ (including a specific additive, space-independent function of time), and that the corresponding TDHF solution for any specified initial value determinant is uniquely prescribed (including its time-dependent phase) by the resulting TDHF equation. For any TDHF Hamiltonian, $\mathcal{H}$, satisfying the familiar variational conditions, this variationally true "Constant-$<\mathcal{H}>$" Hamiltonian is given by

$$\mathcal{H}_C = \mathcal{H} + \langle\Phi|H - \mathcal{H}|\Phi\rangle, \tag{1}$$

where H is the exact Hamiltonian and Φ is the solution of $\mathcal{H}$.

Among such solutions we seek[2] as the TDHF analogs of the Schrödinger stationary eigenstates phase quasi-periodic solutions which exhibit, under the gauge transformation

$$H \to H + \beta(t), \tag{2}$$

the same transformation properties as the exact Schrödinger solutions. Thus we impose upon the TDHF "eigensolutions" the structural form of the time-dependent Schrödinger eigensolutions, as follows:

$$\Phi_C(\underline{\chi},t) = \Phi_G(\underline{\chi},t)\exp\{-i\langle H\rangle t/\hbar\}. \tag{3}$$

With such a choice of phase, Φ_G in (3) must obey the equation

$$[\mathcal{H} - \langle\mathcal{H}\rangle]\Phi_G = i\hbar\dot{\Phi}_G \tag{4}$$

and Φ_G is guaranteed to be completely unaffected by any gauge transofrmation. Then the periodic solutions of Eq. (4) exhibit the same gauge transformation properties as the Schrödinger eigenstates and can be used to construct a TDHF solution, Φ_C, of the form (3) which is guaranteed to have the gauge transformation properties of the exact time-dependent eigensolution.

Furthermore, whenever $\mathcal{H}$ exhibits a set of periodic solutions, Φ_P, continuous in energy, then the corresponding solutions of (4)

$$\Phi_G(\underline{\chi},t) = \Phi_P(\underline{\chi},t)\exp\{\tfrac{i}{\hbar}\int_{t_0}^{t}\langle\mathcal{H}(t')\rangle dt'\} \tag{5}$$

will be periodic if, and only if, the second factor is periodic with the same period as Φ_P. This requires

$$\int_{t_0}^{t_0+T}\langle\mathcal{H}(t')\rangle dt' = 2n\pi\hbar, \qquad (n, \text{integer}) \tag{6}$$

where T is the period of Φ_P. Thus, the condition (6) selects from the continuous periodic spectrum of $\mathcal{H}$ a discrete spectrum of Gauge Invariant Periodic solutions. (As discussed in Ref. 2, (6) can be recast into the Bohr-Sommerfeld form.) Note

that the resulting TDHF "eigensolutions" (3) have two distinct frequencies; one associated with the energy and the other specifying the period of the matter density oscillations described by Φ_G.

Here we apply the Gauge Invariant Periodic Eigensolutions to collective vibrations of ^{16}O. In the parametrized TDHF calculations we use the Skyrme force which leads to the Hamiltonian density of Brink.[3] The determinantal wave function Φ_P is constructed of single particle wave functions in polar form,[4] which are assumed to depend on time only through two time-dependent parameters, $\alpha(t)$ and $\gamma(t)$, as follows:

$$\psi_i(\alpha,\gamma) = u_i(\alpha)\, e^{-i\frac{m}{\hbar}\gamma S(\alpha)} . \tag{7}$$

Here $u_i(\alpha)$ is the harmonic oscillator eigenfunction in the potential dependent on the parameter α, and $S(\alpha)$ (the same for all i) is the velocity field[4] appropriate for the collective oscillations of interest. The restricted TDHF equations of motion for Φ_P are then obtained from the action-integral variational principle,[1] as follows:[2]

$$B\dot{\alpha} = \frac{\partial E}{\partial \gamma}; \qquad B\dot{\gamma} = -\frac{\partial E}{\partial \alpha} \tag{10a,b}$$

where $E(\alpha,\gamma) = \langle\Phi_P|H|\Phi_P\rangle$ and

$$B = 2\hbar\, \mathrm{Im}\left\langle \frac{\partial\Phi_P}{\partial\alpha} \middle| \frac{\partial\Phi_P}{\partial\gamma} \right\rangle . \tag{11}$$

It is always possible to choose γ in ($\dot{}$) to be equal to $\dot{\alpha}$ with the result[5]

$$B = m\int \rho(\nabla S)^2 d\tau . \tag{12}$$

We recast (10) into a canonical form[2] by selecting the collective coordinate and momentum to be, respectively,

$$q = \alpha; \text{ and } p = B\gamma = B\dot{\alpha}. \tag{13}$$

The equations (10) possess a continuous spectrum of periodic solutions.[2] The Gauge Invariance condition (6) then selects the discrete set of periodic solutions which provide the proper analogs of Schrödinger eigenstates.

The calculations were performed separately for giant monopole and quadrupole vibrations of ^{16}O. For the monopoles the collective coordinate q was chosen to be the oscillator scale parameter, b, and for the quadrupoles the deformation parameter β. Then the respective velocity fields are given by

$$S_M = r^2/2b; \text{ and } S_Q = r^{21/20}(\Omega)/12\beta \tag{14}$$

are proportional to those of Blocki, et al.[6] Figure 1 presents the results of the calculations using SKI and the discussion of them (see caption). For other forces and nuclei see Ref. 5.

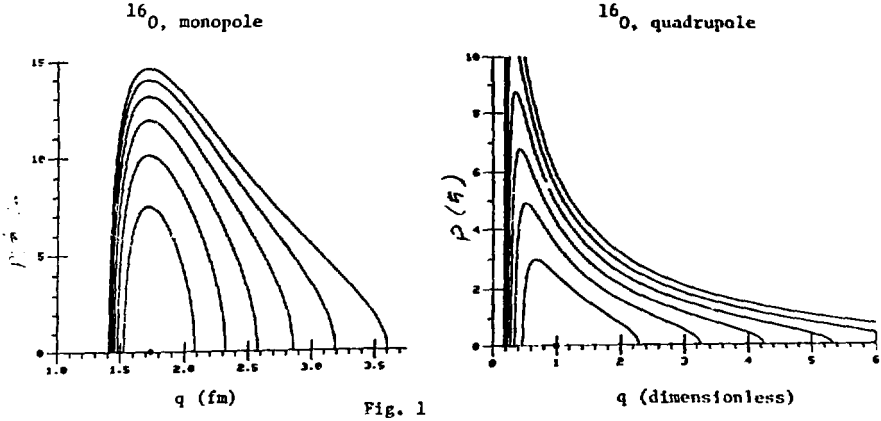

Fig. 1

States	Energy E (MeV)	Period T (fm/C)	ΔE (MeV)	2πℏ/T (MeV)
0	-129.4	0		----
			32.6	
1	-96.8	39.8		31.1
			27.1	
2	-69.7	48.1		25.8
			22.2	
3	-47.5	59.3		20.9
			17.7	
4	-29.8	75.0		16.5
			13.7	
5	-16.1	98.2		12.6
			10.3	
6	-5.8	135.5		9.1

States	Energy E (MeV)	Period T (fm/C)	ΔE (MeV)	2πℏ/T (MeV)
0	-129.4	0		----
			21.5	
1	-107.9	56.7		21.9
			21.1	
2	-86.8	58.1		21.3
			20.6	
3	-66.2	59.4		20.9
			20.3	
4	-45.9	60.7		20.4
			20.0	
5	-25.9	61.8		20.0
			19.7	
6	-6.2	62.8		19.7

Fig. 1: Gauge Invariant Periodic trajectories in phase space for monopole and quadrupole vibrations of ^{16}O. Note that the energies are unequally spaced, the more so in the monopole case, so the spectrum is anharmonic. Also the period, T, of the wave function, Φ_G, of Eq. (4) is state dependent. The tables also provide a comparison of the energy differences, ΔE, of neighboring states and the quantities 2πℏ/T, which exhibit remarkable similarity with the energy differences. Again the monopole deviations exceed those of quadrupole.

REFERENCES

†Work supported by the U. S. Department of Energy.

1. P. C. Lichtner, J. J. Griffin, H. Schultheis, R. Schultheis and A. B. Volkov, U. of Md. tech. rpt. #79-010 (ORO 5126-49); Phys. Rev. C20 (1979) 845.
2. K.-K. Kan, J. J. Griffin, P. C. Lichtner and M. Dworzecka, U. of Md. tech. rpt. #79-113 (ORO 5126-71), Nucl. Phys. A332 (1979) 109.
3. Y. M. Engel, D. M. Brink, K. Goeke, S. J. Krieger and D. Vauthein, Nucle. Phys. A249 (1975) 215.
4. K.-K. Kan and J. J. Griffin, Phys. Rev. 15 (1977) 1126.
5. M. Dworzecka, K.-K. Kan and J. J. Griffin, to be published.
6. J. S. K. Andersen, J. Blocki and A. S. Jensen, to be published.

MEASUREMENT OF THE NON-FUSION YIELD IN $^{16}O + ^{16}O$ AT E_{cm} = 34 MeV

A.Lazzarini, H.Doubre[+], K.Lesko, V.Metag[++], A.Seamster, and R.Vandenbosch
Nuclear Physics Laboratory, University of Washington
Seattle, Washington 98195 USA

Time dependent Hartree-Fock calculations[1,2] indicate that at sufficiently high bombarding energies collisions between two heavy ions for small impact paramters do not lead to compound nucleus formation, but rather proceed to deeply inelastic scattering with a total kinetic energy in the final state characteristic of the Coulomb barrier for the two nulcei. At E_{cm}=34 MeV Koonin and Flanders have calculated that for the $^{16}O+^{16}O$ system the partial waves L=0-6 do not lead to fusion. We have performed an experiment to measure the cross section for the $^{16}O(^{16}O,^{16}O^{*})^{16}O^{*}$ reaction to determine whether the predictions of TDHF calculations are, in fact, borne out.

Particle-particle coincidences were measured using two position sensitive gas ΔE-solid state E telescopes. In this manner, the final state was determined in a kinematically complete measurement. Angular distributions were measured for the inelastic yield from θ_{lab}=10°-40°.

Figure 1 presents energy spectra for one reaction partner of the $^{16}O+^{16}O$ coincidences. Because of the kinematic coincidence requirement the spectra contain limits in the reaction Q-values which could be measured. These are denoted by the diagonally hashed marks in each of the spectra. A broad inelastic bump which shifts with angle is apparent in the spectra. An enhancement of the inelastic yield in the region -22<Q<-20 MeV which was predicted by the TDHF calculations and which arises from the non-fusion of the inner partial waves is not observed here. Figure 2 shows the Wilczynski plot for this system. The dashed curve bounding the upper part of the contours represents the kinematic coincidence window. The entrance channel center of mass energy is marked by the dotted line. The $^{16}O+^{16}O$ Coulomb barrier is indicated by the dashed line labelled V_C. Several features are immediately obvious: 1)The inelastic cross section for this reaction peaks at θ_{cm}=90°. The symmetry about 90° is imposed by the identical boson entrance channel. 2) A peak in the inelastic yield occurs for Q=-14 MeV. Even though the coincidence window closes rapidly for more positive Q-values, it is clear that the maximum cross section for Q>-14 MeV becomes significantly less than for Q=-14 MeV.

Although the data are not in quantitative agreement with the theoretical predictions, they are qualitatively consistent. The agreement would be considerably improved if one assumed that the collison is not yet fully damped for the partial wave L=6. We note that the direction of this disagreement is opposite to that which has been reported in heavier systems where TDHF calculations have underpredicted the degree of damping[3,4]. The TDHF trajectory for the non-fusing partial waves L=0,2,4,6 is marked by the symbols 'x' in Figure 2 (L=0 is at θ_{cm}=0° and L=6 is at θ_{cm}=87°). The increase of the inelastic yield towards θ_{cm}=90° is consistent with the fact that the partial wave L=6, which is predicted to scatter to θ_{cm}=87° carries

$^{16}O(^{16}O,^{16}O')^{16}O'$

E_{CM}=34 MeV

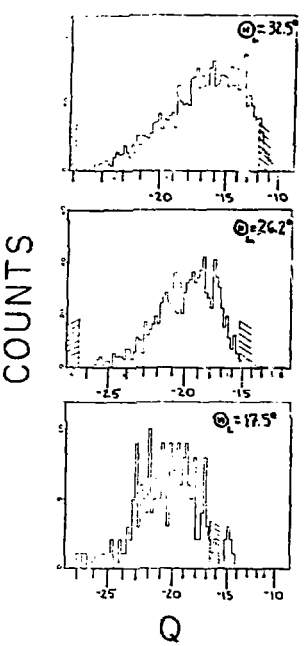

1.

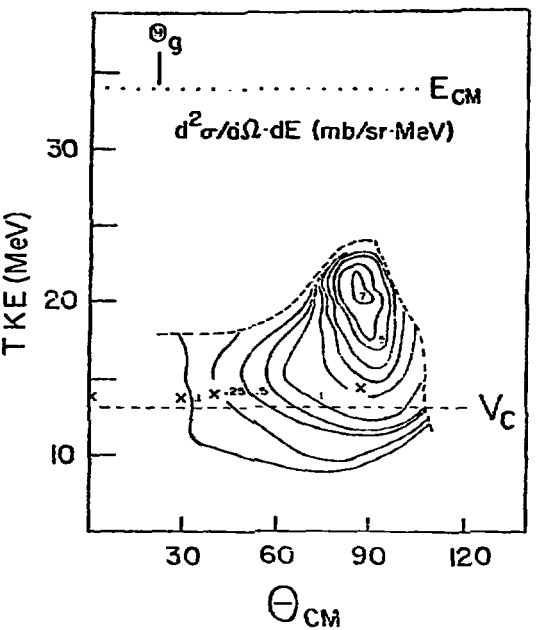

2.

the bulk of the deeply inelastic, non-fusing cross section. Assuming as usual a direct relationship for deep inelastic scattering between reaction Q-value and partialwave, L, the fact that we see a drop in the inelastic yield for Q>-14 MeV implies that the partial waves L>6 are proceeding to fusion.

The magnitude of the effect is in agreement with the TDHF predictions. σ_{TDHF}=132 mb for L=0-6, and we observe an experimental cross section, σ_{exp}=200±50 mb. As a reference, the expected total reaction cross section is σ_R=1450 mb and the measured fusion-evaporation cross section is σ_F=1100 mb[5]. The peaking of the inelastic cross section at θ_{cm}=90° is a novel result when one considers that for this light system the grazing angle is θ_g=20°. The angular dependence we observe is inconsistent with an interpretation that the deep inelastic yield arises from partial waves beyond the fusion limit L=20.

- - - - - - - - - - -

+ Present address: Institut de Physique Nulceaire, B.P. N° 1, Orsay 91406 France

++ On leave from: Max Planck Institut für Kernphysik, D-6900 Heidelberg, P.O. Box 103980, West Germany

- - - - - - - - - - -

1 H.Flocard,S.E.Koonin,and M.S.Weiss,Phys.Rev.C17(1978)1682

2 S.E. Koonin, B. Flanders, private communication.

3 R. Vandenbosch,M.P.Webb,P.Dyer,R.J.Puigh,R.Weisfeld,T.D.Thomas, and M.S.Zisman, Phys.Rev C12(1978)1672

4 K.T.R. Davies,K.R. Sandhya Devi, and M.R. Strayer, Phys.Rev C20(1979)1372

5 B.Fernandez,C. Gaarde,J.S. Larsen,S. Pontoppidan, and F. Videbaek, Nucl. Phys. A315(1978)445

ONE-SIDED FLUX OF FERMIONS*

H. Feldmeier

Institut für Kernphysik, Technische Hochschule Darmstadt

In the one-body window-friction picture for inelastic heavy-ion collisions the one-sided flux of nucleons passing the window in the mean potential plays the role of the frictional form factor.[1] In this contribution we would like to define a quantum mechanical operator for the one-sided flux. Its expectation value calculated with any given many-body wavefunction will yield the number of particles crossing an area element $d\vec{a}$ per time unit in one direction.

Starting out with the regular probability current density in momentum representation

$$\vec{j}(\vec{x}) = \frac{\hbar}{m}\frac{1}{(2\pi)^3}\int d^3k\, d^3k' \,|\vec{k}\rangle \frac{\vec{k}+\vec{k}'}{2} e^{-i(\vec{k}-\vec{k}')\vec{x}} \langle\vec{k}'| \qquad (1)$$

we split up the area of integration into two parts. For a given area element $d\vec{a}$ we have a hemisphere with $(\vec{k}+\vec{k}')d\vec{a}$ greater zero and one smaller zero. The one-sided differential flux through the area element $d\vec{a}$ is defined by integrating only over one hemisphere

$$\vec{j}_+(\vec{x})d\vec{a} = \frac{\hbar}{m}\frac{1}{(2\pi)^3}\int_{(\vec{k}+\vec{k}')d\vec{a}>0} d^3k\, d^3k' \,|\vec{k}\rangle\left(\frac{\vec{k}+\vec{k}'}{2}d\vec{a}\right) e^{-i(\vec{k}-\vec{k}')\vec{x}} \langle\vec{k}'| \qquad (2)$$

The definition of $\vec{j}_+$ only makes sense in conjunction with the area $d\vec{a}$ which determines a direction in space. Integration over the desired area (window) yields the global one-sided flux or the number of particles per time unit crossing the window in a given direction. As can be seen from eq. (2) the operator is hermitean and the two one-sided currents add up to the total current density.

$$\vec{j}_+(\vec{x}) + \vec{j}_-(\vec{x}) = \vec{j}(\vec{x})$$

The matrix elements in coordinate representation are given by

$$\langle\psi|\vec{j}_+(\vec{x})d\vec{a}\,|\psi\rangle = \frac{1}{2}\frac{\hbar}{2mi}\left\{\phi^*(\vec{x})\vec{\nabla}\psi(\vec{x}) - \vec{\nabla}\phi^*(\vec{x})\,\psi(\vec{x})\right\}d\vec{a}$$

$$-\frac{\hbar}{m}\frac{1}{2\pi}\int\frac{\phi^*(\vec{x}-\vec{\xi}/2)\,\psi(\vec{x}+\vec{\xi}/2) - \phi^*(\vec{x})\,\psi(\vec{x})}{\xi^2}\vec{\xi}\,d\vec{a} \qquad (3)$$

where ϕ and ψ are single-particle wavefunctions. The first term is half of the regular differential flux, whereas the second term contains a principal value integral and is nonlocal.

*Work supported by Bundesminister fur Forschung und Technologie.

Starting from the definition (2) it turns out that the expectation value of the one-sided flux can be written as

$$\left\langle \vec{J}_+(\vec{x})\, d\vec{a} \right\rangle = \frac{\hbar}{m} \int_{\vec{k}\, d\vec{a} > 0} d^3k\ \vec{k}\, d\vec{a}\ f(\vec{x}, \vec{k}) \tag{4}$$

where $f(\vec{x},\vec{k})$ is the Wigner transform of the one-body density matrix $\rho(\vec{r},\vec{r}')$

$$f(\vec{x},\vec{k}) = \frac{1}{(2\pi)^3} \int d^3s\ e^{-i\vec{k}\vec{s}}\ \rho(\vec{x}+\vec{s}/2, \vec{x}-\vec{s}/2) \tag{5}$$

The classical definition of the one-sided flux is just the right hand side of eq. (4) where $f(\vec{x},\vec{k})$ would then be the classical phase space distribution. Since the two correspond to each other the quantum and the classical one-sided flux are the same. The nature of the fermions only enters through the shape of the phase space distribution. This well known feature is inherent to all one-body operators. The figure gives an illustration of the quantum one-sided flux compared to the classical one calculated with a uniform momentum distribution up to the Fermi momentum. The wavefunction was taken from a model calculation for a fermion-gas in a one-dimensional box.[2]

1) J. Blocki, Y. Boneh, J. R. Nix, J. Randrup, M. Robel, A. J. Sierk. and W. J. Swiatecki; Ann. Phys. (N.Y.) 113, 330 (1978).

2) H. Feldmeier, P. Buck: A model calculation for mass dispersion in a fermion gas; these Proceedings.

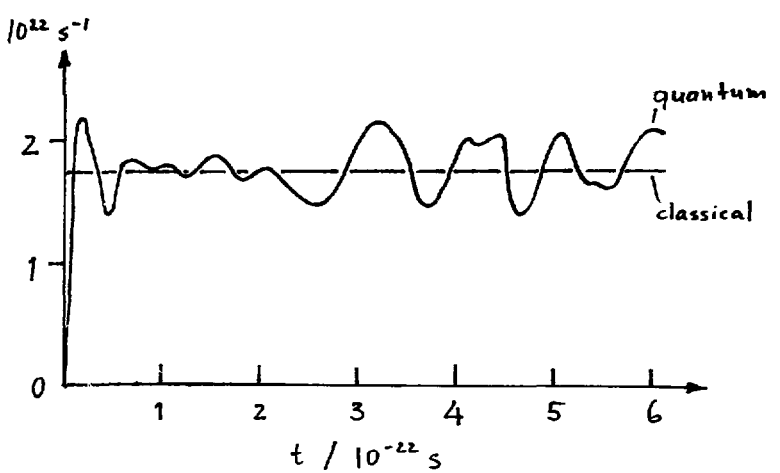

A MODEL CALCULATION FOR MASS DISPERSION IN A FERMION GAS[+]

H.Feldmeier and P.Buck
Institut für Kernphysik, Technische Hochschule Darmstadt, FRG

To gain better understanding of the mass distribution in heavy ion collisions[1,2,3] we solve numerically the time dependent many body Schrödinger equation for a fermion system. The results are compared with different approximations.

The model consists of an infinite square well potential which contains $A=n_1+n_2$ identical fermions. For simplicity we treat only one dimension. The particles interact via a finite-range two-body interaction which can be varied in shape and strength. Initially a wall (strong delta-function) separates the container in two parts with sharp number of particles n_1, n_2 on each side. We start at time t=0 with an eigenstate of the separated system and remove the wall. The wavefunction evolves in time according the Hamiltonian H

$$H = \sum_{i=1}^{A} \left\{ \frac{p_i^2}{2m} + V_{\text{container}}(x_i) \right\} + \sum_{i<j} V_{12}(|x_i - x_j|)$$

and describes the exchange of particles between the two sides. Due to the single particle motion and the two-body collisions the system heats up and reaches an equilibrated situation.

An interesting question would also be to specify what is meant by heating and equilibration for such a system where we know the exact many-body wavefunction and hence the statistical operator represents a pure state with the entropy being zero.

In this contribution, however, we'd like to concentrate on one macroscopic variable, namely the number of particles n_1 on one

[+]Work supported by Bundesminister für Forschung und Technologie.

side of the container. The according operator is given by

$$\mathcal{N} = \sum_{ij} \omega_{ij}\, a_i^+ a_j \quad ; \quad \omega_{ij} = \int \varphi_i^*(x)\, \theta(x)\, \varphi_j(x)\, dx$$

The mean value and the variance

$$\langle \mathcal{N} \rangle = \langle \Psi(t) | \mathcal{N} | \Psi(t) \rangle \; ; \; \sigma^2 = \langle \Psi(t) | \mathcal{N}^2 | \Psi(t) \rangle - \langle \mathcal{N} \rangle^2$$

are calculated with the many body wavefunction $\Psi(t)$ which is the solution of the time-dependent Schrödinger equation. $\Psi(t)$ consists of a superposition of many Slater-determinants Φ_ν.

$$\Psi(t) = \sum_\nu C_\nu(t)\, \Phi_\nu$$

A typical result of the calculation is given in fig. 1. The spread σ^2 is plotted versus time for a system with totally 16 fermions, 8 on each side. The upper-most curve shows σ^2 for distinguishable (classical) particles,[3] where the transition probability for switching sides is given by the mean one-sided current of a fermi gas.[7] The other two curves are the exact results for fermions with an attractive and without any two-body interaction. The latter one corresponds to the TDHF case if one regards the container as the selfconsistent mean potential. Inclusion of the two body interaction almost doubles the mass spread compared with the interaction free fermi gas.

This effect is due to the fact that for an attractive residual interaction the particles sometimes form pairs and thus increase the mass spread. For a residual interaction which is in this respect more realistic the variance is shown in fig. 2. The interaction has a repulsive core and an attractive tail. The mass spread is almost the same as for the not interacting fermi gas.

This is an indication that also a mean field theory including explicitly the two-body collisions will not be able to reproduce the mass spread in heavy ion collisions which is much larger than the exact σ^2 in our model. The reason for this is that the model contains one mean single-particle potential which is, however, also inherent in the TDHF approach. To move a particle from one side to the other one needs energy since the particle can occupy only a level above the Fermi edge. A state with a large particle excess on one side has thus a high energy and becomes unprobable, which in turn keeps the mass spread narrow. It seems that in heavy ion collisions the different channels with different mass numbers develop different mean potentials which accomodate the corresponding larger or smaller number of particles in larger or smaller volumes, where each mean potential can have about the same Fermi energy.

In extended TDHF prescriptions[4,5,6] equations are derived for the non-idempotent one-body density-matrix $\rho^{(1)}_{\alpha\beta}$
To calculate the expectation value of a two-body operator like $\mathcal{N}^2$ the two-body density-matrix is sometimes approximated by

$$\rho^{(2)}_{\alpha\beta\gamma\delta} \approx \rho^{(1)}_{\alpha\gamma}\,\rho^{(1)}_{\beta\delta} - \rho^{(1)}_{\alpha\delta}\,\rho^{(1)}_{\gamma\beta}$$

The validity of this approximation (for a single Slater determinant it is exact) can be judged from the results in fig. 3. Here we first deduce from the exact wavefunction the one-body density $\rho^{(1)}_{\alpha\beta}$ and than calculate with the above approximation the mass spread denoted by σ^2_a. The lower two curves show the comparison if the initial state is the groundstate. The approximated σ^2_a is in this case somewhat larger than the exact σ^2. If we start with the seventh excited state the situation has changed and σ^2_a is much too large. In heavy ion collisions one does not expect to be close to a single Slater determinant and thus the above made approximation is

doubtful. J. Randrup[1] has studied the effect of the Pauli principle on the mass diffusion coefficient D. The result was that D (for our example $F_A=0$, $\omega=0$) is given by

$$D = \tau N'(\varepsilon) \qquad \text{whereas classically} \qquad D_{cl} = N(\varepsilon_F) .$$

$N(\varepsilon)$ is the conbribution to the one-sided flux of particles with energies up to ε. Since $N(\varepsilon) \sim \varepsilon^2$ one gets $N'(\varepsilon) = \frac{2}{\varepsilon} N(\varepsilon)$ and hence

$$D = \frac{2\tau}{\varepsilon_F} D_{cl}$$

In the initial part for small times both the classical mass spread and the exact mass spread behave like

$$\sigma^2 = 2 D t$$

From fig. 2 one gets the ratio of the slopes as $D/D_{cl} = .43$. On the other hand we determined from the calculated mean occupation numbers (not shown here) $\tau \approx 15$ MeV and $\varepsilon_F \approx 70$ MeV. Thus we get $\frac{2\tau}{\varepsilon_F} \approx .43$. With the uncertainties of the fitting procedures this confirms that only the particles in a region around the fermi edge contribute to the diffusion.

1) J. Randrup; Nucl. Phys. A307, 319 (1978) and Nucl. Phys. A327, 490 (1979)

2) C.M. Ko, G.F. Bertsch, D. Cha; Phys. Letters [illegible], 1[illegible] (1978) G. Bertsch, J. Borysowicz; Phys. Rev. C19, 533 (1979)

3) F. Beck, M. Dworzecka, H. Feldmeier; Z. Phys. A289, 113 (1[illegible]

4) C.Y. Wong, H.H.K. Tang; Phys. Rev. Lett. 40, 1070 (1978)

5) H.S. Köhler; Proceedings of the International Workshop on Gross Properties of Nuclei and Nuclear Excitations VIII (1980) p. 39

6) S. Ayik; Proceedings of the International Workshop on Gross Properties of Nuclei and Nuclear Excitations VIII (1980) p. 43

7) H. Feldmeier, these Proceedings.

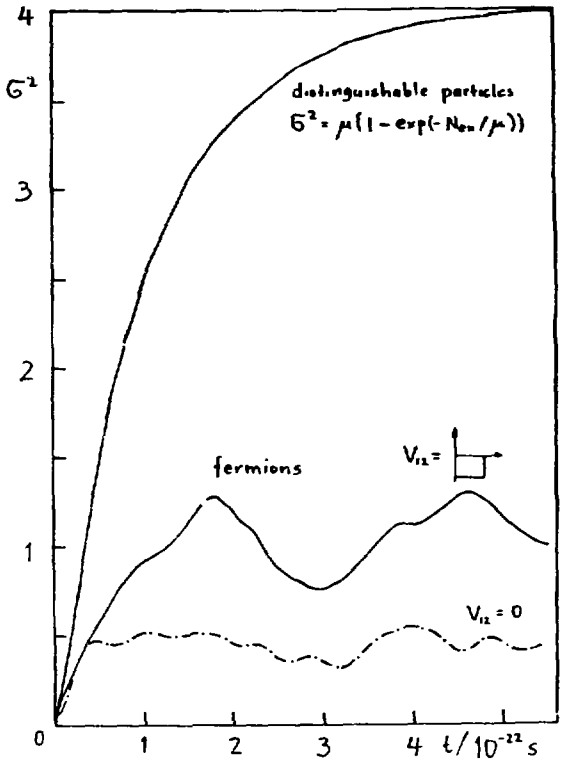

Fig.1: Mass spread for fermions and classical particles in a box of 2 times 15 fm length. Full line: attractive two-body interaction with strength V_0=30 MeV and range 5 fm. Dash dotted line: interaction free fermi gas.

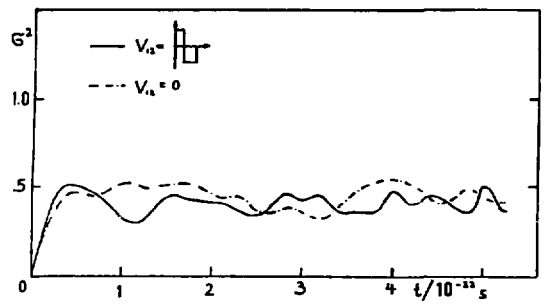

Fig.2: Same as fig. 1 but a different two-body interaction V_1=45 MeV, V_2=-30 MeV, R_1=2 fm, R_2=5 fm.

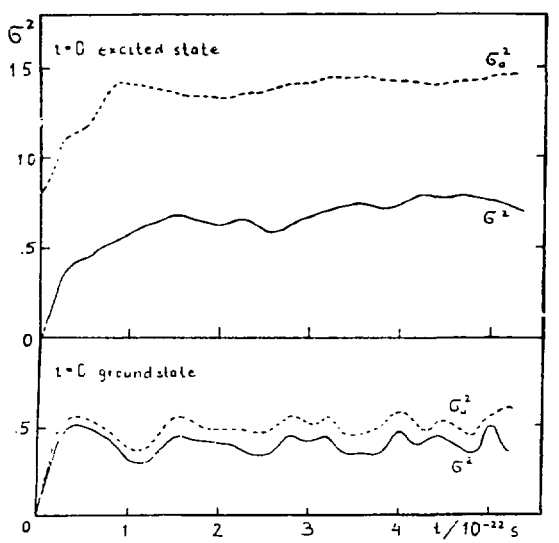

Fig.3: Comparison of the exact σ^2 with an approximated σ_a^2 (dashed line) calculated with the one-body density-matrix.

A DYNAMICAL SIMULATION OF HEAVY-ION COLLISIONS

G. J. Mathews[†]
W. K. Kellogg Radiation Laboratory, Caltech, Pasadena, CA 91125

J. Randrup and L. G. Moretto
Lawrence Berkeley Laboratory, University of California, Berkeley, CA 94720

Many models are currently available for the description of heavy-ion collisions at energies near a few MeV per nucleon. Most of these models rely on what we would call a mean trajectory approximation, i.e., the assumption that at least some of the macroscopic degrees of freedom can be described by deterministic classical equations of motion while perhaps only one or two macroscopic variables are allowed to evolve along this mean trajectory according to transport theory. We would like to begin by pointing out two dangers associated with this approach. One is that if fluctuations along the mean trajectory are large, then the true ensemble of trajectories which characterize the system may deviate significantly from the mean trajectory, leading to a breakdown of the mean-trajectory approximation. A second note of caution is that, at least to some extent, the fluctuations in the macroscopic variables are due to the same microscopic source, namely the random exchange of nucleons between the collision partners. Therefore, fluctuations in one variable are unavoidably coupled with fluctuations in the remaining collective coordinates.

We discuss here an application of transport theory which avoids the above mentioned difficulties by utilizing the method of direct dynamical simulation. That is, nucleon exchange is allowed to occur randomly and discretely according to a time-integrated probability function. The stochastic evolution of the system is then obtained by following a large number of such collisions. The method is quite general and independent of any previous assumptions regarding which aspects of the system one wishes to study. Statistics concerning a collision are obtained in a form quite similar to experimental data and can be analyzed for the features of interest.

The essential ingredients in the dynamical simulation approach are a model of the nucleon exchange transition probabilities and a model for the per-

[†]Supported in part by NSF grant PHY79-23038, and by the Department of Energy.

turbation on the system induced by nucleon exchange. For the present application we rely on Randrup's[1] transport theory based on proximity form factors and one-body dissipation. Ultimately, we have in mind a comparison of various transport theories in the framework of this dynamical simulation, for the present discussion, however, we limit the scope to two points. One is to investigate how well the mean trajectory approximation works. This we do by directly comparing mean trajectories for the several variables with the average trajectory from a large number of simulations. The second point addressed here is how well does this dynamically complete one-body theory compare with another fairly complete one-body theory, namely TDHF. Although TDHF is quite different in accounting of the degrees of freedom available, TDHF is still perhaps the ultimate one-body theory to which comparisons should be made.

Mathematical details of the transport theory can be found in ref. 1. Details of the simulation are to appear in a forthcoming paper.[2] The specific degrees of freedom followed here are: the Z and N of the fragments; the three position coordinates and conjugate momenta of the center of mass of the dinuclear system; the six intrinsic rotational degrees of freedom; the total excitation energy; and the radius of a cylindrical neck joining the fragments.

The major perturbations on the system from nucleon transport can ultimately be reduced to the momentum of the transferring nucleon which has components due intrinsic Fermi motion and collective relative motion.

The transition probabilities in this model have the simple analytical form,[1]

$$P = N'(\varepsilon_f)\varepsilon \left(1 - \exp\left(-\frac{\varepsilon}{T}\right)\right) , \qquad (1)$$

where $N'(\varepsilon_f)$ is the differential current of nucleons at the Fermi surface, ε, is the exciton energy induced by the transport, and T is the nuclear temperature.

The calculation proceeds by following the classical equations of motion until a time, $\Delta t = -\tau \ln \sum_{Z=1,A=1}$ where τ is a random number in the interval (0,1), and the P's are numerically averaged over the direction of the transferring particle (a particular direction is ultimately chosen randomly according to the relative weight associated with each direction possibility). After a transfer the macroscopic variables are adjusted, a new Δt

is determined, and the classical equations of motion again solved during the new interval, the average trajectory of a variable, $\langle x(t) \rangle$ is obtained by summing,

$$\langle x(t) \rangle = \sum_{\text{collisions}} \tilde{x}(t)\Delta t(t) \sum_{\text{collisions}} \Delta t(t \qquad (2)$$

where $\tilde{x}$ is the average of x in the interval Δt. Dispersions in the macroscopic variables as a function of time are also similarly determined.

In figure 1 some results of a preliminary trajectory calculation are displayed. Some striking differences emerge, particularly in the drift along asymmetry and in the evolution of the neck. Any conclusion reguarding the drift in A and Z should be considered tentative since at the present time this difference appears to be due to slight differences in the calculation of available phase space in the two codes, and not due to fluctuations. The differences in the dispersions and the neck evolution, can, however, be traced to the large perturbation induced on the system by discrete nucleon exchange. Clearly a deeper understanding of these discrepancies is in order, for example, perhaps an effective nucleon mass may be appropriate during the exchange. This would produce a closer agreement between the two sets of curves.

Finally, in figure 2 we show a comparison with TDHF of some final quantities as a function of incident ℓ wave for the $^{86}Kr + ^{139}La$ reaction. The differences are in some cases large highlighting the inherent differences in these two approaches. Further investigation along this line is underway.

References

1). J. Randrup, Nucl. Phys. A307, 490 (1979).

2). G. J. Mathews, J. Randrup, and L. G. Moretto, LBL-10[illegible] (1980).

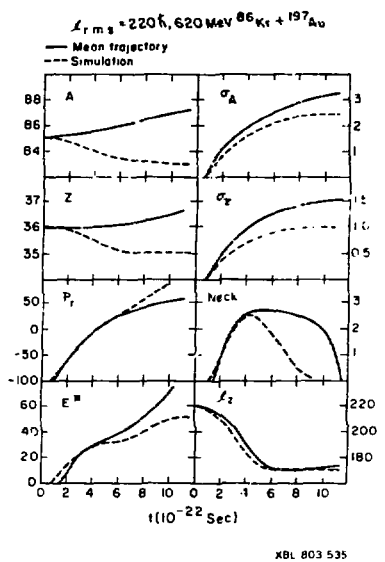

Fig. 1. A comparison of the mean trajectory approximation with the average trajectory from the dynamical simulation.

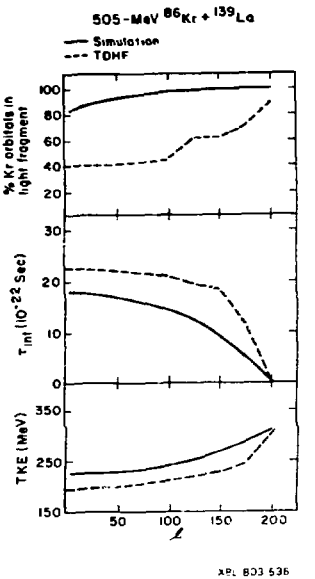

Fig. 2. A comparison of some final qualities with predictions of TDHF theory.

CHARGE AND MASS EXCHANGE IN ^{56}Fe-INDUCED REACTIONS*

H. Breuer, K. Kwiatkowski, A. C. Mignerey, and V. E. Viola
University of Maryland, College Park, MD 20742

B. G. Glagola and K. L. Wolf
Argonne National Laboratory, Argonne, IL 60439

J. R. Birkelund, D. Hilscher, J. R. Huizenga, W. U. Schröder, and W. W. Wilcke
University of Rochester, Rochester, NY 14627

Yields of projectile-like fragments have been measured near the grazing angle with discrete A and Z resolution as a function of energy loss (E_{LOSS}) for both symmetric and asymmetric systems with varying A/Z ratios. Monoisotopic targets of ^{56}Fe, ^{165}Ho, ^{209}Bi and ^{238}U were bombarded with 565 MeV ^{56}Fe ions from the LBL Super-HILAC accelerator. The measured yields and energies were transformed into primary yields and center-of-mass energies by an iterative event-by-event procedure.

Inclusive charge and mass distributions show that, for the asymmetric systems, a drift in the Z towards smaller atomic numbers can be attributed to a charge equilibration process in which protons are preferentially transferred from the Fe-like fragments to the heavy partner.[1] The ratios of average A to average Z, $\overline{A}/\overline{Z}$, are shown in Fig. 1 as functions of E_{LOSS} for ^{56}Fe + ^{165}Ho, ^{209}Bi, and ^{238}U. $\overline{A}/\overline{Z}$ increases smoothly from the A/Z value of the projectile (lower dashed line) towards that of the combined system (upper line) over an E_{LOSS} range of more than 100 MeV for all targets. Nearly identical results are obtained for the ratios $\overline{A/Z}$ calculated for individual events and for $\overline{A}/Z$ for individual isotopes.

The ratios of the variances of the charge and mass distributions, σ_A^2/σ_Z^2 are shown in Fig. 2. The values indicate that the relationship between σ_A^2

and σ_Z^2 is intermediate between correlated (upper dashed lines: $\sigma_A^2/\sigma_Z^2 = (A/Z)^2$; A,Z of combined system) and uncorrelated neutron-proton exchange (lower dashed lines: $\sigma_A^2/\sigma_Z^2 = A/Z$) for the partially damped events. However, with increasing E_{LOSS} all systems evolve toward correlated exchange.

The variances of charge distributions for fixed mass asymmetry, $\sigma_Z^2(A)$, have received much attention recently.[2-7] Data for all our systems indicate that the $\sigma_Z^2(A)$ versus E_{LOSS} curves for individual A values are remarkably similar, as shown in Fig. 3 for the Fe-Fe and Fe+Ho systems. This justifies

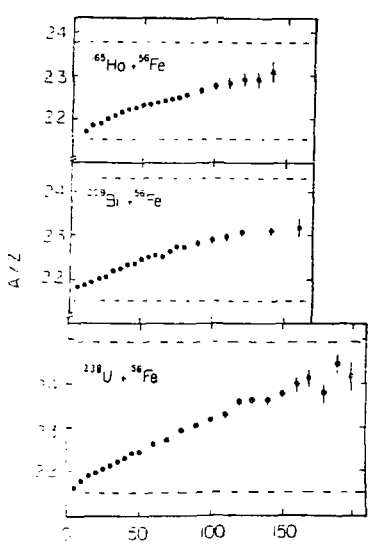

Fig. 1: Ratio of the average mass A to average charge Z as a function of E_{LOSS} for the $^{56}Fe + ^{165}Ho$, $^{56}Fe + ^{209}Bi$ and $^{56}Fe + ^{238}U$ systems.

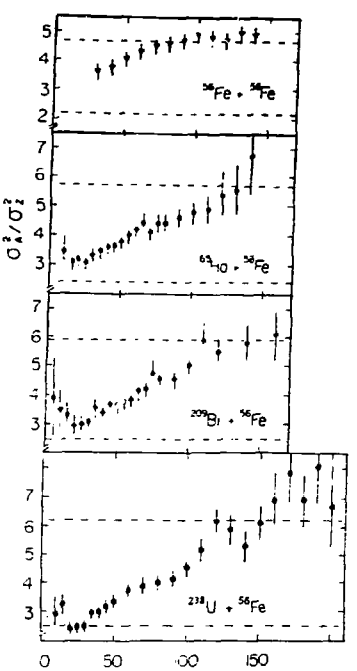

Fig. 2: Ratio of the mass to charge variance σ_A^2/σ_Z^2 as a function of E_{LOSS} for the reactions of ^{56}Fe with ^{56}Fe, ^{165}Ho, ^{209}Bi, and ^{238}U.

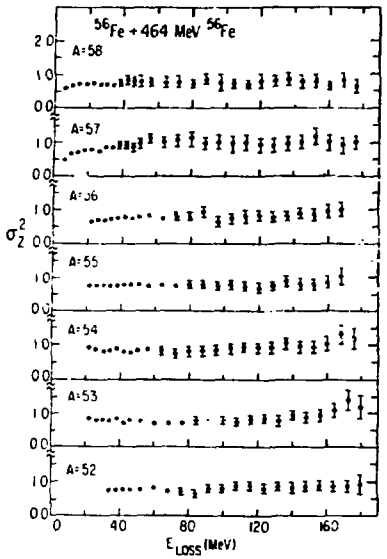

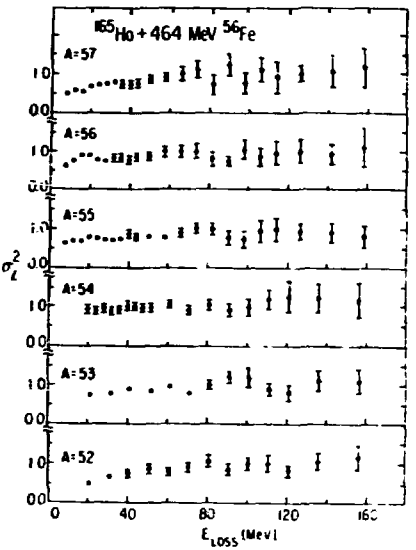

Fig. 3 (above)

Variance of the mass distribution for fixed mass $\sigma_Z^2(A)$ as a function of E_{LOSS} for the ^{56}Fe + ^{56}Fe and ^{56}Fe + ^{165}Ho systems.

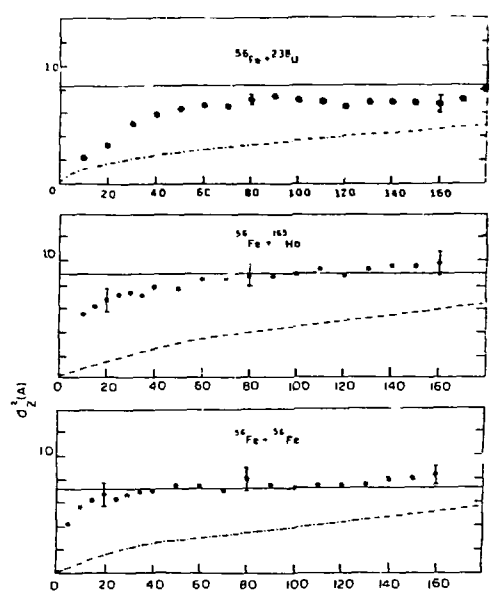

Fig. 4:

Average $\sigma_Z^2(A)$ value as a function of E_{LOSS} for the ^{56}Fe + ^{238}U, ^{56}Fe + ^{165}Ho, and ^{56}Fe + ^{56}Fe systems.

averaging the $\sigma_Z^2(A)$ values for different A; the results for the Fe+Fe, Fe+Ho and Fe+U systems are shown in Fig. 4. All $\sigma_Z^2(A)$ distributions reach a saturation value of $\sim$0.8 within the first 20 to 60 MeV of E_{LOSS}. The data show that with increasing target mass more E_{LOSS} is required to achieve the limiting $\sigma_Z^2(A)$. However, for all systems this E_{LOSS} value corresponds to $\sim$15 MeV excitation energy in the projectile-like fragments, in close agreement with the Kr+Mo data of Berlanger, et al.[2] The data of Fig. 3 and 4 have not been corrected for particle emission and calculations are presently underway to determine its effect. The curves in Fig. 4 represent predictions for σ_Z^2 from statistical fluctuations (dashed-dotted curves: $\sigma_Z^2 = T/C$; T=nuclear temperature, C=stiffness coefficient from liquid drop model) and from quantum fluctuations (full lines: $\sigma_Z^2 = \hbar\omega/2C$, $\hbar\omega=78(A_1^{1/3}+A_2^{1/3})$.

References

*This work was supported in part by the National Science Foundation and the Department of Energy.

1. H. Breuer, et al., Phys. Rev. Lett. 43, 191 (1979).

2. M. Berlanger, et al., Z. Physik A291, 133 (1979).

3. J. Poitou, et al., preprint and VII International Workshop, Hirschegg (1979).

4. H. Hoffman, C. Gregoire, R. Lucas, and C. Ngo, Z. Physik A293, 229 (1979).

5. L. G. Moretto, J. Sventek, and G. Mantzouranis, Phys. Rev. Lett. 42, (1979).

6. S. M. Samaddar and M. I. Sobel, Phys. Lett. 82B, 191 (1979).

7. E. S. Hernandez, W. D. Myers, J. Randrup, and B. Remaud, LBL Report LBL-9761 (1979).

QUANTAL DYNAMICS OF CHARGE EQUILIBRATION IN DAMPED NUCLEAR COLLISIONS*†

E. S. Hernandez,** W. D. Myers, J. Randrup and B. Remaud‡
Nuclear Science Division, Lawrence Berkeley Laboratory
University of California, Berkeley, CA 94720

1. Introduction

In quasi-elastic and deep-inelastic nuclear reactions charge equilibration appears to occur quite rapidly. This rapid movement of protons in one direction and neutrons in the other can be viewed as a collective mode associated with isovector-type hydrodynamical flow in the dinucleus analogous to the Steinwedel-Jensen description of the Giant Dipole Resonance in ordinary nuclei. Since we find that the characteristic energy of such a mode is typically much larger than the nuclear temperatures encountered, the fluctuations in the charge asymmetry degree of freedom are expected to come mainly from zero-point motion.

Such a description of the charge asymmetry mode has already been applied with some success by Swiatecki and Blann to charge and mass distributions seen in fission[1]), and more recently to heavy-ion reactions by Moretto[2]), by Berlanger et al.[3]), and by Hofmann, Gregoire, Lucas and Ngo[4,5]). However, as pointed out by Nifenecker et al.[6]), it is essential to consider the time dependence of the shape of the system in order to correctly establish the connection between the GDR-like collective motion and the width of the charge distribution which is experimentally observed.

Roughly speaking, the inertia associated with the charge asymmetry degree of freedom is inversely proportional to the size of the neck connecting the two colliding nuclei. Trajectory calculations) predict that the pinch-off takes place sufficiently rapidly that the width of the charge distribution is "frozen in" by the increasing inertia.

2. Description of the model

In order to describe the division of charge between the two partners, for a given mass asymmetry, we use the isospin component of the projectile-like nucleus $T = 1/2(N-Z)$. The potential-energy surface of the dinucleus varies rather gently in the A-direction while the strong symmetry energy makes it much steeper in the T-direction. Furthermore, the dynamical evolution along the mass asymmetry proceeds relatively slowly and can often be entirely neglected.

Typical results obtained from the trajectory calculations are shown in fig. 1a. The time evolution of the neck radius c and the neck length d is plotted for the case of 430 MeV ^{86}Kr on ^{72}Mo, at an impact parameter corresponding to an angular momentum of 60ħ.

Under the figure the five small drawings show the appearance of the dinucleus at various stages of the collision.

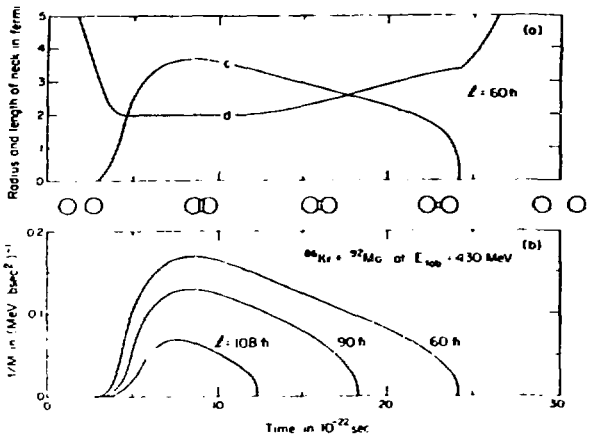

Figure 1

Once the time evolution of the dinuclear geometry has been determined from the trajectory calculation, the dynamical coefficients for the charge asymmetry mode can be calculated. For the stiffness K a conventional nuclear mass formula is used, and for the inertia and damping a rather simplified hydrodynamical model is employed. To estimate M we consider the hydrodynamical flow of the proton and neutron fluids through the neck.

The damping of the charge asymmetry mode has been estimated by using the same value of the hydrodynamical viscosity that is required to reproduce the observed width of the Giant Dipole Resonance in spherical nuclei.

Once the quantities K, M and γ have been expressed in terms of the geometrical properties of the system (c, d and R) their time dependence can be estimated using the classical trajectory calculations above.

3. Quantal treatment of a time-dependent damped oscillator

The model presented in the preceding section describes a particle with time-dependent mass M(t) placed in a harmonic oscillator field with stiffness K(t), and centered at the position $X_0(t)$. Since ordinarily $\hbar\omega$ is several times larger than the expected temperature T we shall in fact assume that the thermal fluctuations arising from the coupling of the oscillator to the rest of the system are neglible; it then sufficies to follow the evolution of only a single wave function throughout the equilibration process.

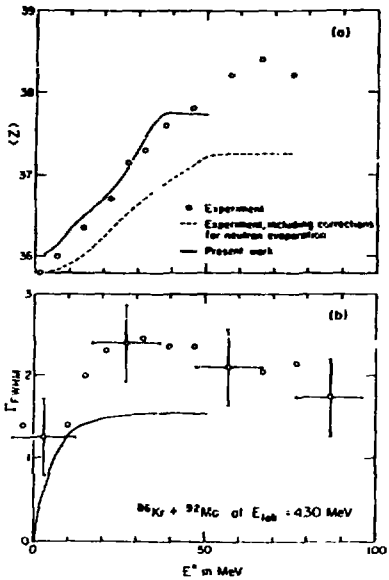

Figure 2

4. Calculated results

In fig. 2 the calculated results are compared with the experimental data of ref. [3]). The upper portion of the figure shows the mean charge $\langle Z \rangle$ and the lower portion shows the width Γ of the final charge distribution at a fixed mass partition; both quantities are plotted as function of the total center-of-mass kinetic energy loss E* which is approximately the same as the induced intrinsic excitation in the fragments.

The primary experimental data are shown as the open dots on the upper portion of the figure and the dashed curve results after correction for neutron evaporation has been made. The calculated values are given by a solid curve.

The present calculations give a quick rise of Γ with E*, followed by a broad maximum. The maximum occurs at around E* = 35 MeV in agreement with the data but it is not as pronounced. The overall magnitude of the calculated curve is seen to fall somewhat below the experimental data. We are encouraged by the fact that these predictions are consistent with the observations. This is especially significant since all the coefficients entering in the various formulas are either fundamental nuclear constants or have been otherwise fixed beforehand so that there are no adjustable parameters.

Footnotes and References

* This work was supported in part by the U. S. Department of Energy.

† Condensed from LBL-9761.

**Permanent address: Departamento de Fisica, Facultad de Ciencias Exactas y Naturales, 1428 Buenos Aires, Argentina.

††Permanent address: Institut de Physique, Universite de Nantes, 2 rue de la Houssiniere, 44072 Nantes, France.

1) W. J. Swiatecki and H. M. Blann, unpublished notes (1961); W. J. Swiatecki, lecture at Princeton University, 7 March 1961
2) L. G. Moretto, J. Sventek and G. Mantzouranis, Phys. Rev. Lett. 42 (1979) 563
3) M. Berlanger, A. Gobbi, F. Hanappe, U. Lynen, C. Ngô, A. Olmi, H. Sann, H. Stelzer, H. Richel, and M. F. Rivet, Proc. Int. Workshop on Gross Properties of Nuclei and Nuclear Excitations VII, Hirschegg, Austria, Jan. 1979; also Z. Phys. A291 (1979) 133
4) C. Gregoire, R. Lucus, C. Ngô and H. Hoffmann, Proc. IVth Balaton Conf. on Nucl. Phys., Keszthely, Hungary, June 1979
5) H. Hofmann, C. Gregoire, R. Lucas and C. Ngô., preprint DPh-N/MF/79/22, CEN, Saclay, July 1979.
6) H. Nifenecker, J. Blachot, J. P. Bocquet, R. Brissot, J. Crancon, C. Hamelin, G. Mariolopoulos and Ch. Ristori, preprint Centre d'Etudes Nucleaires, Grenoble, July 1979

NUCLEON EMISSION FROM A LOCALIZED EXCITED ZONE IN HEAVY ION REACTIONS

S. K. Samaddar**, D. Sperber and M. Zielinska-Pfabe***
Department of Physics, Rensselaer Polytechnic Institute

Recently energy spectra and angular distribution of light particles produced in heavy ion reactions, high above the Coulomb barrier, have been measured. At high bombarding energies there is a component of the spectrum not originating from a fully equilibrated system. One way to account for such a component, is to assume that some of the nucleons are emitted from a hot zone[1] near the interface of the touching ions.

As soon as the ions come into contact they stick and we assume that at the interface a 'layer of nucleons' is excited in each of the ions. We approximate the hot zone by two caps (Fig. 1) of depth d which is about the average distance between the centers of adjacent nucleons in nuclear matter.

We assume that all the available energy is transformed into heat localized in the zone and the rest of the system remains cold. Nucleons emitted from the zone travel freely in the cold nuclear matter and are refracted at the nuclear boundary.

Due to the short time of nucleon emission from the localized hot zone, as compared to the reaction time, the geometry (Fig. 1) is applicable to the study of emission of nucleons both in reactions leading to fusion and in strongly damped collision. Therefore, we include contributions from impact parameters leading to the above mentioned processes.

It is assumed that nucleons are emitted from the surface of the zone with equal probability in all directions. Furthermore, the energy of the nucleons is given by a Fermi distribution $F(E)$ with the temperature $T = (E^*/a)^{\frac{1}{2}}$ here E^* is the available energy for thermal excitation.

The total nucleon flux dN_{1t}/dE at an energy $E > V_o/\cos^2\alpha$ originating from the plane surface of the target is given by

$$\frac{dN_{1t}}{dE} = -\frac{\rho}{4\pi}\sqrt{\frac{2}{m}}\, E\, F(E)(R_t-d)^2\, R_t^2 \int_o^{2\pi} d\phi_1 \int_o^{2\pi} d\phi_2 \int_{\pi-\beta}^{\pi} d\theta_1 \times \int_o^{\pi-\beta} d\theta_2 \frac{\sin\theta_1 \sin\theta_2 \cos\alpha}{(AB)^2 \cos^3\theta_1}\, \epsilon\left(E - \frac{V_o}{\cos^2\alpha}\right) \qquad (1)$$

(For definition of variables see Fig. 1). Here $\beta = \cos^{-1}\frac{R_t - d}{R_t}$. Corresponding to Eq. 1 the contribution from the curve surface of the target is

$$\frac{dN_{2t}}{dE} = \sqrt{\frac{\rho}{2}}\,\frac{2}{m}\,E\,F(E)R_t^2 \int_{\pi-\beta}^{\pi} \sin\theta_o d\theta_o \int_o^{\pi/2} \sin\theta_i d\theta_i \times \int_o^{2\pi} d\phi_i\ \varepsilon(E-V_o/\cos^2\theta_i) \qquad (2)$$

Similar expressions dN_{1p}/dE and dN_{2p}/dE for emission from the projectile are obtained. In the above expressions contribution from nucleons which re-enter the zone are excluded. Finally, the nucleon spectrum $d\sigma/dE$ is given by

$$\frac{d\sigma}{dE} = \Delta t \pi^2 \sum_{\ell=0}^{\ell_{max}} (2\ell+1)\left[\frac{dN_{1t}}{dE} + \frac{dN_{2t}}{dE} + \frac{dN_{1p}}{dE} + \frac{dN_{2p}}{dE}\right] \qquad (3)$$

The nucleon emission time Δt is determined by normalizing the height of the peak of energy spectrum to the data, this time is of the order of 10^{-22} sec. For proton emission the effect of penetration through the Coulomb barrier is included. This barrier has an important effect on the low energy part of the proton energy spectrum.

In Fig. 2 we show the calculated energy distribution of neutrons and protons for the reaction $^{16}O + {}^{197}Au$ at 315 MeV along with the experimental data for protons[2]. Good agreement is obtained both for the position of the peak and the slope of the spectra.

In Fig. 3 we show the double differential cross section $d^2\sigma/d\Omega dE$. The calculated results underestimate the cross section at forward angles. The inclusion[3] of 'PEPs' prior to the formation of a hot zone is expected to improve the agreement.

We would like to conclude that the emission of nucleons from the 'hot spot' is capable of reproducing the main features of both the energy and angular distributions. It would be interesting to have neutron data in order to see whether the peak of the energy distribution occurs at lower energy as compared to the peak of the proton spectra. Furthermore, it would be worthwhile to establish whether the ratio between the cross sections for emissions of neutrons and protons (above the Coulomb barrier) is given by the ratio of their densities.

Figure Captions

Fig. 1. The two nucleus configuration with hot regions (the caps) is shown. The z axis is in the direction of the incident beam and z' is the symmetry axis for the dinuclear system for non central collision. Here (θ_1,ϕ_1) and (θ_0,ϕ_0) characterize the position of a point on the plane and curved surfaces respectively of the hot zone in the target. The vectors $\vec{p}_i$ and $\vec{p}_f$ are the directions of the momenta of a nucleon before and after refraction. For the curved surface (θ_i,ϕ_i) and (θ_f,ϕ_f) denote the directions of $\vec{p}_i$ and $\vec{p}_f$. Here (θ_2,ϕ_2) are the coordinates of the point of refraction P on the cold surface. All the angles are in the z' frame of reference.

Fig. 2. Proton and neutron spectra for the reaction $^{197}Au(^{16}O,p)X$ and $^{197}Au(^{16}O,n)X'$ at E_{lab} = 315 MeV. Sold line denotes proton spectum and dashed line corresponds to neutron spectrum. For comparison the experimental proton spectrum is shown.

Fig. 3. Experimental and calculated double differential cross section $\frac{d^2\sigma}{d\Omega dE}$ for the reaction $^{197}Au(^{16}O,p)X$ is shown as a function of energy for different angles.

Footnotes and References

*Supported by the U.S. Department of Energy.

**On leave from Presidency College, Calcutta, India.

***On leave from Institute for Nuclear Research, Warsaw, Poland.

1. H. A. Bethe, Phys. Rev. 53 (1938) 675, R. Weiner et al., Phys. Rev. Lett. 34 (1975) 1523, R. Weiner et al., Nucl. Phys. A286 (1977) 282, P. A. Gottschalk et al., Phys. Rev. Lett. 39 (1977) 1250, S. I. A. Garpman et al., Phys. Lett. (in press).
2. T. J. M. Symons et al., Preprint LBL-8379 (1978).
3. J. P. Bondorf et al., Nucl. Phys. A333 (1980) 273.

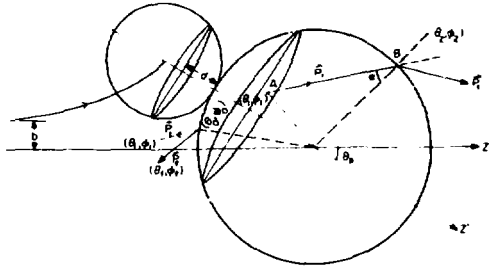

FIGURE 1

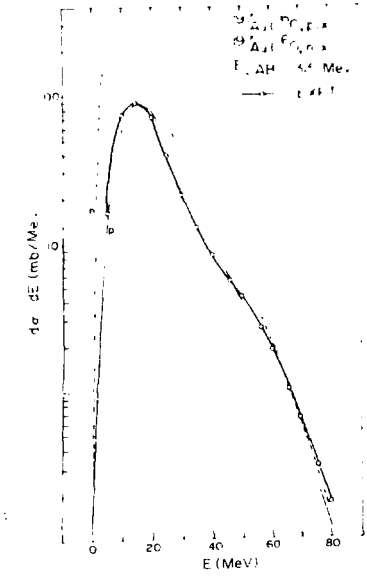

FIGURE 2

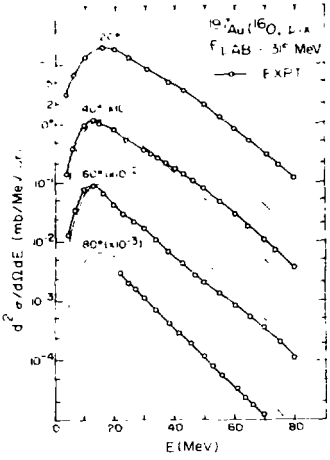

FIGURE 3

POSSIBLE ISOBAR MECHANISM FOR PRODUCTION OF HIGH MOMENTUM PROTONS IN THE BACKWARD DIRECTION IN PROTON-NUCLEUS AND NUCLEUS-NUCLEUS INTERACTIONS

John W. Harris

Lawrence Berkeley Laboratory
University of California
Berkeley, California 94720

ABSTRACT

Inclusive proton distributions at 180^{o} are presented for a range of p-nucleus and nucleus-nucleus reactions at incident energies $0.4 \leq T \leq 2.1$ GeV/n (4.89 GeV for protons). Limiting behavior is evident at the higher energies and features suggestive of correlations in the nucleus are discussed. Exclusive charged-particle production accompanying back-angle particle emission in the streamer chamber is presented. A 180^{o} correlation between the angles of positive charged-particles is observed and provides the first suggestion that $\Delta(3,3)$ isobar production is an important mechanism for the production of higher momentum particles in the backward direction.

Since production of nucleons in the backward laboratory direction is kinematically forbidden in free nucleon-nucleon collisions, nucleon emission in this region from p-nucleus and nucleus-nucleus collisions can only result from internal motion of nucleons in the nucleus -or- multi-step reaction processes. The purpose of this study is i) to obtain information on the possible reaction mechanisms which produce high nucleon momenta in the backward direction, ii) to learn details of the structure of nucleons in the nucleus from the observed nucleon momentum distributions, and iii) to gain an overall understanding of proton-nucleus and nucleus-nucleus interactions.

Results from (e,e'), (e,e'p), (p,2p), and (γ,p) experiments[1] on the distributions of nucleon momenta up to 300 to 400 MeV/c are in agreement with theoretical predictions using known single-particle wavefunctions. Larger momenta observed in (γ,p) and (p,p') experiments[2,3] suggest the existence of high momentum components in the nucleus which cannot be described by single-particle wavefunctions. These high momenta have been interpreted in terms of internal correlations in the nucleus.[4-10] However, there exist inherent problems in relating measured momentum distributions directly to internal momentum distributions in the nucleus. Gottfried[11] suggests that the validity of the impulse approximation assumed in these applications may be jeopardized by deviations from mean field motion in the nucleus. Moreover, Amado and Woloshyn[12] state that final state interactions may forbid a simple interpretation of the observed momentum distributions. Nevertheless, a systematic study the inclusive proton momentum distributions in p-nucleus and nucleus-nucleus interactions[13] furnishes valuable information with which to test possible reaction mechanisms that have been proposed. In the interest of obtaining more-complete-event information to ascertain the production mechanisms associated with backward particle emission, exclusive charged-particle production accompanying back-angle proton emission in the streamer chamber was also studied.[14] These data provide the first suggestion that $\Delta(3,3)$ isobar production with subsequent decay and/or reabsorption plays a major role in the production of particles in the backward direction.

The incident energy dependence of the back-angle proton inclusive momentum distributions is displayed in Fig. 1 for $p+^{12}C$ interactions. In this study 180° protons in the momentum range $300 \leq p \leq 1000$ MeV/c were analyzed in a magnetic spectrometer at the LBL Bevalac. Proton, alpha, carbon, and argon beams in the kinetic energy range $0.4 \leq T \leq 2.1$ GeV/n (4.89 GeV protons) were used to bombard C, Al, Cu, Sn, and Pb targets. The absolute uncertainties in the inclusive cross sections are estimated to be ±15 percent. The data, ranging from 90 MeV to 400 GeV incident energy, are independently normalized and exhibit the onset of limiting behavior in the incident energy range from 2.1 to 4.9 GeV. Over this range of energies the spectra become independent of incident energy. This behavior which is attributed to limiting target fragmentation[15] in the present case is also observed for all projectile masses studied up to argon. Further evidence for this limiting behavior is shown in Fig. 2. The differential cross sections integrated between 300 MeV/C and 1000 MeV/C are observed to be energy independent above an incident energy of 3.5 GeV. The magnitude of these cross sections (σ) depends on the projectile (A_p) and target (A_t) masses in the form $\sigma \sim A_p^{2/3} A_t^{4/3}$. The $A_t^{4/3}$ dependence suggests the involvement of more than one target nucleon in the backward production mechanism and argues against a single hard scattering mechanism.

The dependence of the shape of the proton momentum distributions on projectile mass is displayed in Fig. 3 for 1.05 GeV/n incident energy. The shapes of the distributions from ^{12}C for $300 \leq p \leq 1000$ MeV/c are independent of the mass of the projectile.

When the 1.05 GeV/n ^{12}C projectile fragmentation data from Papp[16] at $\theta = 2.5^0$ is transformed to the projectile rest frame and superimposed on Fig. 3, a break in the proton momentum distribution is observed at $p \simeq 350$ MeV/C. This break is similar to that observed in the extracted momentum distributions in recent (γ,p) data.[2] Furthermore, a similar break in the proton spectra in the fragmentation region of p + α and p + d reactions[17,18] is observed, thus providing evidence against a dominant multiple scattering cascade mechanism.

Recent theoretical work has led to the approximation of internal momentum distributions in the nucleus by two overlapping Gaussians.[4,5] a low momentum Gaussian dominated by single particle characteristics of the momentum distributions, and a high momentum Gaussian which emerges when short range correlations are considered. The solid curve in Fig. 3 is a double Gaussian fit to the $^{12}C + ^{12}C \rightarrow p$ momentum distribution. The value of the momentum dispersion for the low momentum Gaussian ($\sigma_p = 75$ MeV/C) can be derived using the Goldhaber[19] and Feshbach and Huang[20] formulations. The dispersion of the high momentum Gaussian ($\sigma_p = 190$ MeV/C) reaches a limiting value of 190-200 MeV/C, near the Fermi momentum, independent of target mass. Other mechanisms which incorporate nuclear correlations for production of high momentum protons have been proposed.[6-10] Fujita and Hufner[7] proposed a model which included correlations between two nucleons in the target to describe the backward proton data. An extended version[8] which includes multiple-particle correlations describes the incident energy dependence quite well for energies up to 1 GeV. Other models[9,10] which attribute the emission of high momentum protons in

the backward direction to the break-up of correlated pairs of nucleons in the nucleus have also been proposed. The results of the theoretical and experimental investigations suggest that the limiting shapes of the backward high momentum proton spectra are related to the presence of short-range correlations in the nucleus.

An experiment was recently completed in the LBL Streamer Chamber at the Bevalac to study the charged-particle production associated with back-angle proton production.[14] The streamer chamber was triggered on a backward-emitted ($\theta_{lab} > 90^0$) charged-particle. A 2.1 GeV proton beam was used to bombard C, KCl, and BaI_2 targets. The mean positive charged-particle multiplicities associated with events with a backward trigger particle from these targets are $\langle M_+ \rangle$ = 4.70 ± .09, 6.66 ± .23, and 8.00 ± .18, respectively. These multiplicities are higher than would be expected if a single hard scattering mechanism were dominant. Further information on the possible reaction mechanisms associated with backward particle production can be derived from a rapidity plot of the positive charged-particles (mostly protons) in these events as presented in Fig. 4 for the 2.1 GeV p + BaI_2 reaction. The curve designates the kinematic limit for nucleon-nucleon interactions. The most prominent feature is the number of events centered at the target rapidity. This corresponds mainly to target fragmentation processes. In addition, contributions from quasielastic processes are observed as the high-momentum forward-going particles. A third feature in the plot is the presence of events with high perpendicular momentum. Further study of these

events is presently being conducted. Rapidity plots for the C and KCl targets are similar to that of Fig. 4 except an enhancement in the forward cross section is observed as the target mass decreases. Thus, the target nucleus becomes less transparent and the reaction retains less memory of the incident projectile as the target mass increases. This is evidence for the presence to some degree of multiple scattering.

Since isobar production accounts for a major fraction of the pp total cross section at energies from 1-2 GeV [21] the effects of the decay and absorption of an isobar on the spectrum of particles in the backward direction may be substantial. The contribution of these two-step mechanisms to backward spectra can be investigated. Diagrams for the $\Delta(3,3)$ isobar decay and absorption are displayed in Fig. 5 following production in the reaction $pp \rightarrow n\Delta^{++}(1232)$, which is a dominant inelastic mechanism at these energies. Only the production of Δ^{++} isobars from the lower vertex (target proton) in Fig. 5 will contribute appreciably to the yield of particles in the backward direction. Also shown are schematic diagrams of the momenta of the products of Δ^{++} decay and absorption. The production of protons in the backward direction with appreciable momentum in the laboratory frame is indeed possible—the contribution depending upon the direction and momentum of the Δ^{++}. Furthermore, the products of Δ^{++} decay will be emitted back-to-back (180^0 apart) in the Δ^{++} rest frame. Likewise, in the absorption process the products will be emitted 180^0 apart in the $\Delta^{++} + n_{target}$ center-of-mass system.

Since the Δ^{++} production cross section is largest for low momentum transfer, the decay (Δ^{++}) and absorption ($\Delta^{++} + n_{target}$) rest frames will be moving slowly with respect to the laboratory system and the 180^{0} correlation of the products should be preserved to some degree in the lab. Displayed in Fig. 6 is the laboratory correlation for pairs of positive particles (protons, positive pions) as a function of the cosine of the angle between the two particles. One of the pair is always emitted in the backward hemisphere. A strong 180^{0} correlation is observed. This correlation is further enhanced if only particles with momentum p > 300 MeV/C are considered, as depicted by the histogram in Fig. 6. These data suggest that the $\Delta(3,3)$ resonance plays an important role in producing high momentum protons in the backward direction. The laboratory correlation for all four- and five-prong events is shown in Fig. 7. The statistics are lower, however a 180^{0} correlation is observed. For comparison, the phase space predictions for three possible final states are also presented. The correlation at 180^{0} observed in the experiment cannot be reproduced by considering only pure phase space. This lends further support to the possibility of an isobar production mechanism in the production of particles in the backward direction. Additional background analysis and more sophisticated theoretical calculations assuming an isobar production mechanism are necessary to establish the importance of isobar production in the emission of particles of high momentum in the backward direction.

the moment of inertia of one of the two touching spheres and T is the temperature. For the -250 MeV Q-value bin, T = 2.3 MeV and the model predicts a value of σ^2/I^2 = 0.064 and a misalignment angle of 25° which are in close agreement with the experimental values.

In summary, from this preliminary analysis we have observed in the ^{165}Ho + ^{165}Ho reaction, large values for the spin transfer ($I_1 + I_2 \sim 100\ \hbar$) and large values for the in-plane to out-of-plane continuum γ-ray ratio, W(in/⊥) = 2.2. Both the spin transfer and W(in/⊥) are strong functions of the reaction Q-value and the latter also shows a dependence on E_γ. For a reasonable value of the γ-ray cascade multipolarity (80% E2s), a misalignment angle of 26° is extracted for the deep-inelastic region. These data have been compared with the statistical model of Moretto and Schmitt which correctly predicts the magnitude of the observed misalignment and qualitatively explains the trend of W(in/⊥) with Q-value. We conclude that continuum γ-ray anisotropy measurements are a powerful technique for probing the deep-inelastic collision process.

would also like to acknowledge the other collaborators in the experiments that were presented: Steve Chessin, J. Y. Grossiord, Dave Hendrie, Bob Treuhaft, Karl Van Bibber, Jim Brannigan, Herbert Stelzer, and Reinhard Stock. This work was supported in part by the Division of Nuclear Physics of the Office of High Energy and Nuclear Physics of the U.S. Department of Energy under Contract No. W-7405-ENG-48 and the Bundesministerium für Forschung and Technologie (West Germany).

REFERENCES

(1) D.J.S. Findley and R. O. Owens, Nucl. Phys. A292 (1977) 53 and references therein.

(2) D.J.S. Findley et. al., Phys. Lett. 74B (1978) 305.

(3) S. Frankel et. al., Phys. Rev. Lett. 36 (1976) 642.

(4) J. G. Zabolitsky and W. Ey, Phys. Lett. 76B (1978) 527.

(5) O. Bohigas and S. Stringari, IPN-Orsay Preprint (1979) 1.

(6) J. W. Van Orden et. al., Univ. of Maryland Preprint No. 80-080 (1979) 1.

(7) T. Fujita and J. Hufner, Nucl. Phys. A314 (1979) 317.

(8) T. Fujita, Nucl. Phys. A324 (1979) 409.

(9) L. L. Frankfurt and M. I. Strikman, Phys. Lett. 83B (1979) 407.

(10) T. Yukawa and S. Furui, Phys. Rev. C20 (1979) 2316.

(11) K. Gottfried, Ann. Phys. 21 (1963) 29.

(12) R. D. Amado and R. M. Woloshyn, Phys. Lett. 69B (1977) 400.

(13) J. V. Geaga, S. A. Chessin, J. Y. Grossiord, J. W. Harris, D. L. Hendrie, L. S. Schroeder, R. N. Treuhaft, and K. Van Bibber, Lawrence Berkeley Laboratory Report No. LBL-10265 (1979) 1.

(14) Lawrence Berkeley Laboratory/Gesellschaft für Schwerinonenforschung Streamer Chamber Collaboration: J. W. Harris, J. Brannigan, J. V. Geaga, L. S. Schroeder, R. N. Treuhaft, A. Sandoval, H. E. Stelzer, and R Stock.

(15) J. Benecke et. al., Phys. Rev. 188 (1969) 2159.

(16) J. Papp, Lawrence Berkeley Laboratory Report No. LBL-3633 (1975) 1.

(17) A. M. Baldin et. al., Joint Institut for Nuclear Research (Dubna) Preprint P1-11168 (1977) 1.

(18) L. M. Anderson, Lawrence Berkeley Laboratory Report No. LBL-6769 (1977) 1.

(19) A. S. Goldhaber, Phys. Lett. 53B (1974) 306.

(20) H. Feshbach and K. Huang Phys. Lett. 47B (1973) 300.

(21) O. Benary et. al., University of California, Lawrence Radiation Laboratory Report No. UCRL-20000 NN (1970) 1.

(22) Y. D. Bayukov et. al., Phys. Rev. C20 (1979) 764.

(23) J. R. Wu et. al., Phys. Rev. C19 (1979) 698.

FIGURE CAPTIONS

Fig. 1. Inclusive proton distributions as a function of momentum for the present study (▲, ◆, ○), Ref. 22 (□), Ref. 17 (▽), Ref. 3 (–), and Ref. 23 (--).

Fig. 2. Proton invariant cross sections from the present study (●), Ref. 3 (Δ), and Ref. 22 (□) integrated over $300 \leq p \leq 1000$ MeV/c. The cross sections are plotted as a function of incident energy for the $p + Cu \rightarrow p(180^0) + X$ reaction.

Fig. 3. Inclusive proton momentum distributions plotted in the laboratory rest frame for the present data (▽, ♦, □) and in the projectile rest frame for Ref. 16 (○). The solid curve is the double Gaussian representation of the $^{12}C + {}^{12}C \rightarrow p$ momentum distributions.

Fig. 4. Rapidity plot of positive charged-particles from the reaction 2.1 GeV $p + BaI_2$. The kinematic limit of elastic scattering in the nucleon-nucleon system is designated by the curve.

Fig. 5. $pp \rightarrow n\Delta^{++}(1232)$ isobar production; a) diagram for $\Delta(3,3)$ isobar formation and decay; b) associated schematic momentum vector diagram in the laboratory system; c) diagram for $\Delta(3,3)$ isobar formation and reabsorption; d) associated schematic momentum vector diagram in the laboratory system.

Fig. 6. Correlation between pairs of positive charged-particles in each event as a function of the cosine of the angle between the particles. One particle in each pair is emitted at $\theta_{lab} > 90^0$. The histogram represents all pairs with individual particle momentum $p > 300$ MeV/c.

Fig. 7. Correlation analysis (as in Fig. 6) for all 4- and 5-prong events. Pure phase space calculations for three possible final states are also displayed.

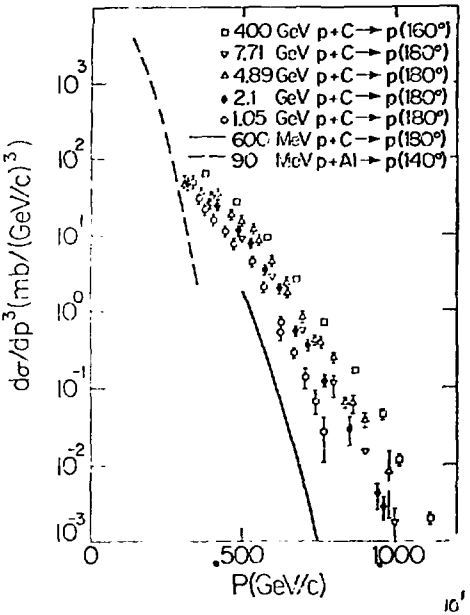
400 GeV p+C→p(160°)
7.71 GeV p+C→p(180°)
4.89 GeV p+C→p(180°)
2.1 GeV p+C→p(180°)
1.05 GeV p+C→p(180°)
600 MeV p+C→p(180°)
90 MeV p+Al→p(140°)
dσ/dp³(mb/(GeV/c)³)
P(GeV/c)

Fig.1

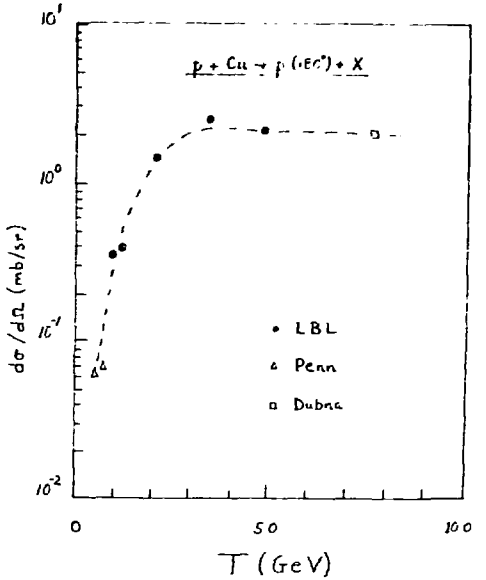
p + Cu → p (140°) + X
LBL
Penn
Dubna
dσ/dΩ (mb/sr)
T (GeV)

Fig.2

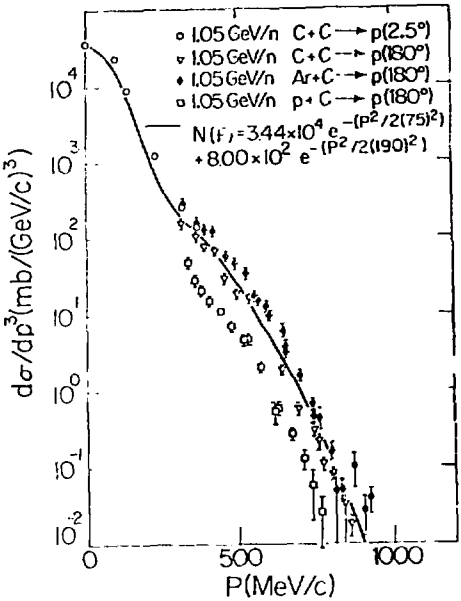
o 1.05 GeV/n C+C → p(2.5°)
▽ 1.05 GeV/n C+C → p(180°)
♦ 1.05 GeV/n Ar+C → p(180°)
□ 1.05 GeV/n p+C → p(180°)
N(P) = 3.44×10⁴ e^-(P²/2(75)²)
+ 8.00×10² e^-(P²/2(190)²)
dσ/dp³(mb/(GeV/c)³)
P(MeV/c)

Fig. 3

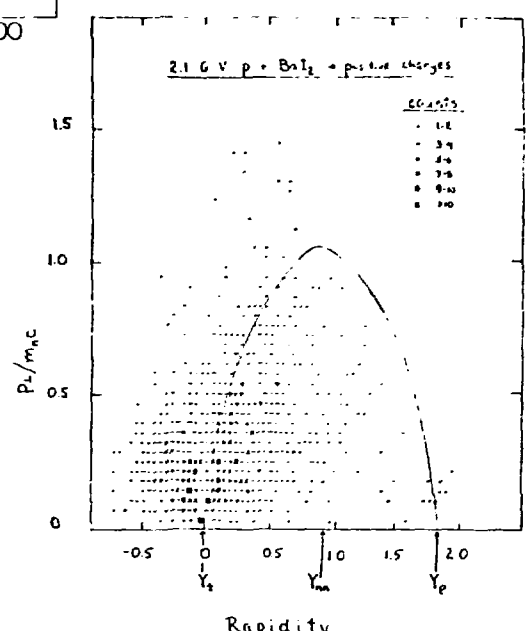
2.1 GeV p + BaI₂ + positive charges
P∥/mc
Rapidity

Fig. 4

Fig. 5

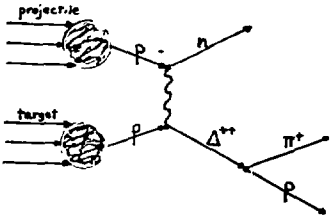
projectile
target
p
n
p
Δ++
π+
p

(a)

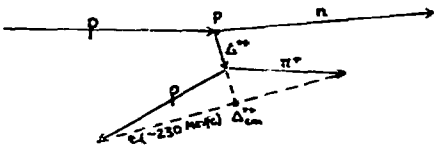
p
p
n
Δ++
π+
p
Δ++ lab

(b)

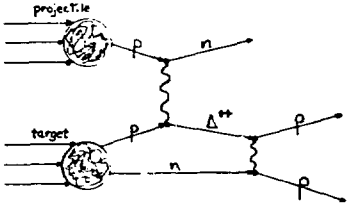
projectile
target
p
n
p
Δ++
p
n
p

(c)

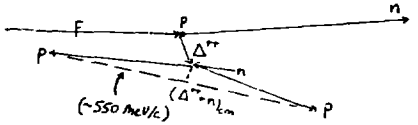
p
p
n
p
Δ++
n
p

(d)

Fig. 6

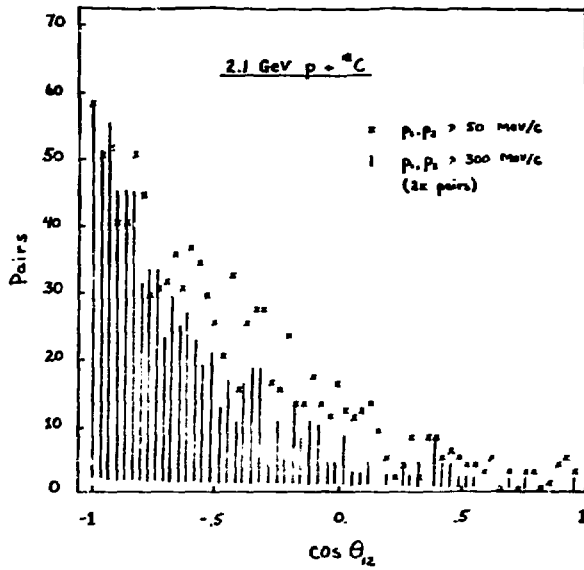
2.1 GeV p + ¹²C
x p₁-p₂ > 50 mev/c
1 p₁-p₂ > 300 mev/c
(2π pairs)
Pairs
cos θ₁₂

Fig. 7

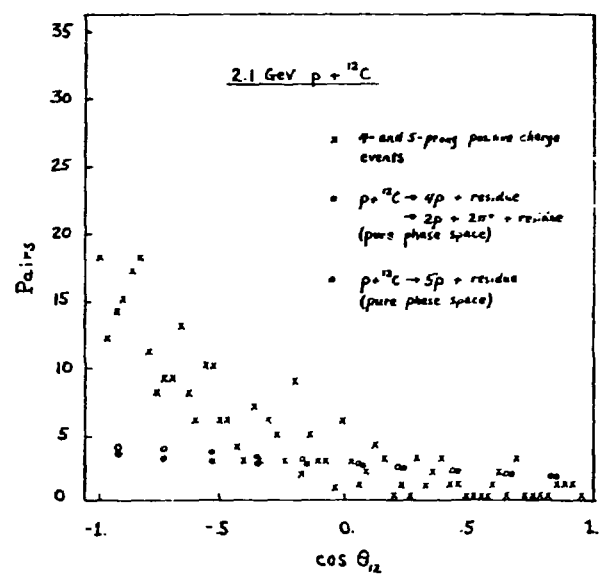
2.1 GeV p + ¹²C
x 4- and 5-prong positive charge events
• p+¹²C → 4p + residue → 2p + 2π⁺ + residue (pure phase space)
• p+¹²C → 5p + residue (pure phase space)
Pairs
cos θ₁₂

NUCLEAR MOMENTUM DISTRIBUTION AND RELATIVISTIC HEAVY-ION REACTIONS*

Cheuk-Yin Wong
Oak Ridge National Laboratory
Oak Ridge, TN 37830

and

R. Blankenbecler
Stanford Linear Accelerator Center
Stanford, CA 94305

Abstract

In terms of a direct fragmentation process and a hard-scattering process, the proton-inclusive data for the reaction $\alpha + {}^{12}C \to pX$ have been successfully analyzed. The extracted semiempirical momentum distribution indicates possible evidence of nuclear correlations and final-state interactions.

The nuclear momentum distribution is a basic nuclear property which is important in understanding the correlation between nucleons and the behavior of many intermediate energy phenomena involving large momentum transfers.[1,2] However, not much is known about this momentum distribution experimentally. In the relativistic heavy-ion reactions, the proton-inclusive spectrum at 0° and 180° comes mainly from a direct fragmentation process (Fig. 1a) in which the proton is emitted from one nucleus without scattering with the other nucleus and, hence, conveys important information on the momentum distribution of a nucleon in a nucleus. Furthermore, as the proton can carry much of the momentum of the nucleus in a cooperative manner, relativistic heavy-ion reactions allow one to extract the high momentum tail of the nuclear momentum distribution which may not be obtained by other means. The nuclear momentum distribution also enters in the hard-scattering process[3] (Fig. 1b) in which the detected proton comes from the collision of a nucleon in the projectile and a nucleon from the target. Such a process is expected to be important for $p_T >> 0.1$ GeV/c.

With a combination of the direct fragmentation and hard-scattering processes, we analyze the forward proton production data of Anderson et al.[4] in the collision of α particles on ^{12}C. We introduce a simple parametrization of the nuclear momentum distribution as the sum of a single-particle

---

*Research jointly sponsored by the Division of Basic Energy Sciences, U.S. Department of Energy, under contract W-7405-eng-26 with the Union Carbide Corp., and by the U.S. Department of Energy under contract DE-AC03-76SF00515.

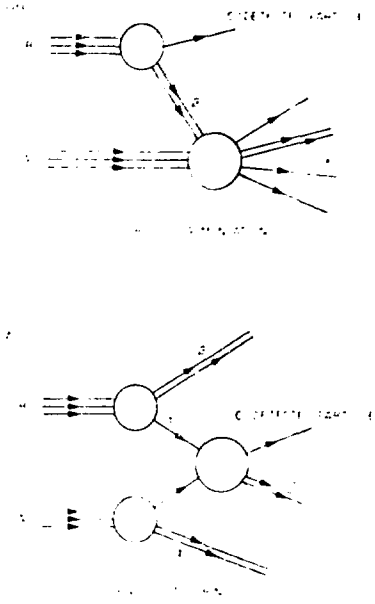

Fig. 1. Diagrams the two dominant processes contributing to the reaction of interest.

component and a correlated component with a greater width and a parameter specifying the relative importance of the direct fragmentation and hard-scattering processes. We show in Fig. 2 the experimental invariant cross section versus the theoretical results as a function of the Feynmann scaling variable x_F defined as $p_{//}/|\vec{p}|_{max}$, evaluated in the center-of-mass system. As one observes, the data of $\alpha + {}^{12}C \rightarrow p+X$ at $p_\alpha = 1.74$ GeV/c/N is fitted very well by the theoretical curves for $x_F \geq 0.2$. In the region $x_F \leq 0.2$ there are contributions from more complicated rescattering processes which are not included. One observes that direct fragmentation dominates the cross section at $p_T = 0$. However, the hard-scattering cross section dominates the quasielastic peak at $p_T = 0.3$ GeV/c. It is clear that a combination of the two processes is needed to fit the data.

We show in Fig. 3 the experimental invariant cross section in the transverse direction when the detected proton has a momentum of 1.75 GeV/c. The solid curve is the theoretical result which is the sum of the direct fragmentation and the hard-scattering components. As one observes, the experimental data are well explained as a combination of these two processes. One also observes how, as a function of increasing p_T, the direct fragmentation process diminishes its importance while the hard-scattering process becomes more important. The cross-over occurs at $p_T \sim 0.2$ GeV/c.

From the present analysis, a semiempirical nuclear momentum distribution for a proton in ^{4}He is obtained. In the frame in which the center of mass of ^{4}He is at rest this distribution is shown as the solid curve (Fig. 4). The other curves are from the theoretical results of Zabolitzky and Fabre. Curves labeled HJ, RSC, and SSCB are theoretical results which include the effects of nuclear correlation and the curve labeled UNC comes from an independent particle model where the nucleons are not correlated. The presence of nuclear correlation is indicated by a change of slope in $\ln n(p)$. Indeed, the nuclear

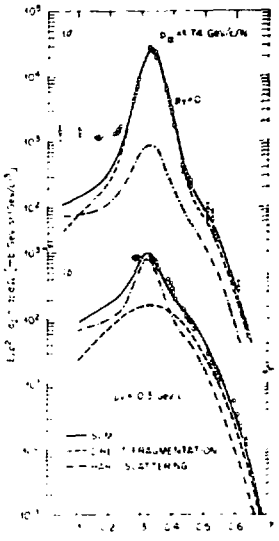

Fig. 2. Experiment invariant cross section for the reaction $\alpha + {}^{12}C \rightarrow p+X$ at $p_\alpha = 1.74$ GeV/c/N as a function of $x_F = (p_{//}/p_{max})_{c.m.}$

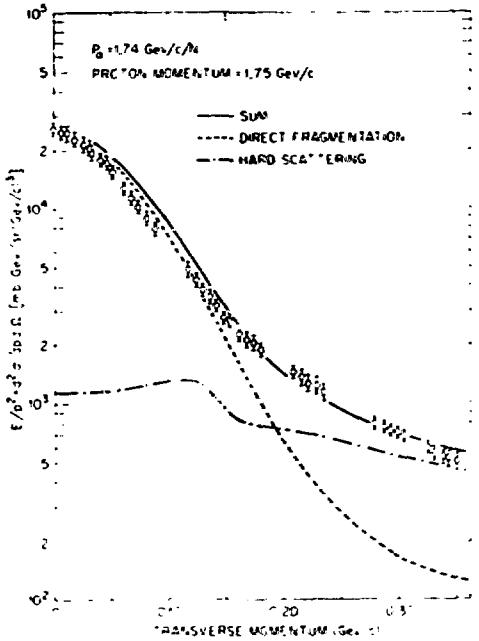

Fig. 3. Experimental invariant cross section for the reaction $\alpha + {}^{12}C \rightarrow p+X$ at $p_\alpha = 1.74$ GeV/c/N as a function of the transverse momentum.

momentum deduced from the present analysis shows a change in the slope of log n(p) which may be taken as a possible evidence for the presence of nuclear correlation. However, the distribution has a narrower width compared with the theoretical distribution. The semiempirical momentum distribution is also narrower than expected for ^{12}C. This indicates that the observed semiempirical momentum distribution may have been subject to a distortion due to the final-state interactions between the observed proton and its complementary partner which suffers a collision with the target. More work is needed to separate our final-state interactions in order to obtain the "true" momentum distribution from the semiempirical distribution.

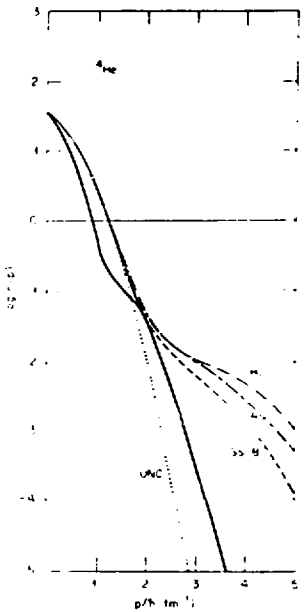

Fig. 4. The extracted semi-empirical momentum distribution for ^{4}He (solid curve) compared with theoretical distributions.

References

1. R. D. Amado and R. M. Woloshyn, Phys. Rev. C15, 2200 (1977).
2. J. G. Zabolitzky and W. Ey, Phys. Lett. 76B, 527 (1978).
3. I. A. Schmidt and R. Blankenbecler, Phys. Rev. D15, 3321 (1977).
4. L. M. Anderson, Ph.D. Thesis, University of California, Berkeley, California, 1977, LBL-6769; L. M. Anderson, et al., LBL-9493, 1979.

SCALING PHENOMENON IN RELATIVISTIC NUCLEUS-NUCLEUS COLLISIONS*

Cheuk-Yin Wong
Oak Ridge National Laboratory
Oak Ridge, TN 37830

and

R. Blankenbecler
Stanford Linear Accelerator Center
Stanford, CA 94305

Abstract

We introduce new scaling variables for proton and pion production in relativistic nucleus-nucleus collisions which are the generalizations of the Feynmann scaling variable. They allow a simple description of the cross sections at the forward and backward angles.

* * * *

Recent experimental and theoretical studies[1-6] of nucleus-nucleus collisions in the energy range of a few GeV per nucleon indicates that the use of the Feynmann variable x_F should lead to scaling in the case of forward pion production.[1,2] However, x_F scaling was not observed in proton production[3,4] or in backward pion production.[5] It is desirable to look for new scaling variables so that the experimental data can be better represented and the underlying physics of the scaling phenomenon understood.

The proper scaling variable depends on the reaction mechanism. In the reaction A+B → C+X, the two dominant processes[7] of interest are the direct fragmentation and the hard-scattering process. In the direct projectile fragmentation process the subsystem C is emitted directly from the beam particle B without scattering, while the complementary partner interacts with the target nucleus A. The cross section is proportional to the probability $G_{C/B}(x_D, \vec{p}_T)$ of finding a subsystem C in the projectile B with transverse momentum $\vec{p}_T$ and fractional momentum x_D defined by

$$x_D = \frac{C_o + C_z}{B_o + B_z} = x_F \, x_{max} \tag{1}$$

where we have used A, B, and C to denote also the four-vectors of A, B, and C, respectively. In terms of the relativistic invariant $s = (A+B)^2$ and the usual λ-function,[2] we have

$$x_{max} = \frac{s - D^2 + C^2 + \lambda(s, D^2, C^2)}{s - A^2 + B^2 + \lambda(s, A^2, B^2)} \tag{2}$$

and D is the missing mass of X. Thus, x_D is a good "direct fragmentation"

*Research jointly sponsored by the Division of Basic Energy Sciences, U.S. Department of Energy, under contract W-7405-eng-26 with the Union Carbide Corp., and by the U.S. Department of Energy under contract DE-AC03-76SF00515.

scaling variable when the direct fragmentation process dominates and when the bombarding energy is high enough. We show in Fig. 1 the experimental data of Anderson, et al.[3] for the reaction $\alpha + {}^{12}C \to p+X$. As one observes, the experimental data scales with x_D when $x_D \geq 0.20$ and $p_\alpha \geq 1.74$ GeV/c/N, for different values of p_T. The analogous scaling variable x_D for target

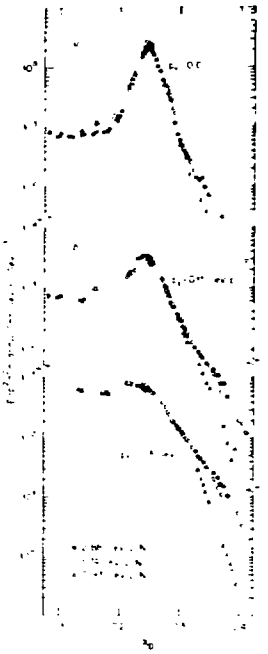

Fig. 1. Experimental invariant cross section for $\alpha + {}^{12}C \to p+X$. Data are from Ref. 3.

fragmentation can be obtained from Eqs. (1) and (2) by replacing $C_Z \to -C_Z$, $x_F \to |x_F|$ and interchanging $B_o \leftrightarrow A_o$, $B_Z \leftrightarrow -A_Z$. The experimental data[4] for backward proton production also scales well with x_D for target fragmentation.

In the hard-scattering process, the target A and projectile B emit subsystems a and b which scatter to produce particle C via the basic process a+b → C+d. Upon examining the six-fold hard-scattering integral,[2] one finds that for projectile fragmentation the integral depends predominantly on the variable

$$x_H = \frac{\gamma^2 + \sqrt{\gamma^4 - b^2(u'+C_T^2)}}{u' + C_T^2}\left[\frac{m_a(A_o+A_Z)}{m_A(B_o+B_Z)} - x_D\right] \quad (3)$$

where

$$\gamma^2 = \tfrac{1}{2}[d^2 - a^2 - u'] \quad (4)$$

and

$$u' = (m_a A/m_A - C)^2. \quad (5)$$

For target fragmentation, the corresponding variable is obtained by replacing $C_Z \to -C_Z$, and interchanging $a \leftrightarrow b$, $A_o \leftrightarrow B_o$, $A_Z \leftrightarrow -B_Z$.

As a pion is *not a normal constituent* of a nucleus, we consider pions to be produced only by the hard-scattering mechanism. The experimental data should scale with the "hard-scattering" scaling variable x_H. Indeed, when the data of p + Cu → p+X (180°) are plotted with respect to x_H, we see that the experimental data scales well with x_H (Fig. 2), in contrast to the absence of scaling with respect to x_F observed earlier.[5,6] For forward pion production, the experimental data of $\alpha + {}^{12}C \to \pi^- + X$ also scale with x_H. In this case, x_H is approximately equal to x_F in the region of interest and thus there is also x_F scaling for forward pion production.[1]

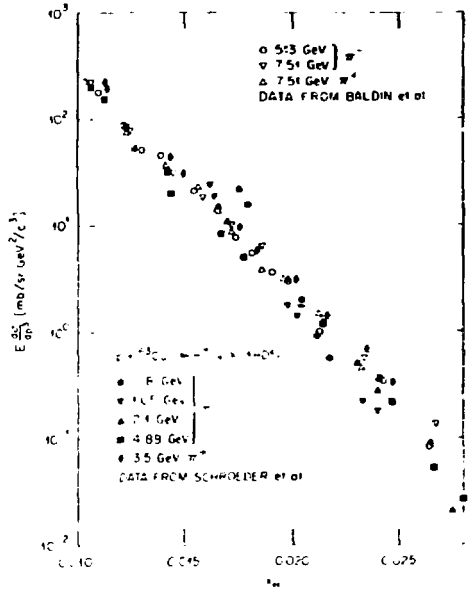

Fig. 2. Experimental invariant cross section for p + Cu → $\pi^{\pm}$+X (180°). Data are from Refs. 5 and 7.

In proton production the hard-scattering process becomes more important as $p_T >> 0.1$ GeV/c. However, in this case $x_H \approx x_D$, and hence, x_D scaling persists even for large values of x_D as we observe in Fig. 2.

It is easy to show that in the projectile fragmentation region, x_D and x_H approaches x_F when $s >> D^2 - A^2$ and in the target fragmentation when $s >> D^2 - B^2$. We see that x_D and x_H are simple generalizations of x_F for the case when the rest masses are not small compared to s.

In conclusion, we have obtained scaling variables which allow the experimental data to scale properly for proton and pion production at the forward and backward angles. Their introduction also clarifies the underlying physics of the scaling phenomenon in nucleus-nucleus collision.

References

1. J. Papp, Ph.D. Thesis, University of California, Berkeley, 1975, LBL-3633; J. Papp, et al., Phys. Rev. Lett. 34, 601 (1975).

2. I. A. Schmidt and R. Blankenbecler, Phys. Rev. D15, 3321 (1977).

3. L. M. Anderson, Jr., Ph.D. Thesis, University of California, Berkeley, 1977, LBL-6769; L. M. Anderson, et al., LBL-9493, 1979.

4. J. V. Geaga, et al. (private communication).

5. L. S. Schroeder, et al., Phys. Rev. Lett. 43, 1737 (1979).

6. R. H. Landau and M. Gyulassy, Phys. Rev. C19, 149 (1978).

7. C. Y. Wong and R. Blankenbecler (to be published and contributed paper to this Workshop).

8. A. M. Baldin, et al., Yad. Fiz. 20, 1201 (1974) [Sov. J. Nucl. Phys. 20, 629 (1975)].

PION CONDENSATION IN A THEORY CONSISTENT WITH BULK PROPERTIES OF NUCLEAR MATTER*

Norman K. Glendenning

Lawrence Berkeley Laboratory, University of California
Berkeley, CA 94720

The theory of nuclear matter at densities higher than normal has acquired particular interest in the last few years, in the context both of astrophysics and relativistic nuclear collisions. At energy densities above normal, new excitations become possible in principle, involving additional particles or field configurations than are present in the normal state. Several such excitations have been studied, known popularly as pion condensate and abnormal or density isomeric states.[1]

In general these states have been discussed in the framework of theoretical models that make little contact with the known bulk properties of nuclei, in particular their saturation energy, density and compressibility. The condensate energy has been calculated as the difference in energy between a state of the theory with and without a condensate. The large discrepancy between the theory and the properties of nuclear matter are assumed to cancel in the subtraction, yielding it is hoped, a reliable estimate of the condensate energy.

This paper makes three contributions to the theory of abnormal states of matter.

1) We have formulated and solved, in a self-consistent mean field approximation, a field theory that possesses condensate states, and reproduces at the same time the three important bulk properties of the normal state.

2) The theory is solved in its relativistically covariant form.

3) A continuous class of pion fields having a space-time dependence is constructed for which the theory can be solved.

We investigate in this paper the implications of self-consistency for the existence of condensate solutions, as well as the dependence of the condensate energy on the nuclear equation of state when the condensate energy does exist.

Formulation

Our starting point is a relativistic field theory like Walecka's[2] with potential terms as studied by Boguta and Bodmer.[3] The ingredients of the theory are a chargeless scalar and vector meson with Yukawa coupling to the neutron and proton fields. The scalar meson is responsible for binding, while the vector meson leads to repulsion at short distance and hence saturation. Nonlinear terms in the field equation for the scalar meson are introduced to reduce the high compressibility of Walecka's theory to an accepted range around $K \sim 250$ MeV. To this theory we add the pions, which are represented by a three component pseudo-scalar field. They can couple to the nucleons by

*Done in collaboration with B. Banerjee and M. Gyulassy.

pseudo-scalar or pseudo-vector coupling. We use the pseudo-vector coupling because it does not possess the unphysically large s-wave interactions of pseudo-scalar coupling, yet leads to the correct p-wave interaction.

The Euler-Lagrange equations derivable from the above described theory are for the scalar, vector, pi mesons and nucleons respectively,

$$(\Box + m_s^2)\sigma = g_s \bar{\psi}\psi - \frac{dU}{d\sigma} \tag{1}$$

$$\partial^\nu(\partial_\mu V_\nu - \partial_\nu V_\mu) = m_v^2 V_\mu - g_v \bar{\psi} \gamma_\mu \psi \tag{2}$$

$$(\Box + m_\pi^2)\underset{\sim}{\pi} = g_\pi \partial^\mu(\bar{\psi}\gamma_5\gamma_\mu \underset{\sim}{\tau}\psi) \tag{3}$$

$$\left(i\partial\!\!\!/ - (m_N - g_s\sigma) - g_v V\!\!\!/ - g_\pi \gamma_5 \gamma^\mu \underset{\sim}{\tau} \cdot \partial_\mu \underset{\sim}{\pi}\right)\psi = 0 \tag{4}$$

$\psi = \begin{pmatrix} P \\ N \end{pmatrix}$, P = 4-component spinor, $\pi = (\pi_1, \pi_2, \pi_3)$

(Slashed quantities denote $a\!\!\!/ \equiv \gamma_\mu a^\mu$). The form of the potential is

$$\frac{dU}{d\sigma}(\sigma) = (bm_N + cg_s\sigma)(g_s\sigma)^2 \tag{5}$$

The parameters are five in number,

$$g_\pi, \left(\frac{g_s}{m_s}\right), \left(\frac{g_v}{m_v}\right), \quad b, \; c$$

The last four are used to generate a desirable equation of state in the absence of a pion condensate. One can think of three of them as being used to define the saturation energy, density and compressibility, and the fourth as determining how soft the equation of state is at high density, as defined for example, by the density at which the binding is zero. We have studied two cases, for which this density is $\sim 2\rho_0$ and $\sim 3\rho_0$.

We solve the field equations in the mean field approximation. The nuclear source currents on the right side are replaced by their ground state expectation values. For infinite homogeneous nuclear matter $\langle \bar{\psi}(x)\, \psi(x) \rangle$ and $\langle \bar{\psi}(x)\gamma_\mu \psi(x) \rangle$ are independent of x. Therefore the σ and V_μ fields are constants which we write as $\bar{\sigma}$ and $\bar{V}_\mu$. These values can be read from the equations of motion as

$$m_s^2 \bar{\sigma} = g_s \langle \bar{\psi}\psi \rangle - \left\langle \frac{dU}{d\sigma} \right\rangle , \qquad m_v^2 \bar{V}_\mu = g_v \langle \bar{\psi}\gamma_\mu \psi \rangle \tag{6}$$

As in other studies,[1] we shall also treat the pions as classical fields whose mean values have a certain space time-dependence. A charged running wave condensate

$$\langle \pi_{\pm} \rangle = \bar{\pi}_c \, e^{\pm ikx} , \quad \langle \pi_0 \rangle = 0 , \qquad kx = k_\mu x^\mu = k_0 x_0 - \underset{\sim}{k} \cdot \underset{\sim}{x} \tag{7}$$

is the functional form that has been studied previously. Boguta has pointed out to us that if we can solve our problem with the above ansatz, then it is also possible to do so for a standing wave

$$\langle \pi_{\pm} \rangle = \bar{\pi}_c \sin kx, \qquad \langle \pi_0 \rangle = \bar{\pi}_c \cos kx \tag{8}$$

Actually both of these are special cases of a continuous class of fields defined by

$$\underset{\sim}{\tau} \cdot \underset{\sim}{\pi}(kx) = \sqrt{2}\, \bar{\pi}_c \, \underset{\sim}{S_v}(kx) \underset{\sim}{\tau} \cdot \underset{\sim}{u} \, \underset{\sim}{S_v}^{+}(kx) \tag{9}$$

where S_v is a unitary operator in isospin space

$$\underset{\sim}{S_v}(kx) = e^{-\frac{i}{2} kx \, \underset{\sim}{\tau}\cdot\underset{\sim}{v}} , \qquad \underset{\sim}{u} \cdot \underset{\sim}{v} = 0 \tag{10}$$

Here $\underset{\sim}{u}$ and $\underset{\sim}{v}$ are unit vectors. After some algebra (9) is found to imply

$$\underset{\sim}{\pi}(kx) = \sqrt{2}\, \bar{\pi}_c \, (\underset{\sim}{u} \cos kx + \underset{\sim}{v} \times \underset{\sim}{u} \sin kx) \tag{11}$$

The Dirac equation that we have to solve is (4) with the σ, V and π fields replaced by the mean values (6, 9-11). In particular

$$\underset{\sim}{\tau} \cdot \partial_\mu \underset{\sim}{\pi} = \sqrt{2}\, \bar{\pi}_c \, k_\mu \, \underset{\sim}{S_v} \, \underset{\sim}{\tau} \cdot \underset{\sim}{v} \times \underset{\sim}{u} \, \underset{\sim}{S_v}^{+} \tag{12}$$

Under the (linear local gauge) transformation

$$\psi = S_v \, \psi_v \tag{13}$$

the Dirac equation is transformed to

$$\left[i\partial - (m_N - g_s \bar{\sigma}) - g_v \bar{V} + \underset{\sim}{\tau}\cdot\left(\frac{1}{2}\underset{\sim}{v} + \sqrt{2}\, g_\pi \, \bar{\pi}_c \, \gamma_5 \, \underset{\sim}{v}\times\underset{\sim}{u}\right) \right] \psi_v = 0 \tag{14}$$

The Dirac operator is by means of this transformation reduced to a finite matrix operator (dimension 8) with no x-dependent terms. Unlike the usual free particle Dirac equation, the spectrum is more complicated than $\sqrt{\underline{p}^2 + m^2}$. In fact the eigenvalues are functions of the field strengths $\bar{\sigma}$, $\bar{V}_0$ and $\bar{\tau}_c$ and of the pion momentum $\underline{k}$, as well as the nucleon momentum $\underline{p}$, and the Fermi surface does not have the usual spherical symmetry but instead is cylindrically symmetric about the direction $\underline{k}$, sometimes consisting of two unconnected regions of momentum. It can be shown that for all fields (9) the energy is degenerate.

It can be verified that the assumed space-time dependence of the pion fields is compatible with their field equations (3), and that $\bar{\tau}_c$ is constrained by the equation

$$(-k_\mu^2 + \underline{k}^2 + m_\pi^2)\,\bar{\tau} - \bar{\tau}_c = -g_\pi\,(\bar{\psi}\gamma_5\,\underline{k}\cdot\underline{\tau}\,\psi) \qquad (15)$$

Now the self consistency problem can be stated. The nucleon fields depend on the mean values of the meson fields through (14). Therefore the source currents of the mesons are implicit functions of the meson mean fields themselves. Because both the momentum p_μ and the vector field V_μ occur in the Dirac equations like $\gamma_\mu(p_\mu - g_v V_\mu)$, the vector field merely produces a shift in the four vector momentum. It is not involved in the self consistency. The remaining field strengths σ and τ_c are coupled and equations (6) and (15) must be solved simultaneously for their self-consistent values. The locus of solutions in the σ, τ_c plane are shown in Fig. 1. As can be imagined and as the figure illustrates, the occurrence of simultaneous solutions for arbitrary density, k and g_π is not assured. Rather they exist only over a limited range.

Results

We have studied condensate solutions for two sets of parameters which yield acceptable equations of state for nuclear matter. They differ in that one is softer at high density, than the other but both yield acceptable values of saturation energy, density, and compressibility.

For both of these we have studied the self-consistent condensate solutions for several values of the coupling constant g_π. The non-relativistic equivalence of the pseudo-vector coupling g_π and pseudo-scalar coupling constant g_0 is $g_\pi = g_0\,(2m_N)$. For the standard value $g_0^2/4\pi = 14$ this gives $g_\pi = 1.41$ fm.

In Figs. 2 and 3 we show the two equations of state without a condensate ($\tau_c = 0$). In each case there are self-consistent condensate solutions some of which are shown, corresponding to several values of g_π and for $k = 1.5$ fm^{-1}, which minimizes the energy. Since it is doubtful that there is a condensate in the normal state, an acceptable equation of state is one which, if there is a condensate at all, it occurs at densities larger than the saturation density. There are such solutions, and they occur for a narrow range of the coupling constants g_π which depends on the softness of the equation of state. Roughly these ranges are

$$1.17 < g_\pi/\text{fm} < 1.2\,; \qquad 1.0 < g_\pi/\text{fm} < 1.15$$

for the stiffer and softer equations of state shown. For values less than the

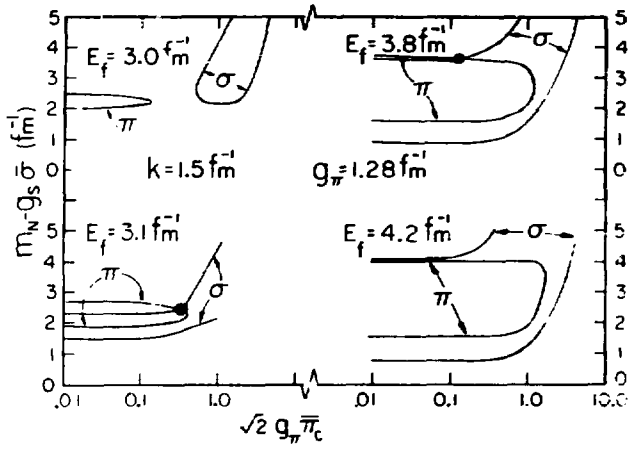

Fig 1. Locus of solutions for σ and π equations for four Fermi energies showing the existence of common self-consistent solutions in a limited range of Fermi energy (related to density).

lower limit, solutions do not exist over the range of densities shown. Effectively for the stiffer equation of state, the condensate energy is zero. For the softer equation, the condensate energy is small and does not exceed about 10 MeV at $\rho \sim 3\rho_0$. This is in sharp disagreement with estimates based on the π model for which the condensate energy is ~30 MeV at this density, and is a very strongly increasing function of density.

A glance at Figs. 2 and 3 reveals a strong dependence of condensate energy on modest variations in the equation of state. This implies that a reliable estimate of the condensate energy cannot be made unless the theory is consistent with the bulk properties of nuclear matter.

Summary

We have solved a relativistic field theory of nuclear matter for the self-consistent field strengths in the mean field approximation. The theory is constrained to reproduce the bulk properties of nuclear matter. We find that a weak pion condensate is compatible with this constraint. At least this is encouraging as concerns the possible existence of a new phase of nuclear matter. In contrast the Lee Wick density isomer is probably not compatible with the properties of nuclear matter.[3,4]

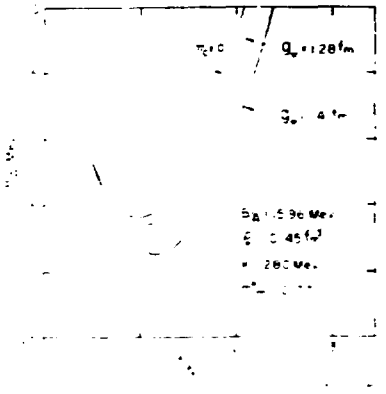

Fig. 2. Binding energy as a function of density in the absence of a pion condensate ($f_c = 0$) and for several self-consistent condensate solutions. The coupling constants and potential parameters are $g_S/m_S = 15/m_N$, $g_V/m_V = 11/m_N$, $b = 0.004$, $c = 0038$, where $m_N = 4.77$ fm^{-1} is the nucleon mass. The pion momentum that minimizes the energy is $k = 1.5$ fm^{-1}.

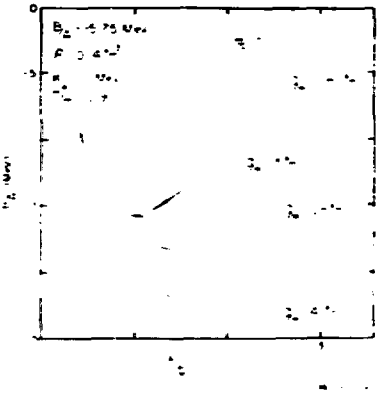

Fig. 3. As Fig. 2 but $g_S/m_S = 9/m_N$, $g_V/m_V = 5/m_N$, $b = -0.192$, $c = 2.47$.

References

1. Cf. reviews by D. K. Campbell, in Nuclear Physics with Heavy Ions and Mesons Vol. 2, ed. by Balian, Rho, and Ripka (North-Holland, 1978) p. 549; G. Baym, op. cit., p. 745.

2. J. D. Walecka, Annals of Physics 83 (1974) 491.

3. J. Boguta and A. R. Bodmer, Nucl. Phys. A292 (1977) 413.

4. A. K. Kerman and L. D. Miller, in Proc. 2nd High Energy Heavy Ion Summer Study, (Lawrence Berkeley Lab. report 3675, 1974) p. 73; C. G. Källman and S. A. Moszkowski, Phys. Lett. 57B (1975) 183; Nucl. Phys. A287 (1977) 495.

LOW ENERGY PIONS AND DENSITY EVOLUTION IN RELATIVISTIC NUCLEAR COLLISIONS[†]

J. Cugnon[††] and S. E. Koonin[†††]

W. K. Kellogg Radiation Laboratory, Caltech, Pasadena, CA 91125

The recent discovery of differences in the π^+ and π^- yields at $\theta_{lab} = 0°$ [1] as well as the observation of different low energy π^+ and π^- spectra in relativistic nucleus-nucleus collisions raise the possibility that such data are sensitive to the matter density distribution during the collision process. There is no way at present to extract such information from proton inclusive cross sections. In a symmetric N = Z system, π^+/π^- differences arise solely from electromagnetic forces and reflect, in principle, the properties of the charge distribution after the pion is created. We report here on some aspects of a classical calculation of these phenomena.

1. Model for the collision process. The nuclear collision is pictured as a succession of relativistic, on-shell, binary, baryon-baryon collisions. The evolution of the system is calculated by means of a Monte-Carlo method [2], which embodies the following important features: (i) relativistic kinematics, (ii) empirical elementary cross sections, (iii) pionic degrees of freedom are accounted for by allowing Δ-production, (iv) Δ's are considered stable against pion emission until the end of the collision process; they may, however, be destroyed in collisions with nucleons. This last point is a reasonable approximation given the present knowledge of the behavior of Δ resonances in nuclear matter [3].

The present model is a very successful parameter-free description of inclusive cross sections (see fig. 1) and two proton correlations at 800 MeV/A [4].

2. Matter distribution. During the collision process, our calculation reveals that the matter can be compressed substantially ($\rho \approx 2\rho_0$) and then expands rapidly. However, pions should not be sensitive to these early stages of the process. At the end of the collision process and at later times, the calculated matter (and charge) distribution of a symmetric system can be

---

[†]Supported in part by NSF grants PHY77-[illegible] and PHY[illegible].

[††]Permanent address: University of Liège, Institut de Physique, B-[illegible] Sart-Tilman, Belgium.

[†††]Alfred P. Sloan Foundation Fellow.

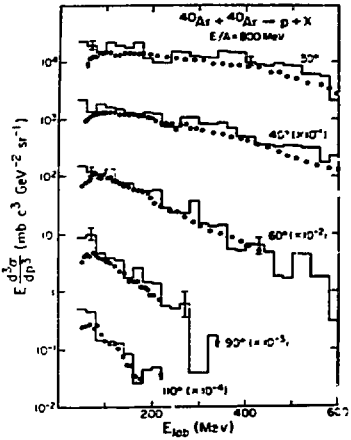

Fig. 1. Invariant proton cross section for Ar + Ar at 800 MeV. The dots are the experimental values and the histograms are the result of the calculation.

fairly well parametrized as

$$\rho(\vec{r},t) = \frac{Q_0}{(r_0^2\pi)^{3/2}} \exp\left(-\frac{r^2}{r_0^2}\right) + \frac{(q-Q_0)}{2} \frac{\gamma}{(a\sqrt{\pi})^3} \left\{ \exp\left[-\frac{(x-x_0)^2 + y^2 + \gamma^2(z-z_0-vt)^2}{a^2} \right] \right.$$

$$\left. + \exp\left[-\frac{(x+x_0)^2 + y^2 + \gamma^2(z+z_0+vt)^2}{a^2} \right] \right\}.$$

Here, q is the total charge of the system, v is the initial velocity in the c.m. frame, and γ is the corresponding Lorentz factor. The beam direction is $\hat{z}$ and the impact parameter is along $\hat{x}$. By fitting this form to the Monte Carlo calculations at each time for a given impact parameter, we find that the participant charge, Q_0, is almost independent of time, while r_0, x_0 and a are linear functions of time. These results support qualitatively the participant-spectator model, except that they predict an expansion of the three parts of the system. Typical expansion velocities are $v_{r_0} \approx 0.4$ and $v_a \approx 0.2$. Q is

close to that predicted by a "clean cut" geometry, except at small impact parameters, where it is somewhat smaller.

3. Electromagnetic effects on the pion spectrum. Let $S(\vec{r},t,b,\vec{p}_i)$ be the source function for creating pions of momentum $\vec{p}_i$ at space-time point $(\vec{r},t)$ in a collision at impact parameter b. The inclusive cross section will be [5]

$$E_f \frac{d^3\sigma}{dp_f^3} = \sum_{\vec{p}_i} \int d^3r \int dt \int d^2b\, S(\vec{r},t,b,\vec{p}_i) \frac{E_f}{E_i} \left| \frac{d^3p_i}{d^3p_f} \right| ,$$

where $\vec{p}_f$ is the final asymptotic momentum after experiencing the electromagnetic field. We have calculated this integral by a Monte Carlo method, sampling the initial value of $\vec{p}_i,\vec{r},t,b$ and solving classical equations of motion in order to find $\vec{p}_f$. The pion source has been factored into functions depending upon each of the arguments. The spatial and impact parameter dependences of the source are described by gaussians, whose parameters are consistent with those of the participant charge distribution at the instant of Δ-decay. The time dependence of the source is taken to be a delta function in time, assuming that the pions are released at the end of the strong interaction process. This is in keeping with the above-mentioned picture of long-lived delta resonances which decay at the end of the decompression stage. The momentum dependence of the pion source is assumed to be thermal (with temperature T), or direct (i.e., related to the N + N → π + N + N data) or a combination of both.

Fig. 2 shows the results for Ar + Ca → π^+ + x at 1.85 GeV. The lines are contours of constant invariant cross sections. The upper left corner shows an undistorted thermal distribution with T = 70 MeV. The distorted cross sections corresponding to different initial spectra as shown in the rest of the figure: Upper Right, the thermal spectrum; Lower Right, Lower Left, two mixtures of thermal and direct spectra, respectively 6% and 8% thermal. The electromagnetic forces produce a depression in the low energy region and therefore a maximum at 90° near $p_\perp \approx m_\pi c$. The position of the peak is sensitive to the initial spectrum. Comparison with experiment [6] would favor a highly thermal initial spectrum, as far as the location of the maximum is concerned. However, the shape of the contour lines near this maximum is not well reproduced. Beyond the region experimentally investigated for this system, we predict a depletion of the pion yield at 0° and 180° at rapidities

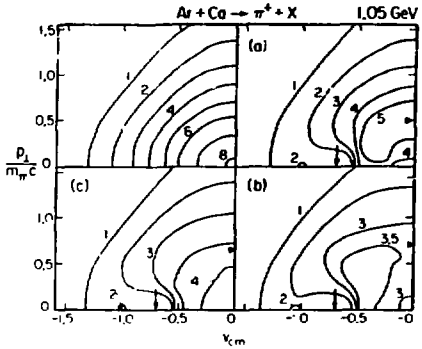

Fig. . Calculated invariant π⁺ cross sections for Ar + Ca at 1.05 GeV. Normalization is arbitrary. Triangles indicate a maximum and arrows indicate the initial c.m. rapidity.

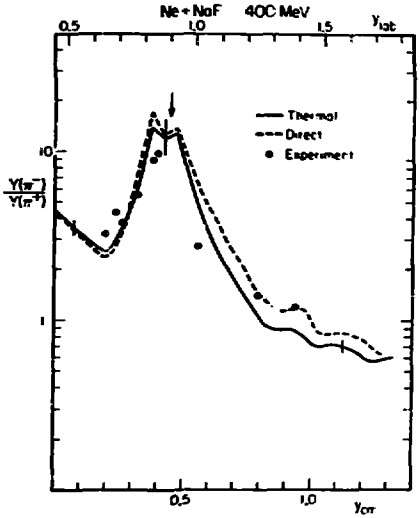

Fig. . Ratio of the π⁻ to π⁺ yield at 90° for Ne + NaF at E/A = 400 MeV.

slightly beyond the incident c.m. rapidity. This is consistent with the measured ratio of π^- to π^+ yields at 90° for Ne + NaF at 400 MeV [1], as Fig. 2 strikingly shows. We find, remarkably, that this ratio is fairly independent of the initial pion spectrum. Negative pions are "captured" by the spectator parts of the system travelling with the incident velocity. Thus, it is very likely that π-mesic atoms are formed in relativistic nucleus-nucleus collisions.

Although there is some uncertainty in the pion source and a classical treatment may be suspect in some regions of phase space, our calculations have revealed that the low energy pion cross sections are sensitive to the evolution of the charge distribution after the strong interaction process. In particular:

(1) the height and the shape of the peak in the π^-/π^+ ratio at 90° are

sensitive to the spatial extent of the spectator part of the system, (2) the high-momentum π^-/π^+ ratio at 0^o depends upon the spatial charge distribution at the end of the strong interaction process, (3) the π^-/π^+ ratio at small momentum depends mainly upon the charge and expansion of the participant part.

We have not yet quantified these dependences and they deserve further attention. The location and the shape of the maximum in the π^+-spectrum at 90^o c.m. also depends upon the properties of the charge distribution, but is quite sensitive to the source parameters. The fact that we cannot reproduce the detailed shape of the maximum may indicate some unusual properties of the pion source.

References

[1] W. Benenson et al., Phys. Rev. Lett. 43 (1979) 683

[2] J. Cugnon, T. Mizutani and J. Vandermeulen, Kellogg preprint MAP-10 (1980)

[3] M. Hiruta, J. H. Koch, F. Lenz and E. J. Moniz, Phys. Rev. Lett. 70B (1977) 281

[4] J. Cugnon, Kellogg preprint MAP-9 (1980)

[5] K. Libbrecht and S. E. Koonin, Phys. Rev. Lett. 43 (1979) 1581

[6] K. L. Wolf et al., Phys. Rev. Lett. 42 (1979) 1448

TWO-PARTICLE CORRELATIONS IN HIGH ENERGY NUCLEAR COLLISIONS

Jörn Knoll* and Jørgen Randrup

Nuclear Science Division, Lawrence Berkeley Laboratory
Berkeley, CA 94720 USA

We discuss the correlations of two particles (proton-proton, proton-pion) in high energy nuclear reactions by means of the linear-cascade model (rows on rows).[1,2] It describes the observed cross sections in terms of contributions arising from dynamically independent groups of interacting nucleons. In addition to a correlated part where both observed particles arise from the same group, there is also a significant background contribution from the particles originating from two independent groups. The construction of the one and two particle spectral functions by means of a Monte Carlo simulation method allows the inclusion of various dynamical effects, such as the production of delta isobars or precritical scattering.

The presently available data[3] express the amount of correlation by a ratio R of the in-plane to out-of-plane coincidence cross sections registered in a tag counter and a spectrometer. Our initial studies indicate that not only the height of the quasi-elastic peak, but also its position in momentum space may be sensitive to the background term and to correlations arising from the sharing of energy and momentum among more than two particles.

Footnotes and References

*On leave of absence from Max Planck Institut für Kernphysik, Heidelberg, Germany; supported by the Heisenberg Stiftung, Germany

1. J. Hüfner and J. Knoll, Nucl. Phys. A290 (1977) 460.
   J. Knoll and J. Randrup, Nucl. Phys. A324 (1979) 445
   J. Randrup, Phys. Lett. 76B (1978) 547
2. J. Knoll, Phys. Rev. C 20 (1979) 773
   J. Randrup, Nucl. Phys. A316 (1979) 509
3. S. Nagamiya, et al., J. Phys. Soc. Japan 44, Suppl. (1979) 378, and I. Tanihata et al., to be published.

THE ROLE OF FINITE PARTICLE NUMBER EFFECTS IN HIGH-ENERGY HEAVY ION COLLISIONS†

Jörn Knoll††

Nuclear Science Division, Lawrence Berkeley Laboratory
Berkeley, CA 94720

During the last few years data of high-energy heavy-ion collisions have been observed that showed significant deviations from thermal predictions (fireball, firestreak). Due to the clean kinematical situation in equal mass systems, these deviations are even found in inclusive spectra[1]): i) anisotropy in CM frame → excludes fireball, ii) mass dependence of the asymptotic slopes and iii) a shouldering at low CM momenta (see fig. 3, below) → excluding firestreak. Are these deviations due to incomplete thermalisation (preequilibrium; strong knock-out) or hydrodynamical effects (compression, blast wave) or other dynamical effects?

As the thermal pictures applied rely on two assumptions i) complete memory loss (→ randomisation) and i) infinite particle number (→ bulk limit), we like to keep the first one but drop the unrealistic second one. By means of a simple phenomenological picture, the nuclear phase-space model[2]), we attempt an initial study of the role of finite particle number effects.

We adopt the simplifications of co-linear collision dynamics (rows on rows)[3]). There inclusive cross sections factorize into geometry coefficients $\sigma_{AB}(M,N)$ and spectral distributions $F_{MN}(\vec{p})$

$$\varepsilon \frac{d^3\sigma}{d^3p} = \sum_{MN} \sigma_{AB}(MN)\, F_{MN}(\vec{p}) \quad .$$

Here in a collision of the two nuclei, A and B, the observed particle (energy ε, momentum $\vec{p}$) results from a collision of M projectile nucleons with N target ones.

The geometrical weights $\sigma_{AB}(M,N)$ are shown in fig. 1 for unselected (inclusive) and selected (central) events. Clearly, for all reactions analyzed the major contributions arise from combinations with $M + N < 6$. This finding seems to cope with results of 3-dimensional cascade calculations[4]), which show a mean collision number per participating nucleon of 3 to 4.

Describing the spectral functions F_{MN} by the corresponding phase space functions $\phi_{MN}(p)$--these are the highest entropy distributions pertaining to a fixed number of particles--we expect significant deviations from the thermal limit ($M+N = \infty$) as the number of nucleons involved stays small, fig. 2.

As a matter of the finite particle number effects retained this way, we arrive at inclusive proton spectra, fig. 3, which precisely reproduce the desired features: the shouldering and the A-dependence of the asymptotic

slopes without any adjustment. The anisotropy of the spectra (e.f. fig. 4) solely arises from fluctuations in M and N (c.f., fig. 1) and results too large in central collisions. This might be due to some lack of transverse communication in this picture. The inclusion of pions[5]) leads to a slight cooling of spectra, an effect which has not been included here.

Altogether we see clear indications that finite particle number effects play a significant role in these reactions. Thus, caution is recommended when extracting temperatures (and this way energy expectation values) from asymptotic slopes of spectra. A study of finite particle number effects on correlations along similar lines has started recently[6]).

[1]) S. Nagamiya et al.. Phys. Lett. 81B (1979) 147, and submitted to Phys. Lett.
[2]) J. Knoll, Phys. Rev. C 20 (1979) 773.
J. Knoll, submitted to Nucl. Phys.
[3]) J. Hüfner and J. Knoll, Nucl. Phys. A290 (1977) 460.
J. Knoll and J. Randrup, Nucl. Phys. A324 (1979) 445
[4]) Y. Yariv and Z. Fraenkel, preprint 1979.
C. Noack, private communication.
[5]) S. Bohrmann and J. Knoll, these proceedings, and to be published.
[6]) J. Knoll and J. Randrup, these proceedings.

*Work supported by the Heisenberg Stiftung, Germany.

**On leave of absence from Max Planck Institut für Kernphysik, Heidelberg, Germany.

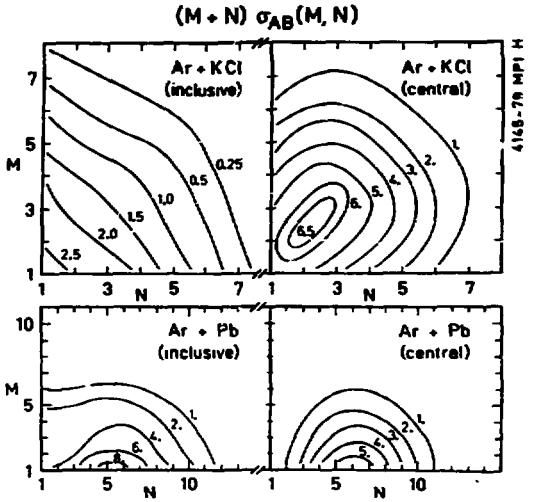

Figure 1: Contour plots of $(M+N)\sigma_{AB}(M,N)$ versus M and N for the reactions of Ar on K Cl and Ar on Pb. The values of the inclusive reactions are in barn, those of the central events in arbitrary units.

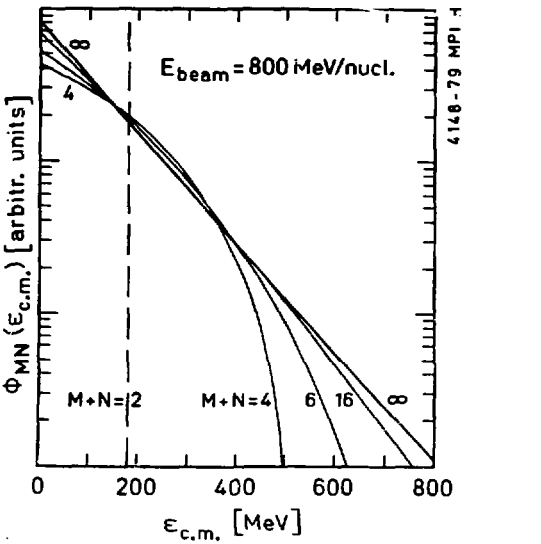

Figure 2: The one-particle spectrum $\Phi_{MN}(\varepsilon_{c.m.})$ as a function of the observed c.m. energy for cluster sizes of M+N = 2,4,6,16 and ∞. The mean c.m. energy per particle is 182 MeV (800 MeV/nucl. beam energy). The spike indicates the position of the δ-function of the M+N = 2 cluster.

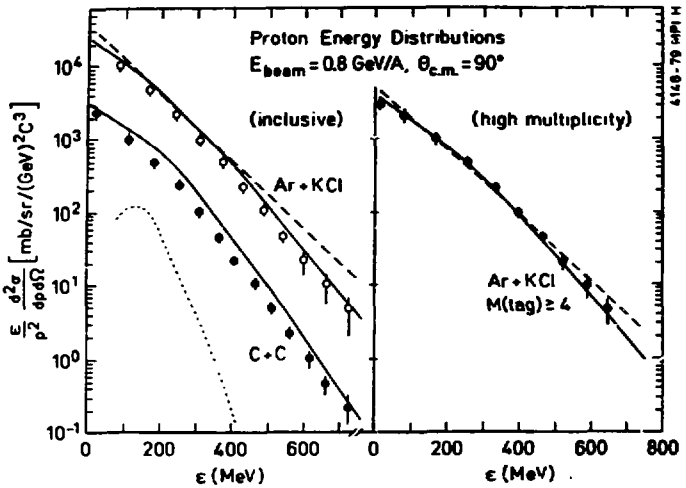

Figure 3: Proton energy spectra at 90° c.m. angle of mass symmetric reactions: a) inclusive spectra and b) spectra with associated high multiplicity compared to central collision calculations $\varepsilon\frac{d^3\sigma}{dp^3} = f^2(p)$. Our result in full lines, for comparison we plott for the Ar + KCl case the thermal limit result (dashed line). The knock-out contribution [illegible] dotted line is negligible in all cases. Data are from ref. [1].

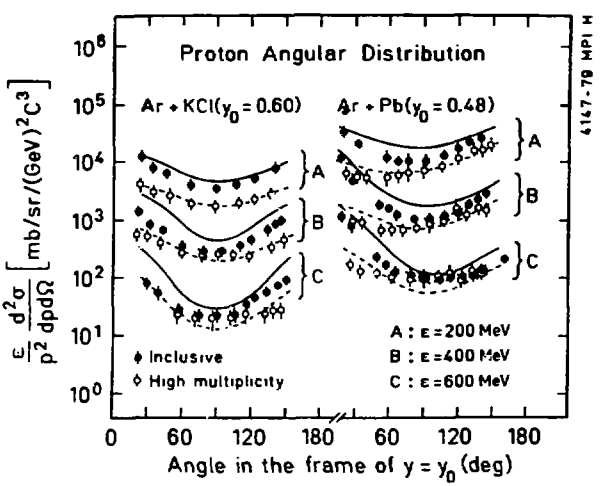

Figure 4: Proton angular distributions viewed from the c.m. frame of the central collision participant matter at rapidities Y_0, for three different c.m. energies of the observed protons. Full data points and full curves correspond to inclusive events, open data points and dashed curves to central collision events. The beam energy is 800 MeV/nucl. Data are from ref. [1].

CALCULATION OF NUCLEAR MASSES WITH A FOLDED-YUKAWA SINGLE-PARTICLE POTENTIAL AND A YUKAWA-PLUS-EXPONENTIAL MACROSCOPIC MODEL

Peter Möller and J. Rayford Nix

Theoretical Division, Los Alamos Scientific Laboratory
Los Alamos, New Mexico 87545

We use the folded-Yukawa single-particle potential[1] and the Yukawa-plus-exponential macroscopic model[2] to systematically calculate the ground-state masses of 4023 nuclei ranging from ^{16}O to $^{279}112$. The ground-state energy is determined by minimizing the total potential energy with respect to ε_2 and ε_4 shape coordinates. We also include an ε_6 shape coordinate, in the form of a prescribed dependence upon ε_2 and ε_4 that is determined by minimizing the macroscopic energy alone. The method is also used to calculate the fission-barrier heights of 28 nuclei ranging from ^{109}Cd to ^{252}Cf within the three-quadratic-surface parameterization.

We introduce several new physical effects, including a smaller nuclear-radius constant, a proton form factor, an exact diffuseness correction, an A^0 term, a charge-asymmetry term, and microscopic zero-point energies. The nuclear-radius constant is determined from elastic electron scattering and microscopic calculations of nuclear density distributions, the range of the Yukawa-plus-exponential folding function is determined from heavy-ion elastic scattering, the surface-energy constant and surface-asymmetry constant are determined from the fission-barrier heights of the 28 nuclei that are considered, and the remaining constants are determined from the ground-state masses of 1323 nuclei ranging from ^{16}O to ^{259}No for which experimental values are known with experimental errors less than 1 MeV.

For the final formula, we compare in Fig. 1 the experimental and calculated fission-barrier heights, for which the resulting root-mean-square error is 1.331 MeV. A similar comparison is made in Fig. 2 for the experimental and calculated ground-state microscopic energy, which is defined as the difference between the ground-state mass and the macroscopic value for a spherical shape. The resulting root-mean-square error in the masses is 0.835 MeV. These values are to be contrasted with a barrier root-mean-square error of 2.050 MeV and a mass root-mean-square error of 1.543 MeV for the original formula of Ref. 2, with the constants adopted there, when the same nuclei are considered.

The improved agreement between the calculated and experimental fission-barrier heights and ground-state masses for the present formula arises primarily because of a smaller surface-asymmetry constant and an A^0 term. Use of an exact diffuseness correction and microscopic zero-point energies are also fairly important. Some of the remaining discrepancies in the ground-state masses evident in Fig. 2 can be understood in terms of instabilities with respect to ε_3 and ε_6 deformations.

We are grateful to John W. Negele for his assistance with the smaller nuclear-radius constant, proton form factor, and charge-asymmetry term. This work was supported by the U. S. Department of Energy and the Swedish Natural Science Research Council.

References

1. P. Möller, S. G. Nilsson, and J. R. Nix, Nucl. Phys. A229, 292 (1974).

2. H. J. Krappe, J. R. Nix, and A. J. Sierk, Phys. Rev. C 20, 992 (1979).

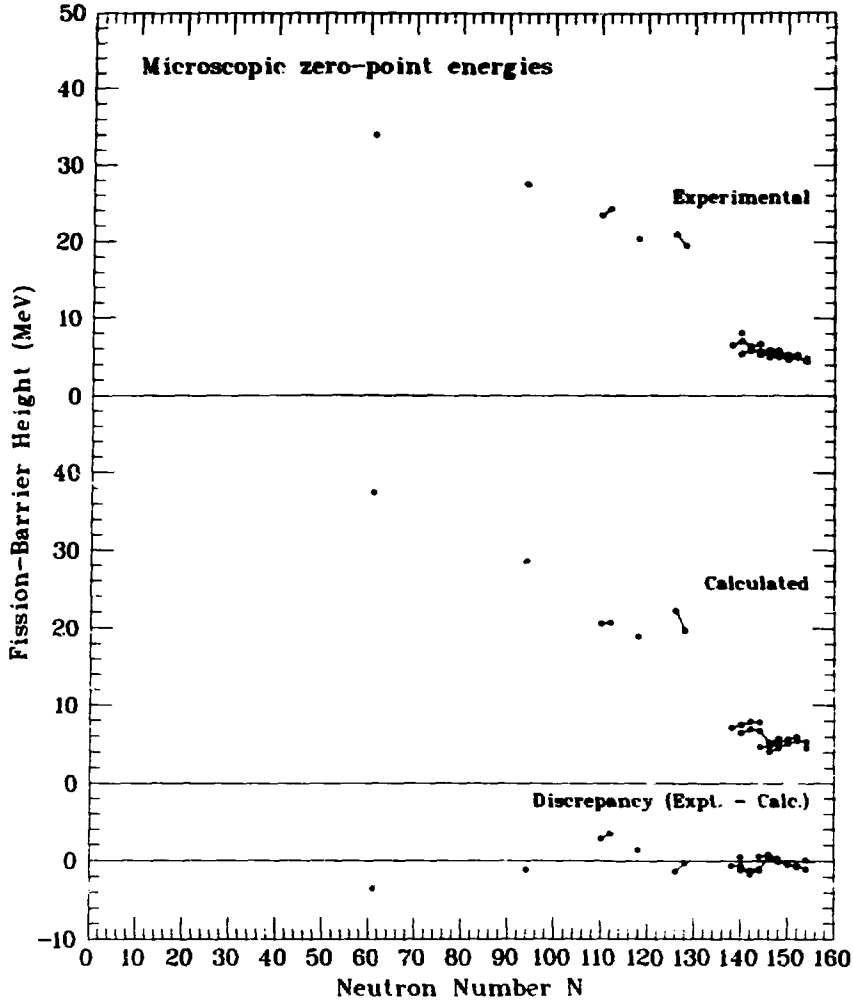

Fig. 1. Comparison of experimental and calculated fission-barrier heights for 28 nuclei. Isotopes are connected by lines.

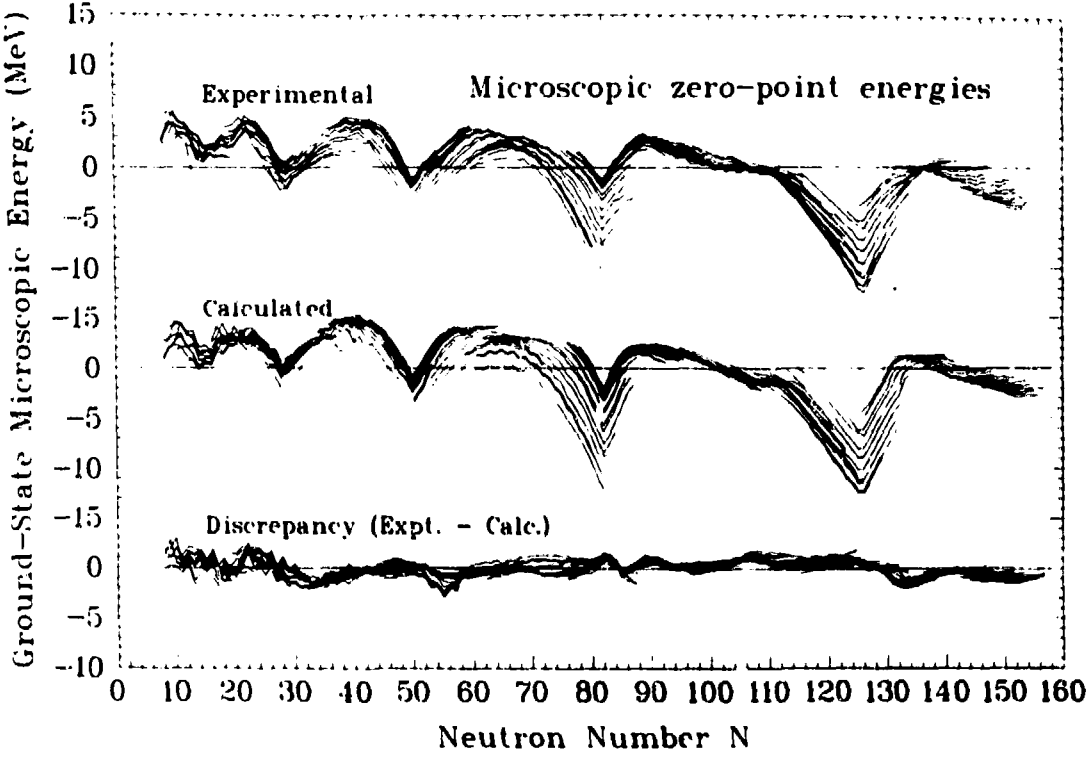

Fig. 2. Comparison of experimental and calculated ground-state microscopic energies for 1323 nuclei. Isotopes are connected by lines.

4π PHYSICS

A. Sandoval

Gesellschaft für Schwerionen forschung
Darmstadt, West Germany
and
Lawrence Berkeley Laboratory
Berkeley, CA 94720

Abstract

Exclusive π^- and charged-particle production in collisions of ^{40}Ar on KCl are studied at incident energies from 0.4 to 1.8 GeV/A. The correlation between the π^- and the total charged particle multiplicity confines the reaction along a narrow ridge with no exotic islands of pion production. For high multiplicities the system reaches the total disentegration of target and projectile into singly charged fragments and pions. Every 200 MeV/A data was taken with a central and inelastic trigger. For central collisions the mean π^- multiplicity increases linearly with the bombarding energy with no marked discontinuities due to the $\Delta(3.3)$ resonance. At 1.8 GeV/A evidence for nonthermal π^- production in central collisions is found. The total c.m. energy in π^- shows linear dependence on the π^- multiplicity with a slope of ϵ = 300 MeV/π^-. Strange particle production in the central collision of 1.8 GeV/A Ar on KCl is seen.

The natural framework for the description of high energy nucleus-nucleus interactions, above the pion production threshold is given by the quark model. For example the production and decay of the $\Delta(3,3)$ isobar, the most important inelastic channel up to bombarding energies of several GeV/A, is described by the quark exchange between two nucleons with the coupling of the quarks in one of them to $I = 3/2$; the decay occurs by the emission of one quark from the Δ and the quark antiquark production from the vacuum to form a nucleon and a pion (Fig. 1). The families of excited states of the nucleon N^*, Δ and strange bayons are higher angular momentum states in the coupling of three quarks; u's and d's coupled to $I = 1/2$ for the N^*, u's and d's coupled to $I = 3/2$ for the Δ and u's and d's with one strange quark s for the strange bayons Λ's and Σ's. Correspondingly the mesons are quark antiquark pairs. The energies at which these states can be formed in an NN collision are given in Fig. 2. At these energies the πN cross sections[1] vary by a factor of 10 resulting in a very energy dependent pion mean free path in nuclear matter.

The aim of this work[2] is to study the energy dependence of the isobar and meson production in central collisions of an equal mass system (Ar + KCl) from below the $\Delta(3,3)$ resonance up to the highest Bevalac energies. Exclusive measurements of all the reaction products are necessary in order to measure the energy flux in pions, the energy flux in certain parts of phase space, to obtain invariant masses to extract isobar decays and search for exotic states with baryon number greater than 1, and to do two and many particle correlations.

At the Bevalac the steamer chamber with it's 4π geometry and 100 percent efficiency for charged particles, is the most suitable detector for such experiments. Nevertheless, all the neutral particles remain undetected. We have measured the central and inelastic interactions of Ar on KCl at 360, 566, 772, 977, 1180, 1385, 1609 and 1808 MeV/nucleon. For each event three pictures are taken, in order to reconstruct the momenta of the charged particles. The events have been scanned, classified according to the number of negative pions, total charged particles, and leading tracks. Scanning results and preliminary results from the negative pion momentum reconstruction will be presented.

In Figure 3 the total charged particle multiplicity distributions and π^- multiplicity distribution for the central and inelastic triggers are shown, together with the correlation of π^- and total multiplicity for the 1.8 GeV/A bombarding energy. For the inelastic trigger the total multiplicity distribution falls off exponentially for small multiplicities, reaches a plateau for multiplicities between 23 and 40 followed by a sharp cut off at higher multiplicities. This plateau is also apparent in the distribution of the number of participant protons, which can be extracted using the multiplicity of leading particles. The fireball and cascade models[3] do not reproduce this extra yield which comes from a larger transverse momentum spread in near central collisions than assumed by these models.

The total cross sections for the inelastic and central trigger are 1.8 barns and 180 mbarns respectively. The π^- multiplicity distribution has a mean of 2.5 for the inelastic trigger and 5.9 for the

central trigger. The fireball and firestreak models overpredict the number of π^- by a factor of 2. This places in doubt the assumption of chemical equilibrium of pions and Δ's as the production mechanism.

The correlation between negative pion and total charged-particle multiplicity is shown in Figure 3 as contour lines of constant cross section. The reaction is confined to a narrow ridge with no discernable exotic islands of pion production. For the higher multiplicities the system reaches the total disintegration into singly charged fragments and pions.

Surprisingly, the energy dependence of the π^- multiplicity distributions is very smooth as one traverses the different N^* and Δ resonances. For the central trigger the mean π^- multiplicity shows a linear dependence on the bombarding energy (Fig. 4). At each bombarding energy and as a function of the number of participant protons in the interaction (Q) and mean π^- multiplicity shows a linear dependence on Q. It is interesting to see if this is compatible with a short pion and Δ mean free path.

A small sample of π^- from the 1.8 GeV/A central interactions have been reconstructed. A scatter plot $p_\parallel$ vs $p_\perp$ plane in the center of mass is shown in Figure 5. The signature of a nonthermal pion source is clearly visible in which the Δ decay's forwards-backward is still present.

It is of great interest to extract the total c.m. energy in negative pions (E_{π^-}) as function of the π^- multiplicity. Figure 6 shows the correlation between M_{π^-} and E_{π^-} for the reconstructed sample. A distribution peaking at 1.2 GeV for 4 π^- is

observed with a linear dependence of E_{π^-} on M_{π^-} with a slope of $c = 300$ MeV/π^-. Further theoretical analysis needs to be done to see if this linear relationship and the dispersions are in agreement with independent nucleon-nucleon isobar production or if some signature of other coherent processes in highly compressed nuclear matter is present.

A clearer signature from the primary most compressed stage of the interaction is expected from the strange particle production.[4] In the streamer chamber the charged decay of neutral strange hadrons can be detected with good efficiency by identifying secondary vertices (Vees). In this way the $K^0 \to \pi^+\pi^-$ and $\Lambda \to p\pi^-$ decays can be measured, identified by their invariant mass and their momenta can be extracted from the decay kinematics. The identified vees in the 1.8 GeV/A central trigger run have been measured and reconstructed. Since we do not have particle discrimination between π^+ and p each event is plotted in the plane of invariant masses assuming it is a $\pi^+\pi^-$ pair or a $p\pi^-$ pair (Figure 7). We see that most of them correspond to decaying Λ's. A c.m. $p_\parallel$ vs $p_\perp$ scatter plot is shown for the identified Λ's in in Figure 8. The distribution in the c.m. is expected to show a forward backward peaking due to phase space, while the K^* distribution is expected to be isotropic. More data is needed to improve the statistics for the strange particle production.

In summary we have presented our first results of charged particle-4π-experiments in high energy nucleus-nucleus collisions. Existing models describing relativistic heavy ion interactions must be

able to provide predictions for more exclusive measurements like the ones reported here. So far, none of the models can coherently explain our data.

I would like to acknowledge my collaborators in this work. Reinhard Stock, Herbet Stelzer, John Harris, Jim Bannigan, Jorge Geaga, Leslie Rosenberg, Lee Schroeder, Kevin Wolf and Reiner Renfordt. In particular I would like to acknowledge the support of Rudolf Bock for this project.

References

*This work was supported by the Bundesministerium fur Forschung and Technologie, West Germany and the Division of Physical Research of the U. S. Department of Energy under contract No. W-7405-ENG-48.

1. Review of Particle Properties, Phys. Lett. 75B (1978).
2. A. Sandoval, R. Stock, H. E. Stelzer, J. W. Harris, J. P. Brannigan, J. V. Geaga, L. J. Rosenberg, L. S. Schroeder, K. L. Wolf and R. E. Renfordt, to be published.
3. Y. Yariv and Z. Frankel, Phys. Rev. C 20, 2270 (1979). J. Cugon, Proceedings of the Winter Workshop on Nuclear Dynamics, Granlibakken 17-21 March 1980, LBL-10688 (1980).
4. Che-Ming Ko, Proceedings of the Winter Workshop on Nuclear Dynamics, Granlibaken 17-21 March 1980, LBL-10688 (1980,

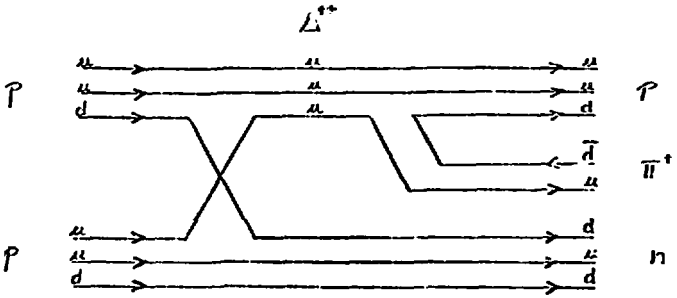

Fig. 1. Quark diagram for the reaction $p + p \rightarrow \Delta^{++} + n$, $\Delta^{++} \rightarrow \pi^+ + p$

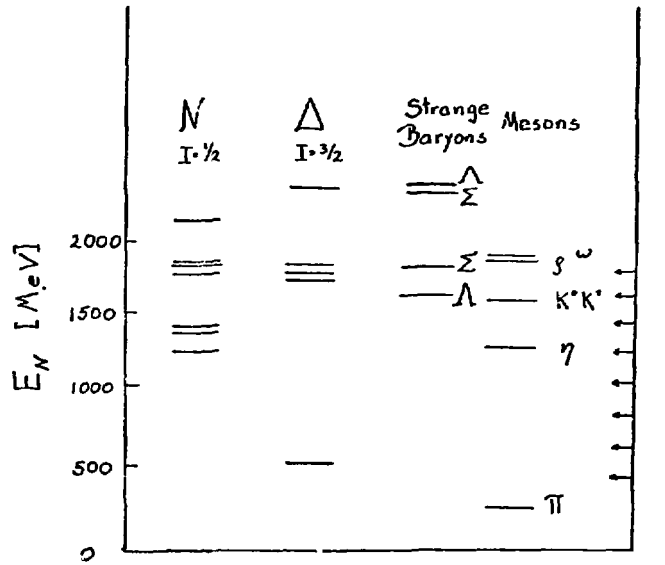

Fig. 2. Known baryon and meson states plotted as function of the laboratory bombarding energy at which they can be excited in nucleon-nucleon reactions. At left the arrows give the energy per nucleon at which we took data.

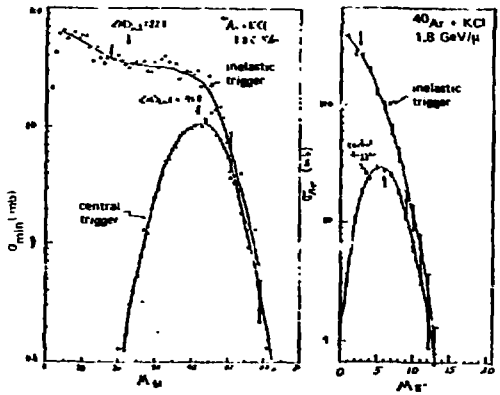

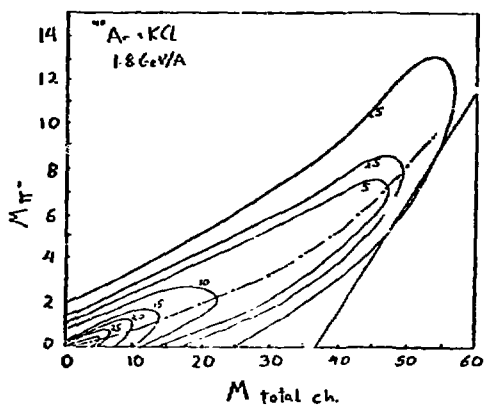

Fig. 3. Top: total multiplicity and π^- multiplicity distributions for the inelastic and central trigger in the interaction of Ar on KCl at 1.8 GeV/A.
Bottom: correlation between total multiplicity and π^- multiplicity for the inelastic trigger as contours of constant cross section (mbarns).

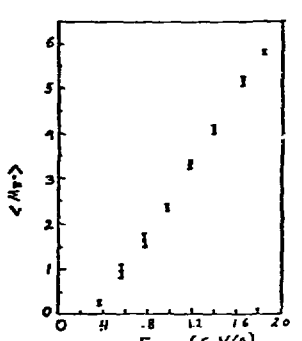

Fig. 4. Energy dependence of the mean π^- multiplicity in the central interaction of Ar on KCl.

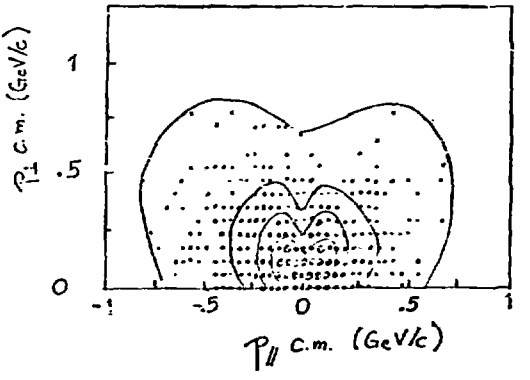

Fig. 5. Scatter plot of the π^- produced in 373 central interactions of Ar + KCl at 1.8 GeV/A, plotted in the center of mass $p_{\parallel}$ vs. $p_{\perp}$ plane.

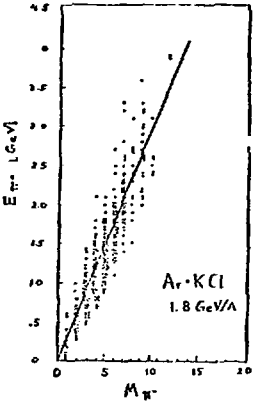

Fig. 6. Total center of mass energy in negative pions of each reconstructed event vs. the π^- multiplicity at 1.8 GeV/A. The straight line corresponds to a slope of 300 MeV/π^-.

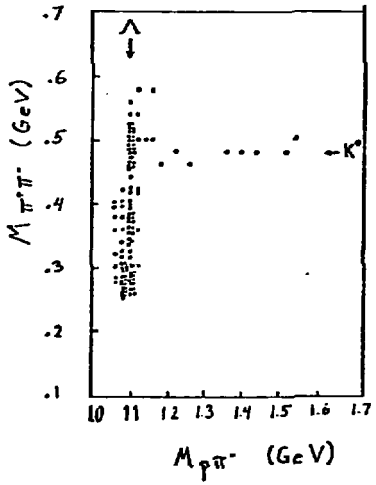

Fig. 7. Scatter plot of the reconstructed vees due to neutral strange particle decay in the streamer chamber for the 1.8 GeV/A energy, plotted in the plane of invariant masses assuming a $\pi^+\pi^-$ or a $p\pi^-$ pair. Most events correspond to Λ decays.

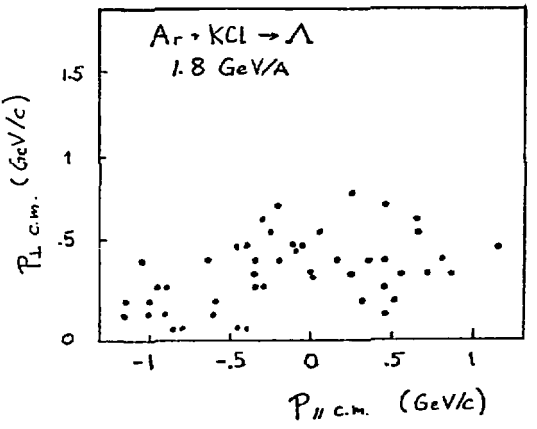

Fig. 8. Scatter plot of the reconstructed Λs center of mass perpendicular and transverse momentum.

PIONS IN THE STATISTICAL PICTURE OF HIGH-ENERGY HEAVY-ION COLLISIONS*

Jörn Knoll and Steffen Bohrmann

Nuclear Science Division, Lawrence Berkeley Laboratory
Berkeley, CA 94720, USA

on leave of absence from
Max-Planck-Institut für Kernphysik and
Institut für Theoretische Physik der Universität
6900 Heidelberg, Germany

Introduction

The preceeding contribution[1] demonstrated that inclusive proton spectra from high energy nuclear reactions clearly show features due to the finite number of particles involved. It is the purpose of this contribution to clarify whether and to what extent finite particle-number effects are important with respect to inclusive pion spectra.

The Model

To answer this question the statistical model of high-energy heavy-ion collisions[2] was extended to include the production of pions. Its main ingredients are the application of the straight-line geometry concept to define independently interacting subsets of participating nucleons and the assumption of complete randomization of available energy and momentum among the particles of each subset. Contrary to thermal limit pictures we treat the subsets as "microcanonical ensembles", retaining strict energy, momentum, and baryon number conservation.

In a completely statistical picture as it was introduced by Fermi[3] the probability to produce a certain number of pions in a subset with a fixed number of nucleons is strictly proportional to the number of states accessible to the system (i.e., the phase space). Whereas the momentum space part of the phase space follows from the conservation laws the coordinate space part, contains the only free parameter of the model; a characteristic baryon density ρ_C which in analogy to bulk limit ("firestreak")[4] models can be interpreted as "freeze-out density".

The Fermi motion of the nucleons in projectile and target modifies the total energy and momentum available to a subsystem. This was taken into account by an appropriate folding procedure.

Results

The above model was used to calculate various pion spectra. For reasons of comparison the same data were calculated in a "firestreak"-simulation by going to the bulk limit for each ensemble.

We observed throughout that the pion yields are overestimated by a factor of about two (also in the thermal limit) if ρ_c were taken to be normal nuclear matter density ρ_0. As we are primarily interested in spectra rather than in multiplicities, we abandoned any physical interpretation of ρ_c and considered it as a free parameter. The observed pion multiplicities at 800 MeV/A require $\rho_c \approx 2\rho_0$. (Regretfully we are only able to present preliminary results calculated with a value of ρ_c giving only half of the observed pion multiplicity at 800 MeV/A. The corrected calculations will accordingly alter the normalization and slightly steepen the asymptotic slopes of the spectra but will not effect their general features in particular if compared to the bulk limit results.) Figure 1 shows 90°-energy-spectra of protons and π^- from 800 MeV/A Ne+NaF in the center of mass of the colliding system. (The data are from Nagamiya[5].) Due to the finite number of particles the statistical model gives steeper asymptotic slopes for the protons (dash-dotted line) than the "firestreak" model (dashed line) even without taking into account the effects of pion production.[1] While "firestreak" calculations require considerable "pion cooling" to get correct slopes for the protons and consequently yield unreasonably high pion rates, our statistical model yields satisfactory agreement already with rates less than the observed ones (solid line). The slope of the associated pion spectrum, however, comes out a bit too flat compared to experiment (solid line) and in fact is identical to the proton slope; the experimentally observed difference cannot be reproduced. However, the model copes with the mass dependence of the slopes of 90°-CM-pion- spectra (C + C gives steeper slopes than Ar + KCl). This the "firestreak" model cannot do from principal reasons.

The apparent "scaling" features of pion spectra in forward direction as observed by Papp et al.[6] were interpreted by Landau and Gyulassy [7] as kinematical effects. The success of the statistical model (Figs. 2,3; solid lines) in reproducing these features as compared to the "firestreak"-model (dashed line) seems to support this conclusion.

In backward direction pion spectra obviously do not scale (Fig. 4; data are from Schroeder et al.[8], lower cross-sections correspond to higher projectile-energy). Gyulassy and Kauffmann interpreted this as scattering on "effective clusters" in the target nucleus and related the slopes of the spectra to the cluster size. As the slopes, however, can be reproduced in the statistical model, too (solid lines; dashed lines: "firestreak"), it seems questionable whether slopes are uniquely related to cluster sizes.

Finally, the correct treatment of kinematics by the statistical model (solid line, Fig. 5) is impressively demonstrated by the comparison to pion spectra which are measured all the way up to the kinematical limit.[9] Here the "firestreak" model (dashed line) fails dramatically. As we kept ρ_c fixed throughout our calculations we underestimated the total rate in this subthreshold pion production experiment.

Conclusions

The rate of pions produced in high-energy heavy-ion reactions still is an open problem and cannot be explained by the assumption of complete randomization. In all cases where kinematical limits are approached finite particle number effects play an important role.

Footnotes and References

*Work supported in part by Bundesministerium für Forschung und Technologie, Germany.

1. Jörn Knoll, these proceedings.
2. Jörn Knoll, Phys. Rev C 20, 773 (1979).
3. E. Fermi, Progr. of Theor. Phys. 5, 570 (1950).
4. J. Gosset, J. I. Kapusta, G. D. Westfall, Phys. Rev. C 18, 844 (1978).
5. S. Nagamiya, L. Anderson, W. Brückner, O. Chamberlain, M.-C. Lemaire, S. Schnetzer, G. Shapiro, H. Steiner, I. Tanihata, Phys. Lett. 81B, 147 (1979), and I. Tanihata, S. Nagamiya, O. Chamberlain, M.-C. Lemaire, S. Schnetzer, G. Shapiro, H. Steiner, Phys. Lett. 87B, 349 (1979).
6. J. Papp, J. Jaros, L. Schroeder, J. Staples, H. Steiner, A. Wagner, J. Wiss, Phys. Rev. Lett. 34, 601 (1975).
7. R. A. Landau, M. Gyulassy, Phys. Rev. C 19, 149 (1979).
8. L. S. Schroeder, S. A. Chessin, J. V. Geaga, J. Y. Grossiord, J. W. Harris, D. L. Hendrie, R. Treuhaft, K. Van Bibber, Phys. Rev. Lett. 43, 1787 (1979).
9. E. Aslanides, P. Fassnacht, F. Hibou, E. Chiavassa, G. Dellacasa, M. Gallio, A. Musso, T. Bressani, G. Puddu, Phys. Rev. Lett. 43, 1466 (1979).

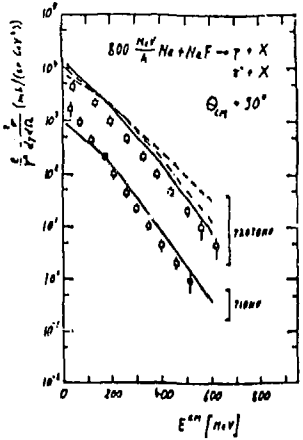

FIG. 1

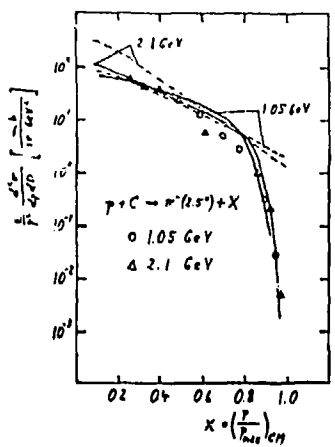

FIG. 2

FOR MORE
DETAILS
SEE TEXT

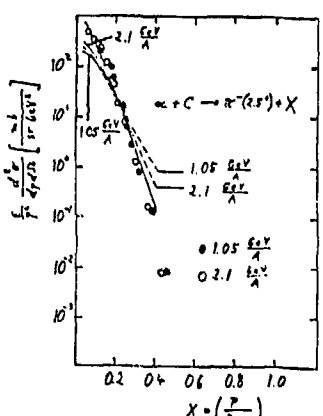

FIG 3

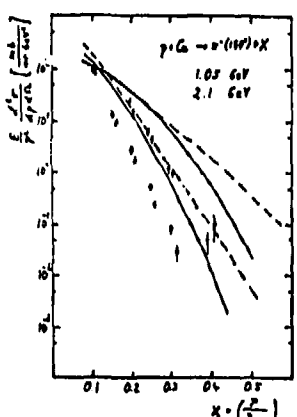

FIG 4

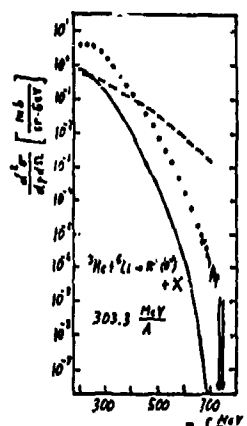

FIG. 5

K^+ PRODUCTION IN RELATIVISTIC NUCLEAR COLLISIONS

Che Ming Ko and Jörgen Randrup
Nuclear Science Division
Lawrence Berkeley Laboratory
Berkeley, CA 94720

Abstract

Kaon production in relativistic nuclear collisions is studied on the basis of a conventional multiple-collision model. The input is the differential cross section for kaon production in elementary baryon-baryon collisions, estimated in a simple model. The inclusive kaon yield is approximately isotropic in the mid-rapidity frame and extends considerably beyond the nucleon-nucleon kinematic limit.

Presently an experiment is underway to measure the spectrum of charged kaons produced in relativistic nuclear collisions.[1] Although the partial cross section for kaon production is relatively small, such an experiment is of great interest because of the important new information it may provide about the nuclear collision dynamics. The positive kaons have a relatively small interaction cross section (~9 mb) with nucleons[2] so that they are more likely to escape unperturbed once created. Since the threshold (~1.6 GeV) for their production is relatively high on the scale of presently available beam energies, the kaons are predominately produced before the initial kinetic energy is substantially degraded. They are therefore expected to be better suited as messengers of the primary violent stage of the collision which might otherwise remain quite elusive.

Our study is based on a conventional multiple-collision picture of the nuclear reactions. In particular, we employ the approximate linear-cascade model developed by Hüfner and Knoll[3] and later extended by Knoll and Randrup.[4] This is probably quite adequate for our present exploratory study. Two baryonic states were included: the nucleon N(940) and the delta resonance Δ(1232). The baryonic cascade then involves the process $NN \gtrless N\Delta \gtrless \Delta\Delta$. Due to the Lorentz dilation factor, which is around 3, the deltas are not likely to decay until after the linear cascade is completed. It is therefore important to note that the pions, whether created during the primary cascade or later, are expected to have too little energy to produce any kaons in their further interactions with the nucleons. We therefore expect that the dominant source of kaons is the primary baryon-baryon collisions. Since the partial production cross section for kaon is so small we may safely employ a perturbative approach in which the dynamical feed-back effect of the kaon production in the further collision process is ignored.

The quantities needed in order to generate the kaon spectra associated with a nucleus-nucleus collision are the kaon spectra associated with the various types of elementary baryon-baryon

collisions. Experimentally, the available information is limited to proton induced reactions at few energies.[5] A simple model in which a pion is exchanged was able to explain reasonably well the experimental data.[6] From both the available experimental information and the theoretical extrapolations based on the one-pion exchange model, we arrive at the following conclusions for the kaon spectra from the baryon-baryon collisions: 1) the angular distribution is isotropic in the center-of-mass system. 2) the momentum distribution can be parametrized by $d\sigma/dp \sim x^2(1-x)$ where $x = p/p_{max}$ is the kaon momentum measured in units of its maximum value. 3) The energy dependence of the isospin-averaged total kaon production cross section is approximately given by $\bar{\sigma}_{NN} = 1.33\ \bar{\sigma}_{N\Delta} = ?\ \bar{\sigma}_{\Delta\Delta} = 144\ \mu b\ p_{max}/m_K c$, where m_K is the mass of kaon.

We have calculated the kaon production cross section for cases of actual experiment interest. The Bevalac experiment in Berkeley,[1] which is being completed, employs p, d, and Ne projectiles with a kinetic energy of 2.1 GeV per nucleon. Targets ranging from NaF to Pb have been used. In Fig. 1, we display the reduced differential cross section $Ed\sigma_K/dp/AB$ as contour plots in the rapidity space for reactions using Ne as the projectile. In the above, A and B denote the mass number of the projectile and the target, respectively. The contours are shown on a logarithmic scale with two solid bands per decade. The solid curves indicate fixed angles in the laboratory frame while the dashed curves corresponding to p_K = 400 GeV/c and 800 MeV/c and approximately bound the experimentally accessible region. The calculations are performed with a Fermi momentum of 270 MeV/c for both projectile and target. From these contour plots it is evident that the present calculation yields kaon distributions which are nearly isotropic and centered near the mid-rapidity $y_c = y_{beam}/2 = 0.92$. The total reduced inclusive kaon (K^+ plus K^0) cross section σ_K/AB are 45 μb and 35 μb for target NaF and Pb, respectively. Therefore the scaling behavior that σ_K/AB is a constant holds within 20 percent. This applies also to calculated results for other reactions not presented here. The decrease of the total reduced inclusive kaon cross section can be understood in terms of multiple collisions. In the first collision there is around a 50 percent chance of converting one of the colliding nucleons into a delta resonance. If a delta is produced, the kinematics is such that its nucleon collision partner is degraded so much in momentum that its ability to produce kaons in its next collision is reduced considerably.

The predictions obtained from the above multiple-collision model are significantly different from what would result in a thermal model. Such a model would predict that kaons are emitted from a source which moves with half the beam rapidity for symmetric systems but with much smaller rapidity for a light projectile incident on a heavy target. Also, the scaling behavior observed in the multiple-collision model is not expected to hold in the thermal model. The kaons should therefore be very well suited for discriminating between the cascade-type picture and the thermal picture.

In Fig. 2, we also show the calculated invariant K^+ spectra at fixed laboratory angles for neon-induced reactions (solid histograms). The light bars indicate the result of a simplified calculation where the nuclear density distributions are taken as sharp homogeneous spheres and the fluctuations in collision numbers are neglected.

The Fermi motion is instrumental in broadening the kaon distribution over a wider domain in rapidty space and thus leads to kaons at considerably larger laboratory angles than that could result in a proton-proton collision. It is thus conceivable that the kaons may be used to probe the intrinsic momentum distribution of the nucleons: this might be a particularly powerful method at beam energies below the nucleon-nucleon kaon production threshold where the kaons are produced exclusively due to the Fermi motion.

Details on this work can be found in Ref. 7. This work was supported by the U. S. Department of Energy under contract No. W-7405-eng-48.

References

1) S. Schnetzer et al., Bevalac Experiment No. 471H

2) C. B. Dover and P. J. Moffa, Phys. Rev. C16 (1977) 1087

3) J. Hüfner and J. Knoll, Nucl. Phys. A270 (1977) 460

4) J. Knoll and J. Randrup, Nucl. Phys. A324 (1979) 445

5) O. Benary, R. Price, and G. Alexander, NN and ND Interactions (Above 0.5 GeV/c) - A Compilation, Berkeley (1970) 112-122

6) Tsu Yao, Phys. Rev. 125 (1961) 1048
W. J. Hogan, P. D. Piroure, and A. J. S. Smith, Phys. Rev. 166 (1967)

7) J. Randrup and C. M. Ko, LBL-10530 and submitted to Nucl. Phys. A.

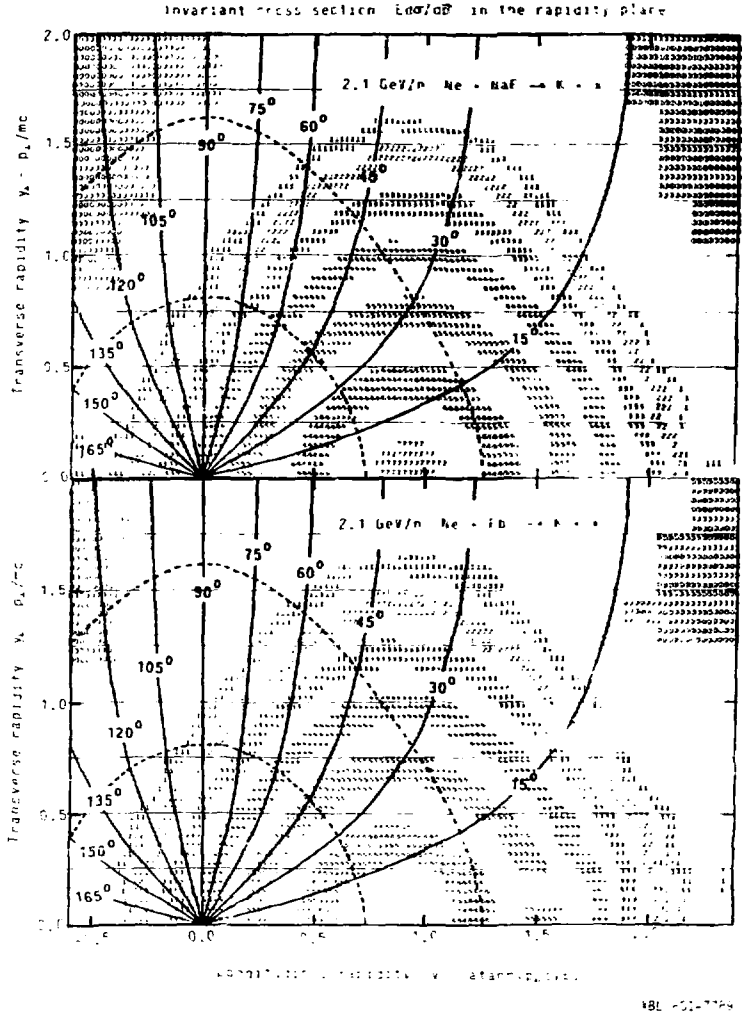

Fig. 1. The calculated reduced invariant differential cross sections for kaon production induced by a 2.1 GeV/n neon beam.

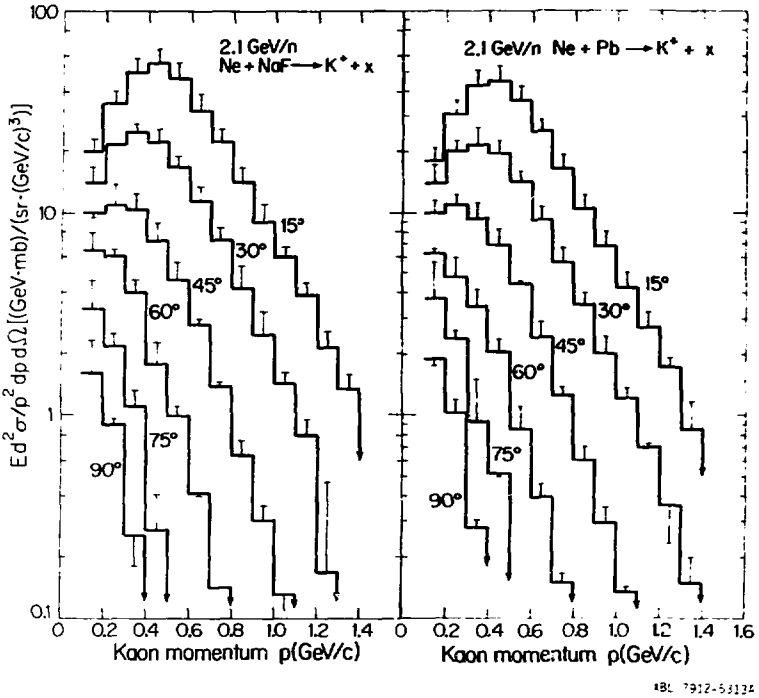

Fig. 2. The calculated invariant K^+ spectra at fixed laboratory angles for neon-induced reactions.

NON-ADIABATIC MASS PARAMETERS

Gerhard Schütte

Theoretical Division, Los Alamos Scientific Laboratory

Los Alamos, New Mexico 87545

It is assumed that the self-consistent single-particle potential for a deforming, especially fissioning, nucleus can be parametrized by time-dependent deformation parameters. The knowledge of their time dependence gives a path in that deformation space leaving a single-particle potential which depends on one deformation parameter only.

In this contribution a fissioning nucleus is described by a Hamiltonian H consisting of the kinetic energy, the above-described single-particle potential and a pairing force. The following arguments are phrased in terms of the adiabatic basis defined as the eigenfunctions $|n\rangle$ of H corresponding to eigenvalues E_n at each deformation. The time-dependent Schrödinger equation is in this basis:

$$\dot{a}_n = -\sum_m \langle n|\partial_t|m\rangle \exp\left(i\int_0^t (E_n - E_m)dt\right) a_m \quad . \tag{1}$$

Two classes of matrix elements can be distinguished: those which create an additional pair $\alpha_\nu^+\alpha_{\bar{\nu}}^+$ out of the BCS ground state $|0\rangle$ are up to one order of magnitude larger than those which break a pair. Accordingly the Hilbert space is split into paired states

$$|0\rangle \quad , \alpha_\nu^+\alpha_{\bar{\nu}}^+|0\rangle \quad , \alpha_\nu^+\alpha_{\bar{\nu}}^+\alpha_\mu^+\alpha_{\bar{\mu}}^+|0\rangle$$

denoted by

$$|0\rangle \quad , |\bar{\nu}\nu\rangle \quad , |\bar{\nu}\nu\bar{\mu}\mu\rangle \quad , \ldots \quad , \tag{2}$$

states with one broken pair

$$|nm\rangle \quad , \; |nm\bar{\nu}\nu\rangle \quad , \; \ldots \quad , \tag{3}$$

and states with more broken pairs. The corresponding projection operators are denoted by P_0, P_{nm}, etc.

Projecting the time dependent Schrödinger equation onto these subspaces gives

$$i\, P_0\dot{\psi}_0 = H\psi_0 - i\, P_0 \sum \dot{\psi}_{nm} \quad , \tag{4a}$$

$$i\, P_{nm}\dot{\psi}_{nm} = H\psi_{nm} - i\, P_{nm}\dot{\psi}_0 - i\, P_{nm} \sum \psi_{nmk\ell} \quad . \tag{4b}$$

The definitions $\psi_0 = P_0\psi$ and $\psi_{nm} = P_{nm}\psi$ have been used. This system is solved through first order in the pair-breaking matrix elements for a nucleus starting in the BCS ground state. Therefore the last term in eq. (4b) which is of second order is neglected. The pair creating or annihilating matrix elements are contained in the ℓ.h.s. and in the first term of the r.h.s. of eqs. (4). These terms constitute homogenous equations which have the solution

$$\psi_0^h = \prod_\nu (d_\nu + c_\nu \exp(-2i \int \varepsilon_\nu d\tau)\alpha_{\bar{\nu}}^+\alpha_\nu^+)\,|0\rangle \quad . \tag{5}$$

ψ_{nm}^h has the same form but $|0\rangle$ is substituted by $|nm\rangle$ and an additional phase $\exp(2i \int (\varepsilon_n + \varepsilon_m)d\tau)$ appears. The usual BCS energies are denoted by ε_n. The coefficients have to fulfill the equations:

$$\dot{c}_\nu = -\langle\bar{\nu}\nu|\partial_t|0\rangle \exp(2i \int \varepsilon_\nu d\tau)\, d_\nu \quad ,$$

$$\dot{d}_\nu = -\langle 0|\partial_t|\bar{\nu}\nu\rangle \exp(-2i \int \varepsilon_\nu d\tau) c_\nu \quad . \tag{6}$$

Since a gap parameter is used common to all basis states one has

$$\langle nm\bar{\nu}\nu|\partial_t|nm\rangle = \langle\bar{\nu}\nu|\partial_t|0\rangle = \langle\bar{\mu}\mu\bar{\nu}\nu|\partial_t|\bar{\mu}\mu\rangle \quad . \tag{7}$$

Together with the initial condition that the system starts essentially in the BCS ground state eq. (7) shows that the amplitudes c and d are identical in ψ_0^h and ψ_{nm}^h. The pair (6) is of Landau-Zener type. Hence c_ν and d_ν are analytic functions [1] of the variables $\varepsilon_\nu^2/\dot{\varepsilon}_\nu$ and $\Delta^2/\dot{\varepsilon}_\nu$. Therefore c_ν does not contain positive powers of the deformation velocity $\dot{\alpha}$.

Through first order in pair breaking matrix elements the solution ψ of the time-dependent Schrödinger equation is

$$\psi \cong \psi_0^h + \sum_{n,m} \left\{ A_{nm} - \int_0^t \langle \psi_{nm}^h | \dot{\psi}_0^h \rangle dt' \; \psi_{nm}^h \right\} \quad . \tag{8}$$

The initial conditions are specified in accord with the Inglis cranking model

$$A_{nm} = \frac{i\langle nm|\partial_\alpha|0\rangle}{\varepsilon_n + \varepsilon_m} \dot{\alpha} \Big|_{t=0} \quad . \tag{9}$$

The matrix element in eq. (8) oscillates in time. Its modulus is a smooth function of deformation except in the vicinity of the crossings α_n or α_m of the single particle energies ε_n or ε_m with the chemical potential λ. The contribution of these regions to the integral in (8) is small. It depends on the deformation α_n or α_m and on the velocity $\dot{\alpha}_n$ or $\dot{\alpha}_m$ at this deformation. In the other subintervals of $(0,t)$ containing smooth parts of the modulus the phase can indeed be partially integrated yielding terms which are linear in $\dot{\alpha}_n$ or in the actual velocity $\dot{\alpha}$.

The total excitation energy is given by

$$E^* = \langle \psi|H|\psi\rangle - \langle 0|H|0\rangle$$

$$= \sum_\nu 2\, \varepsilon_\nu |c_\nu|^2$$

$$+ \sum_{nm} \left| A_{nm} - \int_0^t \langle \psi_{nm}|\dot{\psi}_0^h\rangle \right|^2 \left\{ \varepsilon_n \left(1 - 2|c_n|^2\right) + \varepsilon_m \left(1 - 2|c_m|^2\right) \right\} \quad . \tag{10}$$

In this expression the collective kinetic energy $\frac{1}{2} B\dot{a}^2$ is identified as the term quadratic in the actual velocity. Only the absolute square in the last line contributes due to the analytic properties of c_ν. The above-mentioned partial integration yields the mass parameter:

$$B = 2 \sum_{n,m} \frac{\langle nm|\partial_\alpha|0\rangle^2}{\varepsilon_n + \varepsilon_m}$$

$$+ \sum_{nm} |d_m \frac{\langle nm|\partial_\alpha|0\rangle}{i(\varepsilon_n + \varepsilon_m)} \exp\left(i \int_0^t (\varepsilon_n + \varepsilon_m) d\tau\right)$$

$$+ c_m \frac{\langle nm|\partial_\alpha|m\bar{m}\rangle - M_{nm}}{i(\varepsilon_n - \varepsilon_m)} \exp\left(i \int_0^t (\varepsilon_n - \varepsilon_m) d\tau\right)|^2$$

$$\cdot (\varepsilon_m + \varepsilon_n - 2\varepsilon_m |c_m|^2) \quad . \tag{11}$$

A renormalisation of the coupling matrix element takes the "pole contribution" out as discussed in ref. [2]. No contribution of pair creating matrix elements occurs.

Generalizing this result one may say that the coupling causing pseudo-crossings does not contribute to the collective kinetic energy and therefore not to the mass parameter. It gives rise only to intrinsic excitation.

References

[1] E. T. Whittaker and G. N. Watson, "A Course of Modern Analysis," Cambridge University Press, 1969.

[2] G. Schütte, Los Alamos Scientific Laboratory Preprint LA-UR-80-660, 1980.

EFFECT OF A DENSITY ISOMER ON THE DISTRIBUTION OF OUTGOING MATTER IN HIGH-ENERGY HEAVY-ION COLLISIONS

J. R. Nix and D. Strottman

Theoretical Division, Los Alamos Scientific Laboratory

Los Alamos, New Mexico 87545

Within a conventional nuclear fluid-dynamics model,[1] we study the effect of a density isomer on the distribution of outgoing matter in the reaction $^{20}Ne + ^{238}U$ at a laboratory bombarding energy per nucleon of 393 MeV. For comparison, we also vary the nuclear compressibility coefficient K in an equation of state for which the pressure increases continuously with density above normal nuclear density.

The compressional contributions to the three specific nuclear equations of state that we consider are illustrated in Fig. 1. The ground-state energy per nucleon $E_0(n)$ is specified in terms of curves that join smoothly with continuous value and first derivative at one or more intersection points. For small nucleon number density n, we take $E_0(n)$ to be of the form $an^{2/3} - bn$. In the other regions, we take $E_0(n)$ to be parabolas in the square root of the density. This means that in the limit of infinite compression, $E_0(n)$ increases linearly with density, with the speed of sound approaching the speed of light. The value of $E_0(n)$ at normal nuclear density n_0 is taken to be -8 MeV to simulate the effects of surface and Coulomb energies for finite nuclei. The density isomer is taken to occur at a density that is three times normal nuclear density, with an energy 2 MeV higher than that at normal density and with the same curvature. The thermal contribution to the nuclear equation of state is in each case taken from a nonrelativistic Fermi-gas model.

The equations of relativistic nuclear fluid dynamics are solved numerically in three spatial dimensions by use of a particle-in-cell finite-difference

computing method[1] with an improved treatment of edge cells. By integrating over the appropriate ranges of impact parameter, we compute the double-differential cross section corresponding both to all impact parameters and to central collisions constituting 15% of the total cross section. In constructing the cross section from the velocity vectors of the outgoing computational particles at large time, we use a preliminary Gaussian smoothing technique in energy and angle. To facilitate comparisons with experimental results, we convert the cross section for the outgoing matter distribution into the cross section $d^2\sigma/dEd\Omega$ for outgoing charged particles under the assumption of uniform charge density.

The results calculated for our three equations of state are shown in Fig. 2. To within numerical uncertainties, the results are very similar to one another in all cases except for central collisions at laboratory angle $\theta = 30°$ and for both central collisions and all impact parameters at $\theta = 150°$. In these cases, over certain ranges of energy, $d^2\sigma/dEd\Omega$ is larger for the density isomer than for the two conventional equations of state. Because of our neglect of binding, at low energy all of the calculations lie significantly higher than the experimental data for outgoing charged particles,[2] which are given by the solid circles. At high energy all of the calculations reproduce the experimental data at forward angles, but lie below at backward angles. This discrepancy demonstrates experimentally that the target and projectile are partially transparent to each other.

References

1. A. A. Amsden, F. H. Harlow, and J. R. Nix, Phys. Rev. C 15, 2059 (1977).

2. A. Sandoval, H. H. Gutbrod, W. G. Meyer, R. Stock, C. Lukner, A. M. Poskanzer, J. Gosset, J. C. Jourdain, C. H. King, G. King, Nguyen V. S., G. D. Westfall, and K. L. Wolf, Phys. Rev. C, to be published.

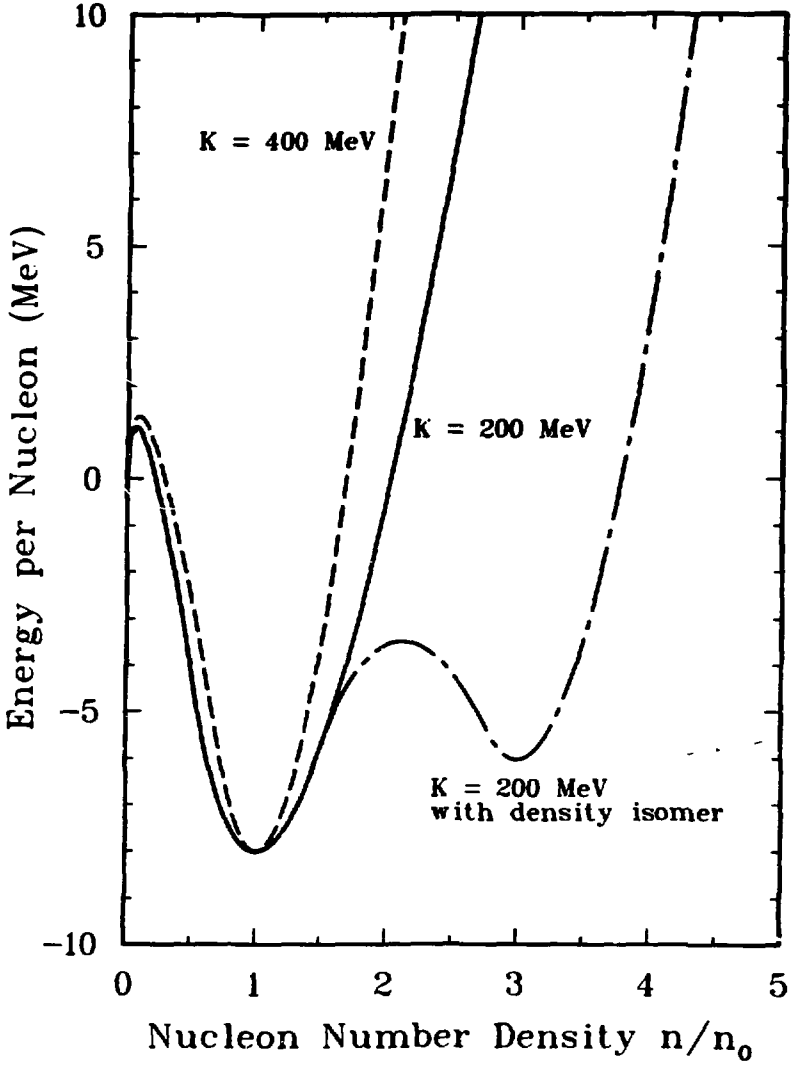

Fig. 1. Compressional contributions to our three nuclear equations of state.

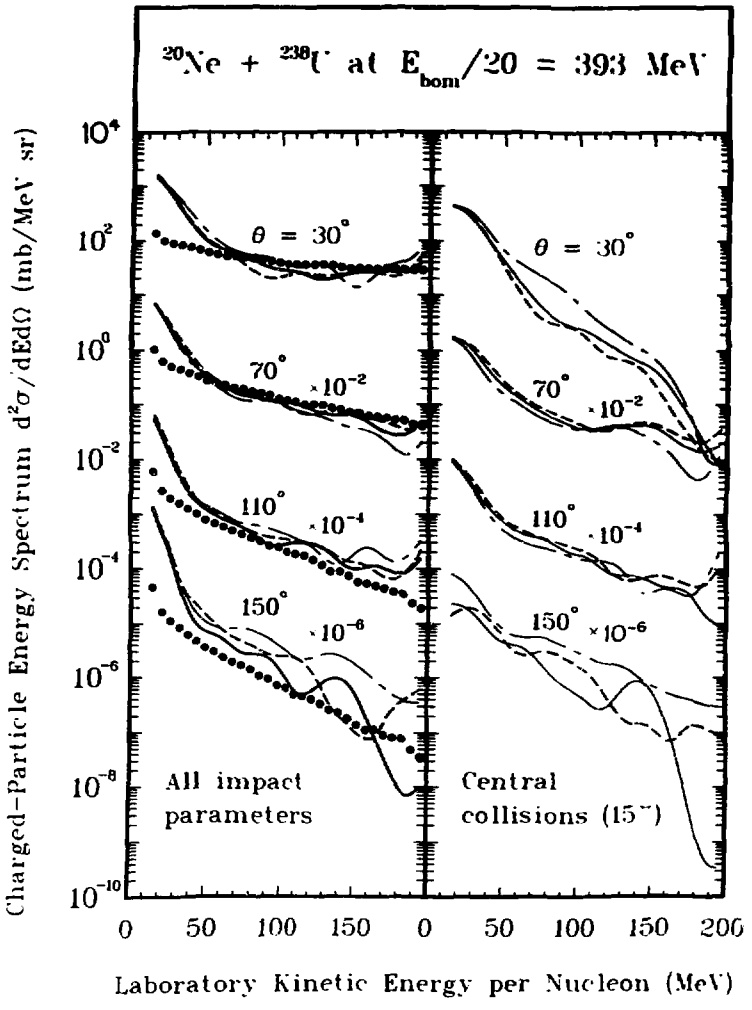

Fig. 2. Dependence of $d^2\sigma/dEd\Omega$ upon the nuclear equation of state, with line conventions corresponding to those used in Fig. 1.

COULOMB EFFECTS IN RELATIVISTIC NUCLEAR COLLISIONS*

M. Gyulassy and S. K. Kauffmann

Nuclear Science Division
Lawrence Berkeley Laboratory
University of California
Berkeley, CA 94720

We derive simple analytical formulas for Coulomb final state interactions and apply them to the analysis of recent data on nuclear collisions. The π^-/π^+ ratio, the π^+ inclusive cross section, and the n/p ratio are studied. A relativistic field theoretic model is used to derive the formulas to first order in $Z\alpha$. Then based on certain well known non-perturbative results, we recast those formulas in an approximate non-perturbative form to increase their domain of applicability and remove unphysical singularities arising from perturbation theory. The final formulas are covariant and take into account multiple independently moving charged fragments of finite size and finite thermal expansion velocities. Our studies demonstrate analytically the complexity and importance of Coulomb distortions in nuclear collisions.

*Abstract from LBL-10279.